MSc Thesis

Portfolio methodology for high level estimation of CO_2 storage potential of saline aquifers

C. Dubbeld

TUDelft

Portfolio methodology for high level estimation of CO_2 storage potential of saline aquifers

by

C. Dubbeld

to obtain the degree of Master of Science
at the Delft University of Technology,
to be defended publicly on Thursday August 12, 2021 at 02:00 PM.

Student number:	4580680	
Project duration:	November 16, 2020 – August 12, 2021	
Thesis committee:	Dr. H. Hajibeygi,	TU Delft, supervisor
	Prof. dr. W. R. Rossen,	TU Delft
	Dr. Y. Wang,	TU Delft
	Ir. T. Huijskes,	EBN B.V.
	Ir. W. Eikelenboom,	EBN B.V.

Delft University of Technology

Abstract

Carbon capture and storage (CCS) is a proven technology for large-scale reduction of CO_2 in the atmosphere to combat the climate change. The captured CO_2, specially from high-concentration areas such as exhausts of power plans, can be stored safely in subsurface geologic formations. These formations range from saline aquifers to depleted gas reservoirs with different storage potential. A reservoir storage potential, typically measured in Mt mass of CO_2, is defined based on the combined effects of the total storage capacity (pore-volume available for storage up to the safe limiting maximum pressure) and operational injection rates [sm^3/day].

Utilization of depleted gas fields has been the main focus of studies performed to estimate storage capacity of the Dutch offshore reservoirs. However, Dutch offshore saline aquifers, despite their greater storage capacities compared with gas fields, in some cases have been completely disregarded. Moreover, many Dutch offshore gas fields are in a mature production phase, and are set to be decommissioned around 2030. The remaining short time left until 2030 might not be sufficient to set-up CO_2 storage projects for them. Due to the near-future decommissioning of depleted gas field, in combination with the large storage capacity of aquifers, it is of great importance to investigate the storage potential of Dutch offshore saline aquifers. This thesis work addresses such an important topic, and presents a scientific methodology to accurately quantify the storage potential of Dutch saline aquifers.

The storage capacity of saline aquifers is often estimated based on a simple volumetric (total pore volume) calculation. The simplicity of this approach makes it convenient, and widely-used. However, this simplistic approach disregards many important physics related to CO_2 sequestration, specially on safety aspects, which raise concerns of whether the existing estimates are applicable.

This study resolves this challenge by constructing a relatively simple, yet accurate, methodology to asses the storage potential of saline aquifers. The storage potential is quantified by combined effects of storage capacity [Mt] (within safe operational pressure) and the injection rate [sm^3/day]. With the use of a numerical simulator, a systematic sensitivity study is then performed for a wide range of uncertain parameters. These parameters include the reservoir porosity, permeability, thickness, depth and radius (i.e. volume). To make the study more realistic, the geologic data is collected from formations that are considered to be possible CO_2 storage formations in the Dutch offshore.

The conceptual model constructed in this study is a cylindrical model with no-flow condition at its external face. The injection of the CO_2 takes place with one well located in the center and perforated all through the reservoir thickness. The well injects CO_2 for 40 years. Only reservoirs deeper than 800 meters are considered. As such, at the studied thermodynamic conditions, CO_2 is always a supercritical fluid.

The storage potential is quantified based on two storage mechanisms: (1) volume limited storage capacity and (2) rate limited storage capacity. This categorization is based on whether the pore volume or the injection rate is limiting the mass of CO_2 that can be stored safely in a certain amount of time. A volume limited storage capacity can be estimated by a linear equation relating the storage capacity with the pore volume, including a storage efficiency factor E. The efficiency factor E is a linear function of the relative injection pressure (ΔP).

Rate limited storage capacity cannot be estimated with a volumetric calculation, but it requires dynamic simulation. However, the storage capacity is conveniently estimated by multiplying the plateau rate with the total time of injection. The rule-of-thumb for the injectivity, which is defined as the injection rate divided by the relative injection pressure (Q / ΔP), is a function of the reservoir injectivity (kh). In this study, the maximum allowed relative injection pressure is determined by the leak-off pressure and by the weight of the CO_2 column in the well. The relative injection pressure directly impacts the volume limited and rate limited storage potential. The relative injection pressure results from the reservoir pressure and maximum allowed bottomhole pressure (BHP), which is set as an operating constraint. In this study the BHP is determined by the leak-off pressure and the weight of the CO_2 column in the well. With these conditions, an optimal injection depth and maximum injection depth are approximated. This study shows that the relative injection pressure is of significant importance on the storage potential, which cannot be neglected in capacity estimation. Moreover, results indicate that a reliable storage estimation is possible with the developed convenient scientific methodology.

Preface

This thesis was written in extraordinary times, where most of my time was spent in solitude in my student room or at the TU Delft library. I don't think any student ever expects to finish their degree during a pandemic.
However, the online support of my TU Delft and EBN supervisors were a great contribution to this project. Thank you for sharing your knowledge and experience with me. Very cliché, but true, without your guidance this project would not have been possible.

First of all, I would like to thank Hadi Hajibeygi. Your critical questions and feedback helped me better understand the goal of this project. Moreover, I would like to thank you for your great lectures during my master track.

Also, a special thanks to Thijs Huijskes. Your daily supervision kept me focused, productive and enthusiastic. You taught me to remain critical of my own work and to analyse the data with a broader and new perspective. I had a great time working with you.

Furthermore, I would like to thank Walter Eikelenboom and Raymond Godderij for their contribution to this project. Your feedback helped me to re-evaluate my research results and apply them in a practical way.

I would also like to thank Yuhang Wang for sharing his knowledge and for hosting the monthly meetings where I got the chance to get feedback from the ADMIRE PhD students.

Additionally, I would like to thank the EBN I&A team for welcoming me in their online meetings. The coffee meetings helped me to start the week fresh and to get to know the EBN staff despite the online work. Thank you for sharing your enthusiasm for the Dutch Energy sector.

Finally, I would like to thank the Technical University Delft for their effort to realise study space during the pandemic. Even after nine months, a student room of 8m^2 can be extremely distracting.

C. Dubbeld
Delft, August 2021

Contents

List of Figures

1 Introduction

The concentration of CO_2 in the atmosphere has significantly increased during the last decades. Currently around 36 billion tonnes of CO_2 per year are emitted by the combustion of fossil fuels, which makes it the largest contributor to green house gas (GHG) emissions [41]. The Kyoto protocol classifies CO_2 as one of the six gasses that contributes most to global warming and accounts for 75% of the global GHG [23]. In May 2019, at the Mauna Loa Observatory in Hawaii, the carbon dioxide levels in the atmosphere surpassed 415 parts per million (ppm) of CO_2 equivalent (CO_2eq) [26]. This concentration is close to the 450 ppm of CO_2eq that the Kyoto Protocol defined as a threshold for a 50% chance that the global average temperature will exceed 2°C. Exceeding this threshold can result into irreversible climatic change [23].

Carbon capture and storage (CCS) is a technology that reduces the CO_2 concentration to combat climate change, while also allowing for the continued use of fossil fuels until green energy production is significant enough to supply the societies' demands for energy [6]. CCS consists of three main steps: (1) separation and capture of CO_2 from the atmosphere or directly from the industrial zones of high concentrations (e.g. power plant exhausts), (2) compressing the CO_2 in order to transport it to the storage location and lastly, (3) storing the CO_2 in the subsurface [6]. CO_2 can be stored in different types of geological formations, such as depleted oil and gas reservoirs, unmineable coal seams and deep saline aquifers [8]. The mass of CO_2 that can be stored in these geologic formations is called the storage capacity, and is typically measured in mega tones [Mt]. The storage capacity [Mt], in combination with the injection rate [sm^3/day], determines the storage potential of a given formation.

The CO_2 is ideally injected in the underground reservoir as a supercritical fluid. In the supercritical phase, CO_2 has a liquid-like density and a gas-like viscosity, which is very efficient for storage and transport. The critical point, at which reservoir temperature and pressure are such that the CO_2 is a supercritical phase, occurs approximately at 800 meters depth. Therefore, reservoirs deeper than 800 meters are suited for storage of CO_2 in supercritical state.

1.1 Prior research on CO_2 in deep saline aquifers

1.1.1 Aquifers versus gas fields

The twenty companies with the highest CO_2 emissions in the Dutch industry and energy sector emit approximately 70 Mt/year [14]. Utilizing depleted gas fields as geologic storage formations has been the main focus of storage capacity estimations in the Dutch offshore, whereas in some cases aquifers have been unfortunately completely disregarded [14]. Note that the total possible storage capacity of only five saline aquifers in the Dutch offshore is estimated to be approximately 1.5 Gt [28]. To achieve the same storage capacity, approximately 104 depleted gas fields are needed. The estimation of the storage capacity of the entire 104 Dutch offshore depleted gas fields is estimated to be approximately 1.7 Gt [14].

The reason that saline aquifers have not been considered during storage capacity estimations is partly due to the scarce geological and technical information of Dutch aquifers compared to gas fields. In addition, the pore pressure in the aquifers is hydrostatic. This means that in order to inject CO_2, the aquifer pressure has to be increased above its original pressure. In contrast, in depleted gas field, injecting CO_2 would not surpass their original non-depleted pressure value.

One of the advantages of utilizing depleted gas fields compared to aquifers is known to be the re-using of facilities, such as wells and platforms. However, this does not hold for many Dutch offshore gas fields. Because, they are in a mature production phase and will be decommissioned around 2030 [14]. The remaining time, approximately nine years, might not be sufficient to set-up projects which utilize this infrastructure or CO_2 storage. Once the depleted gas fields are abandoned, the facilities can not be re-used anymore to accommodate CO_2 storage. In that case, the advantage of re-using facilities no longer holds for depleted gas fields. Which means that for both aquifers and depleted gas fields new facilities are necessary to accommodate CO_2 storage. Due to the large storage potential of aquifers and lower dependency on existing facilities, the offshore aquifers are indeed a good option to complement the storage capacity of depleted gas fields. Therefore, this thesis is focused on storage potential estimation of Dutch offshore aquifers.

1.1.2 Volumetric based capacity estimations

Storage capacity [Mt] is the amount of CO_2 that can be stored in the pore space of an aquifer. In many studies the storage capacity is estimated by a simple volumetric equation (e.g. see [27], [36], [43], [52], [20]). All these equations can be simplified to

$$M_{CO_2} = E * \rho_{CO_2} * \varphi * h * A = E * \rho_{CO_2} * V_p. \quad (1)$$

where M_{CO_2} is the stored CO_2 mass [kg], E the efficiency factor [-], φ the porosity [-], ρ_{CO_2} the in-situ density of the CO_2 [kg/m^3], A the aquifer area [m^2] and h the aquifer height [m]. Equation (1) is proposed by USDOE (2007b) [42]. It suggests that the amount of CO_2 that can be stored (i.e., M_{CO_2}) is related to the pore volume (i.e., V_p) and can be estimated by multiplying the pore volume with an efficiency factor (i.e., E) and the in-situ CO_2 density (i.e., ρ_{CO_2}). The pore volume is calculated by multiplying the reservoir area (i.e., A), the reservoir height (i.e., h) and the porosity (i.e., φ).
The simplicity of equation (1) is an attractive way to assess and compare multiple storage options on portfolio level. However, the simplicity disregards many important aspects of CO_2 sequestration; and can lead to wrong storage potential estimates.

The USDOE, CLSF, USGS and plume evolution methods consider open aquifers [1]. This means that these methods assume full displacement of brine with no pressure increase from CO_2 injection. Apart from relating the pore volume to the efficiency factor, as done with the USDOE, CLSF and USGS method, the efficiency factor can also be related to the CO_2 plume resulting from buoyant forces [1]. This plume evolution method by Owken *et al* (2010) is separated into a calculation before and after injection. Moreover, it is only valid for aquifers with radial symmetry and one injection well. Also, this method only considers buoyant forces and no hydrodynamic forces resulting from the injection pressure [1,30].
The only method that takes into account closed aquifers and water compressibility is the method proposed by Zhou *et al.* (2008). Almost none of the methods take into account dissolution, mineral and residual trapping, but only include stratigraphic and structural trapping. Only Owken *et al.* (2010) takes into account residual trapping after injection of CO_2.

It is important to emphasise that the volumetric calculations lack an overarching method that can be applied to a wide range of aquifers. Also, the volumetric calculations are not time-dependent. Therefore there is no indication of injection rate or the time necessary to fill the aquifer to each the estimated storage capacity. All of these limitations motivate development of a new approach to accurately assess the storage potential of aquifers.

USDOE method
The USDOE method [42] calculates the mass of CO_2 trapped in the aquifer with the aquifer area, average height, porosity and efficiency factor E, as stated in equation (1). The method oversimplifies the calculation by only taking into account structural and stratigraphic trapping. Moreover, it assumes full displacement of water to make place for the CO_2 [1] [12]. This means no trapped water behind the injected CO_2 front is considered. In the USDOE method, an efficiency factor (E) is used, which is calculated by the approach proposed by Goodman *et al.* (2011) [18]. The calculation is based on a Monte Carlo simulation of the efficiency factor for dolomite, limestone and clastic lithologies. Therefore, the USDOE method can be considered to be deterministic-probabilistic, where the aquifer parameters, such as porosity, area and height, are based on the specific aquifer. Whereas, the efficiency factor E is determined probabilistic by the Monte Carlo simulation [1].

CLSF method
Just like the USDOE method, the CLSF method also uses aquifer area, average height and porosity to calculate to potentially stored mass of CO_2, i.e.,

$$M_{CO_2} = C_c * \rho_{CO_2} * A_{av} * h_{av} * \varphi_{av}(1 - S_{w,irr}). \quad (2)$$

The difference between equation (2) and equation (1) is that the CLSF method (i.e., equation (2)) takes into account the residual water saturation (i.e., S_{wirr}), therefore it considers the pore volume portion that will not be available for CO_2 storage. Whereas, the USDOE method does not take into account the residual water saturation and therefore all pore volume is available for CO_2 storage. Also, an efficiency coefficient C_c is introduced into the calculation of CLSF method, as indicated in equation (2). For the USDOE method this efficiency factor is established probabilistic, whereas for the CLSF method the coefficient is determined with dynamic simulations and experiments to take into account heterogeneity, buoyancy and mobility. However, no value for C_C is provided in the literature [1].

USGS method
As the USDOE and the CLSF method, the USGC method is also a volumetric-based procedure. The volumetric equation only takes into account structural and stratigraphic CO_2 trapping. Moreover, just like the CLSF method the USGC method takes into account the residual water saturation. Therefore not all the pore volume is available for CO_2 storage.
Unlike the USDOE and CLSF method, the USGS method is entirely probabilistic. The pore volume, the irreducible water saturation and CO_2 density are determined probabilistic, based on the USGS methodology used for oil and gas assessment [1].
In the USGS method the efficiency factor is determined problematically. The estimation of the efficiency factor is based on regional scale, long-term, steady state CO_2 storage in 192 assessment units. This method includes two depth categories and two permeability classes. The efficiency factor is determined by the plume evolution method after injection [1], as will be described in the next paragraph (and presented in (3) below).

Plume evolution method
Another method to calculate the E factor is by considering the shape of the CO_2 plume, i.e.,

$$E = \frac{(S_{CO_2,irr}/(1 - S_{w,irr})^2}{0.9\lambda + 0.49}, \tag{3}$$

where λ is the mobility. This method is only valid for a horizontal aquifer with radial symmetry and one fully-perforating vertical injection well [1]. This method is developed by the analogy that the flow of CO_2 in an aquifer is driven by hydrodynamic and buoyant forces, where the hydrodynamic forces mainly result from the pressure difference caused by the injection pressure. These forces are opposed by capillary and viscous forces. The ratio between the buoyant and viscous forces can be expressed by a gravity number [12]. In the calculation of the efficiency factor for homogeneous aquifers by Owken *et al.* (2010) the gravity number is used to find the maximum radius of the CO_2 plume. The plume evolution method includes the injection rate and time, aquifer thickness and porosity. Owken *et al.* (2010) also developed a formula for isotropic sloping aquifers [30].
It is important to note that these two methods from Owken *et al.* (2010) are applicable only during injection phase, and not after the injection stops. McMinn *et al.* (2010) developed a formula for the efficiency factor calculations during post-injection phase [24]. It assumes that the flow of CO_2 is resulting from buoyant forces only (as the hydrodynamic forces are insignificant because no injection pressure is applied anymore) and the main trapping mechanism results from residual trapping and the mobility of the CO_2 [1].

Compressibility-based
The CLSF, USDOE, USGS and plume evolution methods can only be applied to open aquifers, assuming full displacement of brine. The method by Zhou *et al.* (2008) is for closed aquifers of limited size with no-flow boundaries [53]. In closed aquifers the storage volume is realized by water and rock compressibility, i.e. βw and β_r, respectively. The efficiency factor E is then calculated as

$$E = (\beta_r + \beta_w)(P_{max} - P_{res,ini}), \tag{4}$$

using the maximum allowed pressure (i.e., P_{max}), initial reservoir pressure (i.e., $P_{res,i}$), and as mentioned before water and rock compressibility (i.e. βw and β_r, respectively). The maximum allowed pressure is set by regulatory measurements, which define a maximum allowed pressure, such as the fracture pressure [1].

1.1.3 Volumetric based capacity estimations for Dutch offshore fields

Storage capacity estimations of saline formations in the Dutch offshore have been previously studied, as summarized in table 1. TNO (2012) executed a screening on high-capacity CO_2 storage sites [28]. Apart from favourable structures, such as anticlines, they also included connected volumes (compartments) of saline formations. The saline formations that were considered in the TNO (2012) study include the Rotliegend, Triassic, Upper Jurassic and Lower Cretaceous formations. The storage capacity of the selected formations is calculated with the volumetric USDOE approach, using a storage efficiency factor of 2%. In an earlier assessment from TNO (2011), they also include the injection rate as an important requirement for CO_2 storage capacity estimations. Which partially depends on geological parameters, such as the reservoir pressure, but also on well-placement, such as number and type of wells [27].

TNO (2021) released a small scale feasibility study to find suitable geologic areas for CO_2 storage. In this study they focus on aquifer storage sites that can be drilled from an existing platform produces from a nearly depleted gas field. The two areas under consideration are the P18 area near offshore Rotterdam and the Vlieland Sandstone Formation. The Tertiary sandstone has also been studied, because of their large connected pore volume and unfaulted areas. However, in the considered P18 area the Tertiary formations lie too shallow for supercritical CO_2 injection. In the report the storage capacity is not estimated, instead an estimation of the pore volume is given [17].

Ramirez *et al.* (2009) developed a screening method to identify potential CO_2 storage options in the Dutch offshore. The three criteria that are set are based on potential storage capacity estimation, costs and effort to manage risks. The minimum capacity threshold for potential CO_2 storage is set to 2 Mt, which is calculated with the same method as TNO (2012). In total the study identified 34 potential saline CO_2 storage formations. In a follow-up study from Ramirez (2010) the storage potential from those 34 saline storage formations is estimated to be 1.8 Mt/y [35,36].

Table 1: Previously studies on storage capacity estimations of saline formations in the Dutch offshore.

Study	Geologic age	Area / formation	Capacity estimation [Mt]	Injectivitiy [Mt/y]
TNO (2012)	Lower Cretaceous	Q1	110 - 225	10
	Lower Cretaceous	P, Q	360	10
	Triassic	F15, F18	650	1 - 3
	Upper Rotliegend	L10, L13	60	5
	Triassic	step graben	190	1 - 3
TNO (2021)	Cretaceous	P18 North	pore volume only	-
	Cretaceous	P18 South	pore volume only	-
	Cretaceous	P18-04 dome	-	-
	Cretaceous	P18-02 dome	pore volume only	-
	Lower Cretaceous	Q01	135 - 235	-
	Paleogene	P15/P18	pore volume only	-
Ramirez (2010)	Lower Cretaceous	Vlieland SST	-	0.5
	Upper Jurassic	Friese front Fm	-	0.2
	Lower Triassic	Buntsandstein	-	0.2
	Permian	Zechtstein Slochteren	-	0.6
	Carboniferous	Limburg Group	-	0.2

1.1.4 Numerical simulation based capacity estimations

Numerical simulators can be used to estimate storage capacity. Compared to volumetric storage capacity estimations, numerical simulators can include many physical and chemical aspects of CO_2 sequestration and their interaction. Whereas volumetric estimations have already been applied to Dutch offshore saline formations, the numerical estimations mainly study the effect of geologic parameters on the storage capacity in general. In most cases, the studies only consider a limited number of geologic parameters on one test model.

Nghiem *et al.* (2009) published essential features for simulation of CO_2 storage in aquifers with the numerical CMG GEM simulator. The study includes solubility trapping, residual trapping, mineral trapping, water vaporization, mineral dissolution and precipitation reactions. In the study a low-permeability and a high-permeability aquifer are studied, 100 and 500 mD respectively. All other aquifer parameters, such as depth, thickness, porosity and size are set constant. The study does not include an estimated storage capacity, but sets the injection rate to 1.0E+06 std m^3/day [29].

Ranjith *et al.* (2012) executes a more detailed sensitivity study. The paper includes a sensitivity on three geological parameters, the reservoir depth, temperature and salinity. Also, it includes a sensitivity analysis on the of the well.
The effect of reservoir depth on the storage capacity is tested from 800 to 1800 meters. The reservoir temperature is tested from 20 to 110 degrees °C. The salinity is tested from 1.00E+05 to 1.60E+05 ppm. The injection pressure is tested from 150 to 230 bar. The sensitivity study does not relate reservoir temperature to depth, so no geothermal gradient is included. Therefore it tests shallow hot to cold reservoirs, i.e. a reservoir at 800 meters depth with a temperature varying from 20 to 110 degrees °C. Or deep cold reservoir, i.e. a reservoir at 1800 meters depth with a temperature of 37 °C. Moreover, the porosity, permeability and reservoir dimensions are kept constant in the sensitivity study. The size of the saline aquifer model is 1000m x 1000m x 184m (l x w x h), with a porosity of 0.25 and a permeability of 100 mD [37].

Preuss *et al.* (2001) studies the amount of CO_2 that can be trapped in various phases (gas, aqueous and solid) for a range of reservoir conditions for a certain amount of injected CO_2. The study mainly focuses on including geochemical reactions that take place between CO_2 and typical aquifer minerals. The reservoir conditions that are included range from temperatures of 40 to 100 °C and pressures from 10 to 45 MPa. Even though the study is looking at the effect of different reservoir conditions on the storage capacity, they only include an infinite-acting reservoir with a constant injection rate of 11 Mt/y. The above discussed studies all make use of a simple, homogeneous radial or Cartesian test models. Instead, some studies include models constructed from isopatch and depth maps in order to better represent real-field aquifers. For instance, Smith *et al.* (2011) studied the effects of boundary conditions (open, semi-closed and closed) on the storage capacity of a Bunter Sandstone formation.

Table 2: Advantages and disadvantages of using volumetric and numerical storage capacity estimations.

Volumetric storage capacity estimation		
Method	**Advantage**	**Disadvantage**
USDOE	1. Simple calculation 2. Structural trapping	1. Only open aquifer boundaries (no pressure increase included) 2. No time dependency 3. No residual, solubility or mineral trapping 4. No heterogeneous permeability 5. Probabilistic E (based on three lithologies)
CLSF	1. Simple calculation 2. Structural trapping	1. Only open aquifer boundaries (no pressure increase included) 2. No time dependency 3. No solubility or mineral trapping 4. Simplified residual trapping 5. No heterogeneous permeability 6. No E provided
USGS	1. Simple calculation 2. Structural trapping	1. Only open aquifer boundaries (no pressure increase included) 2. No time dependency 3. No residual, solubility or mineral trapping 4. No heterogeneous permeability 5. Probabilistic E
Plume evolution	1. Simple calculation 2. Structural trapping 3. Isotropic sloping	1. Radial symmetry 2. Only one injection well 4. No residual, solubility or mineral trapping 5. No heterogeneous permeability 6. No hydrodynamic forces
Compressibility -based	1. Simple calculation 2. Structural trapping 3. Closed aquifer boundaries 4. Maximum allowed pressure	1. No residual, dissolution or mineral trapping 2. No heterogeneous permeability

Numerical storage capacity estimations		
Study	**Advantage / Includes**	**Disadvantage / limitation**
Nhgiem et al. (2009)	1. All four trapping mechanisms 2. Geochemistry	1. Limited sensitivity study: 1a. Two permeability cases 2. Constant depth, thickness, porosity and size 3. Pre-defined injection rate
Ranhith et al (2001)	1. Extensive sensitivity study: 1a. Depth, temperature, salinity 1b. Injection pressure	1. No geothermal gradient included 2. Constant thickness, porosity, permeability and size 3. No mineral trapping
Preus et al. (2001)	1. Geochemical reactions	1. Limited sensitivity study 1a. Temperature and reservoir pressure 3. Open aquifer boundaries 2. Pre-defined injection rate
Smith et al. (2011)	1. Open and closed aquifers	1. Case study 1a. Structural model 1b. Heterogeneity

1.2 Research questions

The main focus of this study is to develop a methodology to estimate the storage capacity [Mt] and injection rate [sm^3/day] of CO_2 in water bearing sand formations, also called aquifers, in the Dutch offshore. In other words: what is the mass of CO_2 that can be stored and how fast can the CO_2 be injected into the water bearing reservoir? This study focuses on injection of supercritical CO_2. This means that reservoir should lie below 800 meters depth, at the critical point, where reservoir pressure and temperature are high enough for the CO_2 to be in the supercritical phase. In the initial stage the aquifer pore volume is completely filled with brine, and a no-flow boundary condition is imposed on the the model. The model can be thought of as a tank in the subsurface. The tank is initially filled with brine and when the CO_2 is injected into the tank, the brine can not escape past the boundaries.

The goal of this study is to develop a methodology to quickly assess the storage potential of a portfolio of aquifers. The storage potential includes the in-situ storage capacity [Mt] and the injection rate at standard conditions [sm^3/day]. This allows for fast screening among many aquifers in order to select potential aquifer candidates, which can be used to enhance future studies.
For simple and quick assessment a rule-of-thumb will be constructed to estimate the storage potential. This rule-of-thumb will be based on the results of a numerical sensitivity study on geologically realistic aquifer parameters. In contrast to the volumetric and numerical storage capacity calculations in previous studies which can only be applied to specific aquifers, the method developed in this work allows for application over a wide range of aquifer parameters.
In order to find the rule-of-thumb approach to accurately estimate the storage capacity of a Dutch offshore aquifer, the following research questions are proposed:

- What is the range of geologic parameter values for potential aquifer formations in the Dutch offshore, including:

    1. Porosity [-]
    2. Permeability [mD]
    3. Top depth [m]
    4. Thickness [m]
    5. Radius [m]

- How do the geologic parameters affect the storage capacity [Mt] and injection rate [sm^3/day];

- Is it possible to set up a rule-of-thumb for the storage efficiency factor E to estimate the storage capacity. If yes, how can the rule-of-thumb for the efficiency factor E be used on a portfolio level;

- Is it possible to set up a rule-of-thumb for the injection rate. If yes, how can the rule-of-thumb for the injection rate be used on a portfolio level;

- Can the rule-of-thumbs be applied to estimate the reservoir parameters (porosity, permeability, top depth, thickness and radius) which are necessary in order to store a certain amount of CO_2 on project scale and within project time (t=40 years).

The following chapters present the steps taken to achieve the research goal. In chapter 2 mechanisms of CO_2 storage in saline aquifers are described. This includes constitutive relations for the multiphase system composed of CO_2 and brine. The next chapter presents the simulation set-up, including the model description and physical values used in the study. Chapter 4 describes the methodology of the geologic data collection, the calculation of the operating constraints, the preliminary sensitivity study and the geologic parameter sensitivity study. In chapters 5 to 8 the results from the sensitivity study are present. The results are subdivided into three separate chapters, which is based on the effect of the pore volume on the storage capacity. These chapters also presents the rule-of-thumbs and how these rules can be practically applied. A workflow can be found in chapter 9. Moreover, in chapter 10 the rule-of-thumbs are applied to two case studies. The results are discussed and concluded in chapters 11 and 12. Recommendations for future work are given in the last chapter.

2 Fluid-rock characteristics and governing equations

Immiscible two-phase flow occurs during CO_2 injection in porous rock filled with brine. The governing equations are presented in this chapter.

2.1 Multi-phase flow

Modelling CO_2 storage in an aquifer requires solving three main equations: (1) the component transport equations, (2) thermodynamic equilibrium and (3) the equilibrium of geochemical reactions.

2.1.1 Component transport equation

The mass conservation law states that within a system mass can not be destroyed nor created. Therefore, the rate of mass increase within the system equals the net rate of mass entering [50]. The mass balance equation for each component can be written as

$$\nabla \cdot \left[\sum_{\alpha=1}^{N_p} \rho_\alpha \; x_{i\alpha} \; \vec{v_\alpha} \right] + Q_i = \sum_{\alpha=1}^{N_p} \frac{\partial}{\partial t} (\varphi \; \rho_\alpha \; x_{i\alpha} \; S_\alpha) \qquad i = 1, ..., N_c \tag{5}$$

Here, N_c and N_p are the number of components and phases in the system, respectively. Moreover, φ is the porosity, ρ_α is the density of phase α, S_α is the saturation of phase α, $x_{i\alpha}$ is the mole fraction of component i in phase α and v_α is the flow rate of phase α. In addition, Q_i is the injection rate of component i.

The flow rate velocity v_α of phase α is calculated with Darcy's multiphase flow equation [50], which is defined as

$$\vec{v_\alpha} = -\frac{k_{r,\alpha} \, \mathbf{K}}{\mu_\alpha} (\nabla P_\alpha - \rho_\alpha \; g \; \nabla h). \tag{6}$$

Here, $\mathbf{K}$ is the rock permeability tensor, $k_{r,\alpha}$ is the relative permeability of phase α, μ_α is the viscosity of phase α, ρ_α is the density of phase α. Moreover, P is the pressure and h the corresponding height. Adding the Darcy multiphase flow equation into the mass balance equation results into

$$\nabla \cdot \left[\sum_{\alpha=1}^{N_p} \rho_\alpha \; x_{i\alpha} \; \frac{k_{r,\alpha} \, \mathbf{K}}{\mu_\alpha} (\nabla P_\alpha - \rho_\alpha \; g \; \nabla h) \right] + Q_i = \sum_{\alpha=1}^{N_p} \frac{\partial}{\partial t} (\varphi \; \rho_\alpha \; x_{i\alpha} \; S_\alpha). \tag{7}$$

The volume consistency equation forces the consistency in the system between the number of components, the density, the saturation and the porosity [11], i.e.,

$$V \frac{\sum_{i=1}^{N_c+1} N_i^{n+1}}{(\rho_g S_g + \rho_w S_w)^{n+1}} - V \varphi^{n+1} = 0. \tag{8}$$

In this equation, the first term is the volume occupied by the fluids and the second term is the pore volume. Also, the superscript n+1 indicates the new time-step. The saturation of the water and the gas phase in the volume consistency equation are related by the following equations

$$S_w = \frac{N_{n_c+1}}{\varphi \; \rho_w} \tag{9}$$

and

$$S_g = 1 - S_w. \tag{10}$$

In order to complete the system, two constraints regarding the saturation and mole fraction are considered, i.e.,

$$\sum_{i=1}^{N_c} S_i = 1 \tag{11}$$

and

$$\sum_{i=1}^{N_c} x_{i\alpha} = 1 \qquad \alpha = 1, ..., N_c. \tag{12}$$

2.1.2 Thermodynamic equilibrium

The equality of the fugacities is used to calculate the thermodynamic equilibrium of a component distributed in 2 different phases of e.g. aqueous and gaseous, i.e.,

$$f_{i_g} - f_{i_w} = 0 \quad for \quad i = 1, .., N_c. \tag{13}$$

The thermal equilibrium states that the fugacity of component *i* in the gas phase is equal to the fugacity of the component in the aqueous phase. In the numerical simulators, the supercritical CO_2 is considered to be a gas phase (just for convenience of referral).
Henry's law is used to calculate the fugacity of a component in the gaseous phase [21], i.e.,

$$f_{i_w} = x_{iw} H_{h,i}. \tag{14}$$

The fugacity is expressed as the product of the molar fraction (x_i) and Henry's constant ($H_{h,i}$) for component i. Henry's constant is a function of pressure, temperature, molar volume (V_m) and the universal gas constant (R), i.e.,

$$ln(H_i) = ln(H^*_{h,i}) + \frac{\overline{V_{m,i}}(P - P^*)}{RT}. \tag{15}$$

In the equation the star symbol * indicates the reference condition and $\overline{V_{m,i}}$ the partial molar volume of component i.
Methane gas (CH_4) is also added as a trace component within gaseous phase. The fugacity of gas mixtures is then calculated as

$$ln(\frac{f_i}{x_i P}) = \frac{1}{RT} \int_V^\infty (\frac{\partial P}{\partial N_i} - \frac{RT}{V}) dV - ln(Z), \tag{16}$$

where Z is the compressibility factor of the mixture. The partial derivative of pressure (P) to the number of moles (N_i) within the volume (V) is calculated by the Peng-Robinson equation of state (PR EOS) [10].
In general an equation of state is a semi-empirical relationship between pressure, volume and temperature of a pure substance. The equation of state can be applied over a wide range of temperatures, pressures, mixtures and also for supercritical phases [34]. The Peng-Robinson equation of state (PR EOS) can be stated as [11]

$$P = \frac{RT}{V - b} - \frac{a(T)}{(V - 0.41b)(V + 2.414b)}, \tag{17}$$

with

$$a = \frac{27}{64} \frac{T^2_{crit} R^2}{P_{crit}} \tag{18}$$

and

$$b = \frac{1}{8} \frac{T_{crit} R}{P_{crit}}. \tag{19}$$

For a mixture of gas components, a mixing rule is applied to evaluate the a and b parameters in the PR EOS. The mixing rule treats all the component equally [10], i.e.,

$$a = \sum_{i,j=1}^{Nc} x_i x_j (1 - d_{ij})(a_i a_j)^{1/2} \tag{20}$$

and

$$b = \sum_{i=1}^{nc} x_i b_i. \tag{21}$$

Here, x_i and x_j are the mole fraction of the components i and j in the mixture. The binary interaction parameter (i.e. d_{ij}) for CH_4 with CO_2 and H_2O is 0.103 and 0.4907, respectively. Moreover, the interaction parameter between CO_2 and H_2O is 0.200 [10].

Salinity
The salinity of the brine affects the solubility of a component into the brine. Therefore Henry's constant is modified accordingly to equation (22). The salting-out coefficient (K_{salt}) depends on the component type and temperature of component i, and in the case of CO_2 it can be calculated as

$$log_{10}(\frac{H_{salt,i}}{H_i}) = k_{salt,i} m_{salt}, \tag{22}$$

where

$$k_{salt,CO2} = 0.11572 - 6.0293 \times 10^{-4} T + 3.5817 \times 10^{-6} T^2 - 3.7772 \times 10^{-9} T^3 \tag{23}$$

holds [11]. In the equation H_i and $H_{salt,i}$ is Henry's constant of component i at zero salinity and at molality of the dissolved salt m_{salt}.

2.1.3 Chemical equilibrium

The chemical reactions during CO_2 storage can be separated into two categories. The first type is a heterogeneous chemical reaction, in which chemical components are not in the same phase [11]. This is the case for mineralization, see equations (37), (38) and (39). However, these heterogeneous chemical reactions are not taken into account in this study. The second type is a homogeneous chemical reactions, in which all components remain in the aqueous phase. The homogeneous chemical reaction that is taken into account in this study is the dissolution of CO_2 in water, see equation (36). The dissolution of CO_2 in water represents one of the three CO_2 trapping mechanisms, namely solubility trapping. The reaction rate of homogeneous chemical reactions is much faster than those of heterogeneous chemical reactions, and therefore the former can be represented by the chemical equilibrium reaction [11]. The chemical equilibrium reaction is shown by equation (24). Where $k_{eq,\alpha}$ is the chemical equilibrium constant and the square brackets refer to the molarity of the component at chemical equilibrium. Q_α is the activity product, which is related to the activity of the component and stoichiometry coefficient [11] stated as

$$Q_\alpha - K_{eq,\alpha} = 0 \tag{24}$$

with

$$K_{eq} = \frac{[CO^2][H_2O]}{[HCO_3^{-1}][H^+]}. \tag{25}$$

2.1.4 Well model: Injector

The well model relates the injection rate (Q_{inj}) to the pressure difference between the wellbore bottomhole pressure (P_{BHP}) and the pressure of the reservoir (P_{res}). Moreover, the well index (WI) and phase mobility (λ_α) are necessary to calculate the injection rate. To be able to inject the CO_2 it is required that the bottomhole pressure is larger than the reservoir pressure ($P_{BHP} > P_{res}$). The injection rate is calculated with

$$Q_{inj} = WI\, \lambda_\alpha\, (P_{BHP} - P_{res}). \tag{26}$$

The well injectivity index (WI) depends on well geometrics. Where wfrac is the well fraction, ff the fraction of completion, r_d and r_{well} the drainage and well radius, and s the skin factor. For a 360° radial injection model the well fraction is assumed to be 1 [11]. The well injectivity is calculated with

$$WI = 2\pi\, ff\, kh\, \frac{wfrac}{ln(r_d/r_{well}) + s}. \tag{27}$$

The drainage radius (r_d) is calculated with the Peaceman formula [11]. For vertical wells holds equation (28), where k_x and k_y are the permeability in the x and y direction, and dx and dy the corresponding dimensions. The drainage radius is calculated with

$$r_d = \frac{0.28\,(dx^2\, k_y + dy^2\, k_x)^{1/2}}{k_x^{1/2} + k_y^{1/2}}. \tag{28}$$

2.1.5 Thermal injection

When the reservoir temperature changes over time, for instance by injecting a fluid which is warmer or colder than the reservoir fluid, the energy balance equation has to be solved. In order to calculate the temperature distribution in the reservoir, the energy balance equation has to be solved. Solving the energy balance equation also requires solving the volume constraint equation, the component flow equations and the phase equilibrium equations [11,50]. The energy balance equation is expressed as

$$\nabla \cdot \left[\sum_{\alpha=1}^{N_p} \rho_\alpha \, H_\alpha \, \frac{k_{r,\alpha} \, \mathbf{K}}{\mu_\alpha} (\nabla P_\alpha - \rho_\alpha \, g \, \nabla h) \right] + \sum_{\alpha=1}^{N_p} (H_\alpha \, Q_\alpha) = \frac{\partial}{\partial t} \left[\varphi \sum_{\alpha=1}^{N_p} (\rho_\alpha \, U_\alpha \, S_\alpha) + (1-\varphi) \, C_r \, (T - T_i) \right]. \tag{29}$$

This equation is based on the mass balance equation and the Darcy multiphase flow equation, see equation (5), (6) and (7). Some extra terms are added to account for the thermal mode. It includes H_α and U_α, which are the enthalpy and the internal energy of phase j. Moreover, the heat loss to the reservoir rock can be included by considering the temperature T and heat capacity of the rock C_r.

The enthalpy of gas at conditions different from the ideal gas enthalpy, at zero pressure and temperature, is the excess enthalpy [11]. The excess enthalpy (H^e) can be calculated with the EOS, see equation (30). Where H^{**} is the enthalpy at zero pressure and temperature, V_m the molar volume, Z the compressibility factor. The excess enthalphy is expressed as

$$\Delta H^e = H - H^{**} = RT \, (Z-1) \, + \int_{\infty}^{V_m} \left[T \left(\frac{\partial P}{\partial T} \right)_{V_m} - P \right] dV_m. \tag{30}$$

2.1.6 Relative permeability

During multi-phase flow in porous rock the permeability of both fluids is decreased due to the presence of the other fluid and the rock. Relative permeability is a empirical description that quantifies the extent to which two fluids interact with each other and the rock surface as they migrate through the porous media [3]. The relative permeability ($k_{r,i}$) is the ratio between the effective permeability (k_i) of the fluid and the absolute permeability (k) of the rock [32] at a given saturation. The relative permeability is calculated with

$$k_{r,i} = \frac{k_i}{K}. \tag{31}$$

The Corey equations are used to find the relative permeability as a function of saturation, see equation (32) and (33). These two equations are empirical functions that are often used because of their reasonably good fit with experimental data [3]. Where k_{rw} and k_{rCO_2} are the the relative permeability of the wetting and non-wetting phase, S_w and S_{nw} the saturation of the wetting and non-wetting phase, $S_{w,irr}$ and $S_{nw,irr}$ the irreducible saturation of the wetting and non-wetting phase. Also, the formula includes the end-point relative permeabilities for the wetting and non-wetting phase k^o_{rw} and $k^o_{rCO_2}$, as well as the fitting exponent of the wetting and non wetting phase. The relative permeability of the wetting and non-wetting phase are calculated with

$$k_{rw} = k^o_{rw} \left(\frac{S_w - S_{w,irr}}{1 - S_{nw,irr} - S_{nw,irr}} \right)^{n_w} \tag{32}$$

and

$$k_{rCO_2} = k^o_{rCO_2} \left(\frac{1 - S_w - S_{nw,irr}}{1 - S_{nw,irr} - S_{w,irr}} \right)^{n_{CO_2}}. \tag{33}$$

Relative permeability is fundamental to predict the spatial and temporal distribution of CO_2 saturation in the porous rock. As well as to estimate the residual trapping during the migration of the CO_2 plume [31].

2.1.7 Capillary pressure and wettability

Capillary pressure results from the interaction of cohesive and adhesive forces. The cohesive force acts within the liquid, whereas the adhesive force acts between the liquid and the bounding surface. A fluid is called the wetting phase if the adhesive forces are greater than the cohesive forces, therefore clinging onto the bounding surface. On the other hand, a fluid is called non-wetting if the cohesive forces are greater than the adhesive forces. Capillary pressure (P$_{c}ap$) is the pressure required to force the non-wetting phase to displace the wetting phase [45].

The CO_2-brine system in the porous rock can be simplified to a bundle of capillary tubes representing the pores. The capillary tubes are originally filled with the wetting brine phase, but is displaced by the injected non-wetting CO_2 phase. The capillary pressure can be described by equation (34). Where σ is the interfacial tension between the wetting and non-wetting phase, r_{cap} is the radius of the capillary tube and θ is the contact angle between the two fluids and the bounding surface. The capillary pressure is calculated with

$$P_{cap} = \frac{2\sigma cos\theta}{r_{cap}}. \tag{34}$$

The Brooks-Corey equation can be used to find the capillary pressure as a function of saturation from experimental data [15], see equation (35). Where P$_{cap}$ is the capillary pressure [bar], P$_{e}$ is the capillary entry pressure [bar], I_{pore} the pore size distribution index, S and S$_{w,irr}$ are the water and irreducible water saturation [-]. The Brooks-Corey equation is stated as

$$P_{cap} = P_e \frac{S - S_{w,irr}}{1 - S_{w,irr}}^{-1/I_{pore}}. \tag{35}$$

2.2 Gas and aqueous phase properties

2.2.1 Phase behaviour of CO_2 and brine

CO_2 is ideally injected as a supercritical fluid. In the supercritical phase the CO_2 has a liquid-like density and a gas-like viscosity, which is very efficient for storage and transport. The density of the supercritical CO_2 (690 kg/m^3) is approximately twice as large compared to the density of the CO_2 in gas phase (300 kg/m^3). This means that approximately half the volume is required to store supercritical CO_2, compared to storing CO_2 at standard conditions. Moreover, the viscosity of the CO_2 only increases slightly when changing from a gas phase to a supercritical phase [44], which is important for how easily a fluid flow through a pipe or porous medium. The combination of the gas-like viscosity and the liquid-like density of the supercritical CO_2, result into the fact that more mass can be transported and stored compared to CO_2 in gas phase.
The critical point is reached at a pressure of 73.8 bar and a temperature of 31.0 °C. These conditions are often present at around 800 meters depth [25].

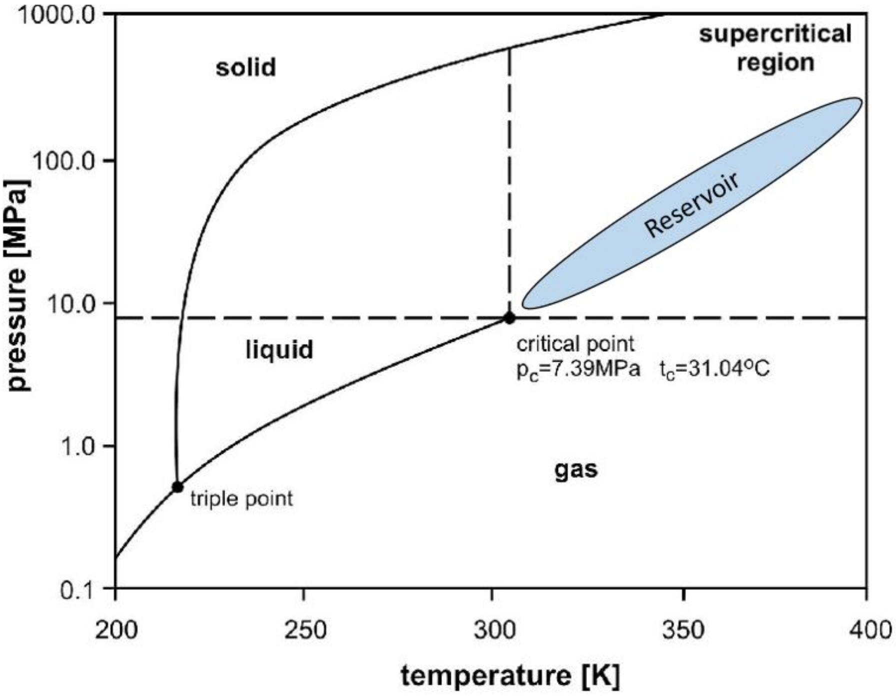

Figure 1: Phase diagram of CO_2 as a function of temperature and pressure. The reservoir conditions below 800 meters fall within the supercritical phase for CO_2. Source: Modified from Witkowski *et al.* (2014) [49]

2.2.2 Density of CO_2 and brine

The supercritical CO_2 phase in CMG GEM is accounted for as a gas and its density is based on Peng-Robinson EOS [11], see equation (17). The density for brine is calculated using the Rowe and Chou (1970) correlation [11], which is a pressure-volume-temperature relation for aqueous NaCl solutions. The molarity of the brine in the simulations is set to 0.5 M.

Even though the CO_2 density is variable with temperature and depth, the temperature and pressure gradient in the subsurface coincidentally results in a relatively constant in-situ CO_2 density at reservoir conditions. Figure 2 shows two estimated CO_2 densities from 800 to 3000 meters. One of the two CO_2 densities is estimated with a look-up table from a VLP (vertical lift profile) calculation. Whereas the other CO_2 density is a calculation from the numerical simulator used in this study. The density obtained from the numerical simulator varies from 519 kg/m^3 to 727 kg/m^3. Whereas the density obtained from the look-up table varies from 654 kg/m^3 to 710 kg/m^3.

The lower density of CO_2 compared to brine, as can be seen in figure 3, results into the upward movement of CO_2 in the reservoir due to buoyant forces. The viscosity of the CO_2 is lower than that of brine, see figure 3. Moreover, the viscosity of the CO_2 at reservoir conditions is less variable than the viscosity of brine.

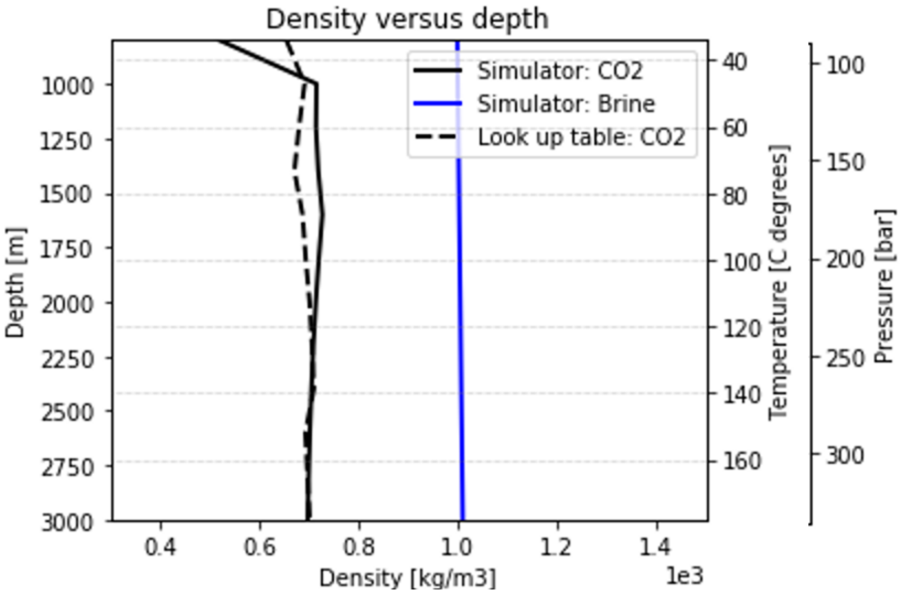

Figure 2: Density of CO_2 and water under reservoir conditions.

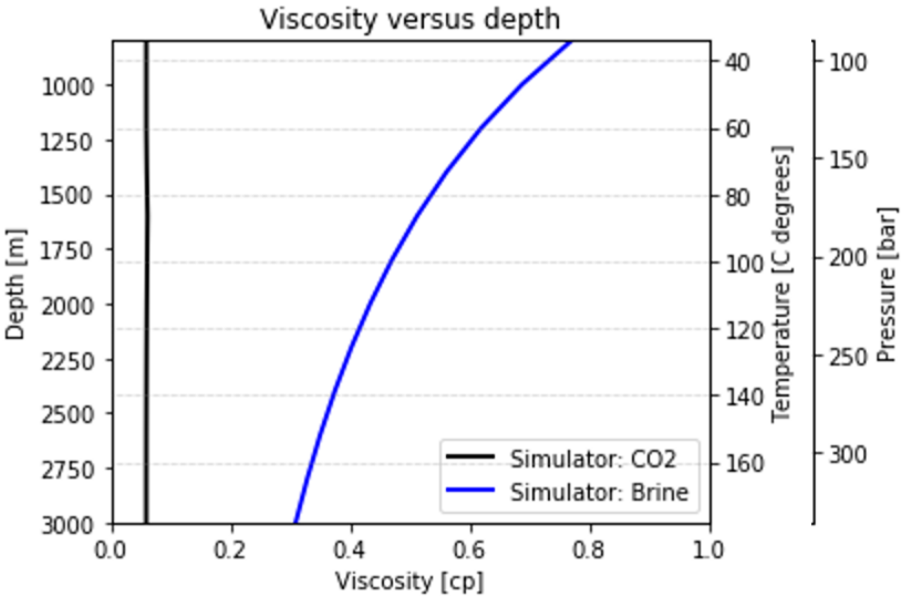

Figure 3: Viscosity of CO_2 and water under reservoir conditions.

2.3 Trapping mechanisms

CO_2 trapping is a combination of physical and geochemical processes that trap and immobilize CO_2 within the formation [33]. The processes occur on different time scales and exhibit different degrees of permanency [7,25], see figure 4. Physical trapping mechanisms include stratigraphic-, structural- and residual trapping. Geochemical trapping mechanisms include solubility and mineral trapping [25].

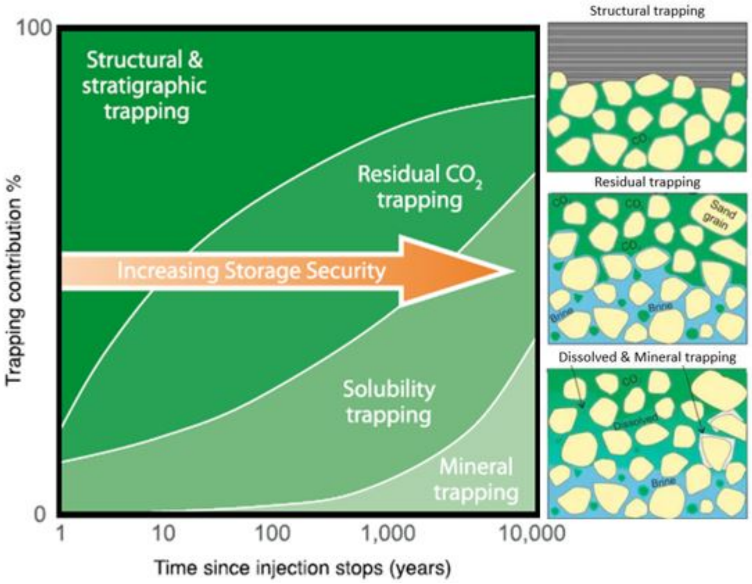

Figure 4: Time scale and contribution of different trapping mechanisms playing an important role in CO_2 sequestration. Modification from IPCC (2005) [25] and Flude & Alcade (2020) [16]

2.3.1 Physical trapping

After injection CO_2 migrates upwards due to its low density compared to brine. The key contributors of short term trapping of CO_2 are stratigraphic and structural trapping. In the case of stratigraphic trapping the upward migration of CO_2 is obstructed by a low-permeability seal, such as shales or salts. Stratigraphic traps result from changes in rock type due to change of environment in times of sedimentary deposition [25]. In the case of stratigraphic trapping the migration is obstructed by a structural trap, such as a fold or fracture [25].

Another type of physical trapping is residual trapping, also called hydrodynamic or capillary trapping. The relative permeability of the CO_2 and brine play an important role during residual trapping. Trapping of CO_2 occurs when imbibition occurs after drainage, see figure 5. During the drainage stage the brine saturation decreases and the CO_2 saturation increases, plotted by the curves k^d_{rw} and k^d_{rg}. With decreasing saturation the relative permeability decreases, and vice versa. The maximum gas saturation (S_{max}), in this case that is the maximum amount of CO_2 saturation, occurs when the relative permeability of the brine reaches zero. At this point the brine is immobilized and the pores can only be partially filled with CO_2. If after this point brine is able to re-occupy the pore space, so called imbibition, the relative permeability and saturation of the brine and CO_2 follow the dotted curves in figure 5. Part of the CO_2 is immobilized and remains in the pores as trapped CO_2. For the intruded fluid, in this case the brine, the relative permeability (k^i_{rw}) is higher at a specific saturation than before re-occupation. For CO_2 the relative permeability (k^i_{rg}) is lower at a specific saturation than compared to before re-occupation. Therefore the residual CO_2 saturation (S_t) is immobilized and trapped [7].

Residual trapping is controlled by physical factors, such as pore-network geometry, rock-fluid interactions and fluid-fluid interaction. Rock properties that influence residual trapping include intrinsic rock permeability, porosity, wettability and capillary entry pressure [7]. Residual trapping occurs in reservoirs when brine intrudes (imbibition) into the tail of the relatively buoyant CO_2 plume while migrating upwards [7]. Residual trapping occurs within 10's of years and significantly contributes to CO_2 sequestration, see figure 4. In sandstones the residual gas saturation is quantified to be on average 10-30% [2].

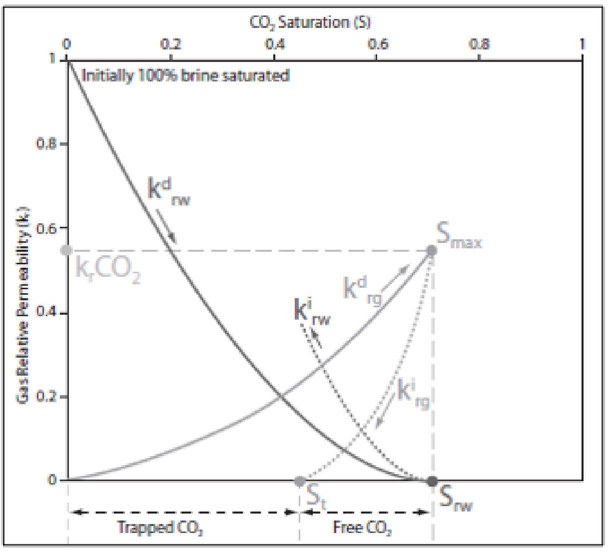

Figure 5: Relative permeability curve for CO_2 and water.
Source: Burnside and Naylor (2014).

2.3.2 Geochemical trapping

The injected CO_2 can react with the rock minerals and with the formation water [25]. Geochemical trapping mechanisms, such as solubility trapping and mineralization, act on a longer timescale compared to physical trapping mechanism [25], see figure 4. When the CO_2 dissolves in the formation water a chemical process called solubility trapping occurs. During CO_2 sequestration the CO_2 dissolves into the formation water and forms weak carbonic acid (H_2CO_3), which rapidly dissociates to form a bicarbonate ion (HCO_3^-) [51] The chemical process can be described by:

$$CO_2(g) + H_2O <-> H_2CO_3 <-> HCO_3^- + H^+ \tag{36}$$

The solubility of CO_2 depends on temperature, pressure and chemical composition of the brine [33]. The solubility of CO_2 in formation water decrease as temperature and salinity increase [25] and pressure decreases [33]. Moreover, the dissolution rate of CO_2 is controlled by diffusion and convection rates [25]. In general solubility trapping has a very low leakage risk because it only comes out of solution when a significant pressure drop or temperature increase occurs [33].

The second type of geochemical trapping is mineralization. The CO_2 which dissolves during dissolution produces weak carbonic acids and bicarbonate ions, see equation (36). The dissolved bicarbonate ions can react with divalent cations causing precipitation of carbonate minerals. The reaction with divalent cations CA^{2+}, Mg^{2+} and Fe^{2+} is the main way of mineral trapping [51]. The corresponding reations are

$$HCO_3^- + Ca^{2+} -> CaCO_3(s) + H^+ \tag{37}$$

and

$$HCO_3^- + Mg^{2+} -> MgCO_3(s) + H^+ \tag{38}$$

and

$$HCO_3^- + Fe^{2+} -> FeCO_3(s) + H^+. \tag{39}$$

The chemical reaction between the CO_2 and the rock minerals can occur within days, for instance for carbonate-bearing rocks, but can also take hundreds to thousands of years in the case of silicate-dominated rocks [25].

3 Numerical simulator

3.1 CMG GEM

GEM is a multidimensional, equation-of-state (EOS) compositional numerical simulator developed by the Computer Modelling Group LTD (CMG). GEM is often used as a simulator for oil and gas. GEM can be used for reservoir modelling, such as CO_2 storage in saline aquifers, but is more commonly used for oil and gas reservoir simulation. Modelling CO_2 storage in aquifers involves solving component transport equations, thermodynamic equilibrium equations and chemical equilibrium equations [11]. Moreover, GEM can include thermal mode to calculate the temperature distribution in the reservoir for compositional processes. This can be included for instance when the injected fluid is at a different temperature than the reservoir temperature [11]. The processes included in the GEM simulations are noted in table 3.

Table 3: Specification of physical processes included in GEM.
Source: Modified from Creusen (2018).

Process	**GEM**	**Note**
Multi-phase	✓	
Non-isothermal	✓	
Components	✓	CO_2-H_2O-NaCl-CH_4(trace component)
Equation of state	✓	Peng-Robinson
Salt precipitation	**X**	
Permeability reduction	**X**	
Water vaporization	**X**	
CO_2 solubility	✓	Henry's Method (1996)
Residual trapping	✓	
Relative permeability	✓	tabular
Capillary pressure	✓	tabular
Imbibition	**X**	tabular

* Included: ✓

* Optional but not used in this research: X

3.2 Reservoir model

3.2.1 Radial sensitivity model

For the sensitivity study a 2D radial model is used with an injector well in the middle, see figure 6. The cell size in the I direction is logarithmic decreasing away from the well in order to have proper resolution near the well, without increasing the total number of cells in the model. This is done because close to well is where most changes in pressure and saturation occur. The grid exist of 79 cells in the I direction and 10 cells in the k direction.

This study considers a base case with a radius of 2 kilometers and a thickness of 100 meters.

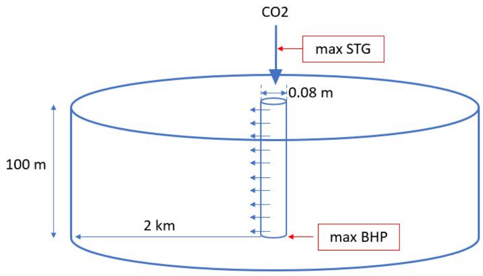

Figure 6: 2D logarithmic radial model with operating constraints: maximum bottomhole pressure (BHP) and maximum surface gas rate (STG).

3.2.2 Well conditions

The injector well is placed in the center of the radial model. Injection of pure super critical CO_2 will take place for 40 years, after which injection is stopped. The well diameter is 0.08 meters and is perforated in every layer in the K-direction, resulting into a total of 10 perforations over the total reservoir thickness. Moreover, a skin factor of 0.1 is applied.

The injection rate depends on the pressure difference between the reservoir pressure and the bottomhole pressure. Moreover, a bottomhole pressure and injection rate constraint are applied to the injector. These constrains make sure that the bottomhole pressure and injection rate do not surpass a certain limit. A detailed description of the operating constraints can be found in section 4.2.3 and 4.2.2.

Table 4: Well conditions set for the radial model.

Well conditions	**Specification**
Injection time [years]	40
Injection fluid	Pure super critical CO_2
Injection rate	Dependent on relative injection pressure ΔP
Injection constraints	Maximum BHP and STG
Well bore radius [m]	0.08
Tubing radius [m]	0.057
Skin factor [-]	0.1
Number of perforations	10

3.3 Boundary conditions

3.3.1 No-flow boundary

The aquifer model can be imagined as a tank in the subsurface where no flow of brine nor CO_2 occurs across the boundary. This increases the reservoir pore pressure, because both the brine and the CO_2 are not able to escape. Due to the increase in pore pressure (P_{res}) the relative injection pressure (ΔP) decreases, which consequently results in a decrease of the injection rate, see equation (26).

3.3.2 Operating constraints

The main operating constraint is the bottomhole pressure (BHP) of the injector. Constraining the bottomhole pressure results into a limit on the relative injection pressure (ΔP) and therefore on the amount of CO_2 that can be injected.

For reservoirs at a depth between 800 and 1600 meters the maximum bottomhole pressure is based on the maximum acceptable formation pressure (leak-off pressures). For reservoirs at a depth between 1600 and 3000 meters the bottomhole pressure results from the tophole pressure and the gravitational pressure in the tubing.

The maximum bottomhole pressure is used to calculate the density of CO_2 at bottomhole conditions and the corresponding erosional velocity. This erosional velocity is set as a maximum injection rate (STG), to prevent erosion of the tubing. See sections 4.2.2 and 4.2.3 for a detailed methodology of the BHP and STG calculations.

3.4 Model assumptions

Several assumptions are made in order to simplify the model. The model simplification allows for better understanding of the effects of the sensitivity study.

The base case is a radial model. The reservoir porosity, temperature and rock-compressibility are assumed to be homogeneous. The permeability is anisotropic, such that the permeability in the k-direction is a 1/10 of the permeability in the horizontal direction. Moreover, one relative permeability and capillary curve is applied to the whole reservoir.

It is assumed that initially the pores are totally filled with brine which has a molarity of 0.5. The study only considers injection of pure supercritical CO_2, which corresponds to reservoir conditions (temperature and pressure) below 800 meters depth.

The injection of supercritical CO_2 takes place with one well in the center of the cylinder for 40 years. To simplify the model several processes are excluded. The excluded processes are water vaporization near the well and the corresponding effects of salt precipitation and permeability reduction. Moreover, geochemical reactions with minerals in the reservoir rock are excluded. Therefore mineralization, which is one of the four trapping mechanisms, is not taken into account. The other three trapping mechanisms, structural/stratigraphic, residual and solubility trapping are taken into account.

Table 5: Model simplifications.

Reservoir parameter	**Note**
Model	Radial
Temperature	Homogeneous
Rock-compressibility	Homogeneous
Porosity	Homogeneous
Permeability	Anisotropic
Relative permeability	Homogeneous
Capillary pressure	Homogeneous

Table 6: Process simplifications.

Process	**Note**
Water vaporization	Excluded
Salt precipitation	Excluded
Permeability reduction	Excluded
Thermal mode	Tested
Mineral trapping	Excluded
Structural / stratigraphic trapping	Included
Residual trapping	Included
Solubility trapping	Included

4 Methodology

4.1 Geolgic data

4.1.1 Geologic data collection

Geologic data from Lower Cretaceous, Late Jurassic, Triassic and Permian formations are collected to get an insight of the parameter range needed in the sensitivity study. The above mentioned formations are chosen because of their relative shallow depth and sandstone content. The collected data includes the porosity [-], permeability [mD], aquifer thickness [m] and top depth [m]. Because the quantity and quality of geologic aquifer data in the Dutch offshore is scarce, the data is collected from various sources and can be seen as a rough proxy, see table 7.

TNO Reservoir Properties and Coreplug Measurements Database
The coreplug measurements are a non-public database of EBN and TNO. It contains porosity and permeability measurements from onshore and offshore wells. It also includes the depth at which the porosity-permeability measurements are taken.

Permeability-porosity maps
Porosity and permeability well data from EBN and TNO is used to create permeability-porosity reservoir property maps. The maps are constructed with the well data, maximal burial depth and poroperm correlation.

ThermoGIS
ThermoGIS is an open source database developed by TNO to map the potential of geothermal energy in the Netherlands. The Mapviewer tool shows the depth, thickness, permeability and temperature of potential geothermal aquifers from different stratigraphic formations. A drawback of thermoGIS is that is shows only onshore data for formations which have a potential for geothermal energy, therefore not all selected formations for CO_2 storage can be found here.

Dinoloket
Dinoloket is an open source database which gathers subsurface information from the DINO and BRO (Basisregistratie Ondergrond) database. The lithological description, despositional setting, age, depth and geographical distribution can be found for many young to very old stratigraphic formations in the Netherlands.

Pressure SNS database
The Pressure SNS database is a non-public TNO database. It includes the the leak-off pressure from several formations in the Dutch offshore.

Table 7: Data source and type for the geologic parameters of the sensitivity study.

	Data source	Data type
Porosity	1. TNO Reservoir Properties Database (EBN) 2. Coreplug Measurements Database (EBN) 3. Permeability-porosity maps (EBN)	min, max
Permeability	1. TNO Reservoir Properties Database (EBN) 2. Coreplug Measurement Database (EBN) 3. Permeability-porosity maps (EBN) 4. Thermogis (P50)	min, max
Thickness	1. ThermoGIS (P50) 2. Dinoloket	min, max
Depth	1. ThermoGIS 2. Coreplug Measurement Database (EBN)	min, max
BHP	1. SNS Pressure and Temperature	leak-off pressure

4.1.2 Geologic data integration

In total 17 formations are identified as potential CO_2 storage formations from the lower Cretaceous, Late Jurassic, Triassic and Permian geologic age, see table 8. The collected data from these formations includes the minimum and maximum porosity [-], permeability [mD], net thickness [m] and depth [m]. The collected data for each formations can be found in appendix B.

The geologic data is used to set up a grouping system, which results into a several unique base cases. The base cases are used in the sensitivity study. Each base case has a unique combination of reservoir porosity, permeability and depth and corresponding sensitivity range. This grouping system ensures that all the potential storage formations are represented in the sensitivity study. The grouping system results into nine unique base cases and corresponding sensitivity ranges to ensure that all 17 formations are represented in the sensitivity study.

Table 8: Overview of the 17 formations of which geologic data is collected.

	code	**formation**		**code**	**formation**
1	KNGLG	Holland Greensand Member	10	RNSOB	Basal Solling Sandstone Member
2	KNNSL	De Lier Member	11	RBMH	Hardegsen Formation
3	KNNSY	Ijselmonde Sandstone Member	12	RBMDU	Upper Detfurth Sandstone Member
4	KNNSB	Berkel Sandstone Member	13	RBMDL	Lower Detfurth Sandstone Member
5	KNNSR	Rijswijk Member	14	RBMVU	Upper Volpriehausen Sandstone Member
6	KNNSF	Friesland Member	15	RBMVL	Lower Volpriehausen Sandstone Member
7	KNNSI	Rijn Member	16	ROSSL	Upper Slochteren Member
8	SLDND	Delft Sandstone Member	17	ROSLU	Lower Slochteren Member
9	SLDNA	Alblasserdam Member			

🟩	Lower Cretaceous	🟪	Triassic
🟦	Late Jurassic	🟥	Permian

4.2 Reservoir model

4.2.1 Initial conditions: reservoir temperature and pressure

The reservoir temperature and pressure are both dependent on the reservoir depth. The reservoir temperature is determined by a general geothermal gradient. The average temperature gradient is 31.2 °C/km with a surface temperature of 10.1 °C [5], this is simplified to equation (40).
A similar approach is taken for the reservoir pressure, which is determined with the hydrostatic gradient obtained from the SNS pressure and temperature dataset from EBN, see equation (41). Where P_{res} is the reservoir pressure [bar] and z the reservoir top depth [m]. The reservoir temperature and pressure are calculated with

$$T_{res} = 0.03 \times z_{top} + 10 \tag{40}$$

and

$$P_{res} = 0.112 \times z_{top}. \tag{41}$$

Both the reservoir temperature and reservoir pressure increase linearly with depth, see figure 7. For a reservoir depth of 800 to 3200 meters the temperature increases from 34 to 178 °C degrees. The pressure increases from 90 to 385 bar.

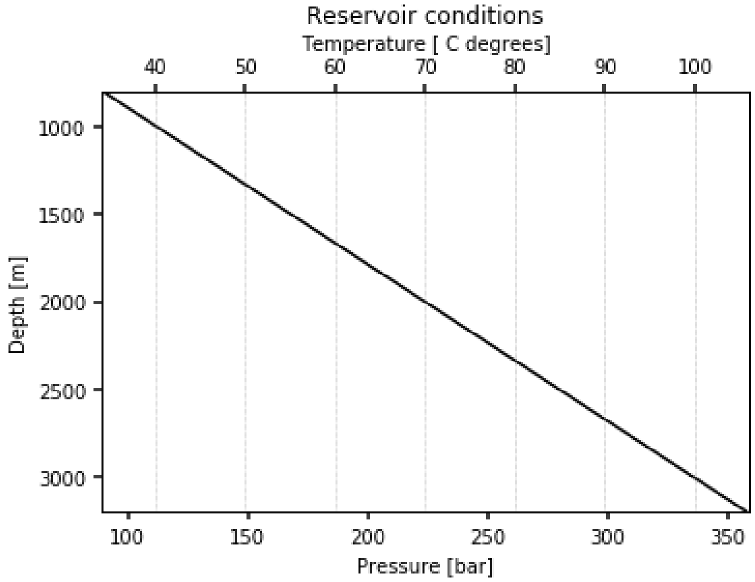

Figure 7: Reservoir pressure and temperature versus depth.

4.2.2 Operating constraint: BHP

The bottomhole pressure (BHP) is dependent on the aquifer depth and tophole conditions. In order to execute the sensitivity simulations at different depths, a corresponding BHP has to be implemented. The main BHP results from weight of the CO_2 column and the CO_2 compressibility For shallow depths an extra constraint on the BHP is set to take into account the strength of the rock. The maximum allowed bottomhole pressure is determined from the leak-off pressure (LOP) test. The LOP test is a pumping pressure test to asses the fracture strength of the rock. During the LOP test drilling mud is pumped into the borehole, which increases the pressure. At a certain point a pressure is reached at which the drilling mud is able to escape into the formation through the pressure-induced fractures, this point is called the leak-off pressure [48]. In order to inject the CO_2 safely, the BHP always has to remain below the LOP. The LOP data originates from offshore Lower Cretaceous, Late Jurassic, lower Triassic and Permian formations from the SNS pressure dataset from EBN. The datapoints which are used to construct the upper limit of the BHP can be found in appendix A.

For deeper depths the maximum allowed bottomhole pressure results from the pressure exerted by the CO_2 column itself. The CO_2 is compressed and is assumed to arrive at the platform at 90 bar at 5 ° C. The tophole pressure and temperature define the tophole density (ρ_1). The CO_2 density is variable with temperature and pressure, which has to be taken into account during the calculation of the bottomhole pressure. Therefore, it is not accurate to calculate the pressure exerted by the CO_2 column with only one value for the density. A constant injection temperature of 35 °C is assumed in the calculation. However, for every increasing depth the pressure increases due to the column weight, which changes the density of the CO_2 at that depth. Therefore, the the BHP is calculated consecutive to take into account the changing CO_2 density with pressure resulting from the CO_2 column itself, see figure 8 and the corresponding equations

$$P_{BHP1} = P_{THP} + \frac{\rho_1 + \rho_2}{2}\, g\, h_1 \tag{42}$$

and

$$P_{BHP2} = P_{BHP1} + \rho_3\, g\, h_2. \tag{43}$$

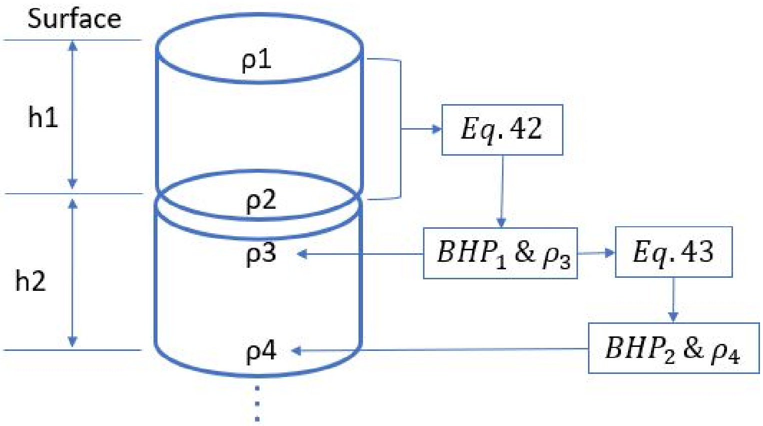

Figure 8: Graphic representation of the bottomhole pressure calculation.

The bottomhole pressure and the reservoir pressure are used to calculate the relative injection pressure with

$$P_{inj} = P_{BHP} - P_{res}. \tag{44}$$

4.2.3 Operating constraint: STG

In the hydrocarbon industry a velocity constraint is frequently applied during injection in order to limit erosion of the equipment. This means that the flow is restricted to the 'erosional velocity', under which no erosion occurs [22]. Due to its simplicity the API RP 14E equation is often used to estimate the erosional velocity, see equation (45). With the erosional velocity the maximum allowed injection rate set as an operating constraint can be calculated with

$$V_{erosion} = \frac{C}{\sqrt{\rho_{CO_2}}} = \frac{350}{\sqrt{\rho_{CO_2}}} \tag{45}$$

and

$$Q_{STG} = \frac{C A_{tubing}}{\sqrt{\rho_{CO_2}}} = \frac{350 A_{tubing}}{\sqrt{\rho_{CO_2}}}. \tag{46}$$

It must be noted that a correct empirical C factor has to be applied for specific circumstances and the erosive nature of the fluids. The recommended C factor of a solid-free fluid lies between 150 and 200 for a continuous operation and 250 for an intermittent operation [47]. An optimised calculation for UGS (underground gas storage) reports a C factor of 275 when the fluid is in gas phase [46]. However, the completion design from TAQA for the Porthos project, which is investigating CO_2 storage into a depleted gas reservoir near the port of Rotterdam, reports higher C values. The completion design with corrosion resistant alloys, solid-free CO_2 stream, smooth well trajectory and the presence of supercritical phase reports a C factor of 350 for supercritical CO_2 [39].

4.3 Preliminary sensitivity study

A preliminary sensitivity study is executed on the relative permeability curve and on the thermal mode, see table 9. This is done in order to give more insight in how significant input parameters are on the injection rate. If the effect of these two parameters are minimal, they can be disregarded in the geologic parameter sensitivity study. Both preliminary sensitivity studies are only executed on base case 2.

Table 9: Overview of the preliminary sensitivity study.

Preliminary sensitivity study		
	Relative permeability curve	**Thermal mode** **CO_2 temperature: 35 °C**
Group	2	2
Test 1	Capillary number	Depth: 1200 & 3000 meters
Test 2	Wettability	Permeability: 10 and 1E+03 mD

4.3.1 Relative permeability

Testing the effect of the relative permeability curve on the injection rate is executed by varying the capillary number and the wettability of the relative permeability curve. The interfacial tension, the viscosity and the Darcy velocity determine the dimensionless capillary number, where increasing the viscosity or decreasing the interfacial tension result into a higher capillary number [19].
In a two-phase system, the capillary number only has an effect on the shape of the relative permeability curve. For high capillary numbers ($N_{cap} >> 10^{-6}$) the shape is linear, whereas for low capillary numbers ($N_{cap} << 10^{-6}$) the shape is curved. For CO_2 storage the capillary number is generally $N_{cap} << 10^{-6}$ [19].
The wettability of a rock is defined as the tendency of a fluid to spread on the rocks surface in presence of another fluid. In general the relative permeability of a phase decreases with increasing rock wettability, because the phase clings onto the rocks surface [19].

The dataset by Chen *et al.* (2014) is used to study the effect of the relative permeability curve on the injection rate. The Chen *et al.* (2014) dataset can be found tabulated in appendix A. The experimental study executes four cycles (primary and secondary drainage and imbibition) and determines the relative permeability curve using the pressure drop of five independent rock sections and corresponding flow rate (Darcy's law). The experiment is performed on a Berea sandstone, which is commonly used due to its homogeneity and uniformity [9]. The sample has a porosity of 0.1346 and a permeability of 49 mD. The experiment is carried out at a temperature of 20 °C degrees and at a pressure of 10.3 MPa.

The experimental data is fitted with the Corey equations [9], which are two empirical functions that are often used because of their reasonably good fit with experimental data [3], see equation (32) and (33). The Chen *et al.* (2014) dataset is used as the base case. The Corey equations are used to construct curves for a higher and lower capillary number than the base case (see figure 9). The same is done for a stronger and weaker wetting case (see figure 10).

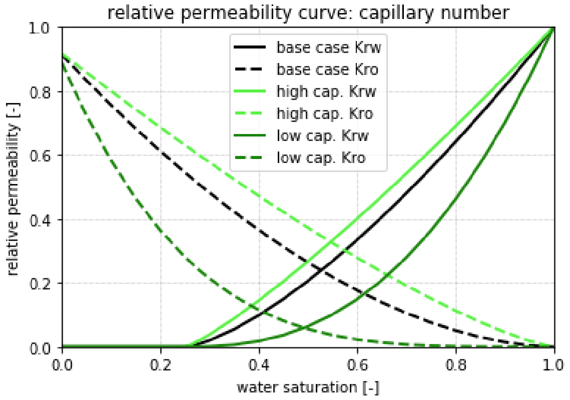

Figure 9: Relative permeability curve for a high and a low capillary number compared to the base case.

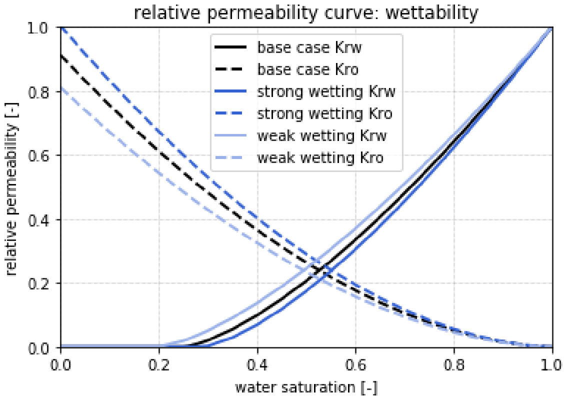

Figure 10: Relative permeability for a strong and a weak wetting rock compared to the base case.

4.3.2 Thermal mode

The thermal mode takes into account the temperature of the injected CO_2 into the warmer reservoir. In this preliminary sensitivity study an injection temperature of 35 degrees °C is assumed. Because the difference between the injected CO_2 temperature and reservoir temperature increases with depth, the thermal mode is tested for two depth cases, 1200 and 3000 meters. Moreover, the flow of the cold CO_2 depend on the permeability in the reservoir, therefore two permeabilities are tested: 10 and 1E+03 mD.

4.4 Sensitivity study

The impact on the storage capacity [Mt] and injection rate [sm^3/day] for varying aquifer top depth z [m], porosity φ [-], permeability k [mD], reservoir thickness h [m] and radius r [km] are obtained from a sensitivity study on a 2D radial model. An overview of simulations is listed in table 10 and 11. Moreover, as an example the input parameters for group 2 are listed in table 50. The input parameters for the remaining eight groups groups can be found in appendix A.

Table 10: Overview of the input parameters for the nine base cases in the sensitivity study.

Sensitivity study					
Group	φ **[-]**	**k [mD]**	**Depth [m]**	**Thickness [m]**	**Size [km]**
	base case	**base case**	**base case**	**base case**	**base case**
1	0.2	10	1800	100	2
2	0.2	100	1800	100	2
3	0.2	500	1800	100	2
4	0.1	50	1800	100	2
5	0.1	10	1800	100	2
6	0.1	100	3000	100	2
7	0.1	50	3000	100	2
8	0.2	500	3000	100	2
9	0.2	50	3000	100	2

Table 11: Overview of sensitivity range for the nine base cases in the sensitivity study.

Sensitivity study					
Group	φ **[-]**	**k [mD]**	**Depth [m]**	**Thickness [m]**	**Size [km]**
	range	**range**	**range**	**range**	**range**
1	0.05 - 0.40	1 - 100	800 - 3000	20 - 200	0.05 - 1000
2	0.05 - 0.40	1 - 1E+04	800 - 3000	20 - 200	0.05 - 1000
3	0.05 - 0.40	1 - 1E+05	800 - 3000	20 - 200	0.05 - 1000
4	0.05 - 0.25	1 - 1E+03	800 - 3000	20 - 200	0.05 - 1000
5	0.05 - 0.25	1 - 100	800 - 3000	20 - 200	0.05 - 1000
6	0.05 - 0.25	1 - 1E+04	800 - 3200	20 - 200	0.05 - 1000
7	0.05 - 0.25	1 - 1E+03	800 - 3200	20 - 200	0.05 - 1000
8	0.05 - 0.40	1 - 1E+05	800 - 3200	20 - 200	0.05 - 1000
9	0.05 - 0.40	1 - 1E+03	800 - 3200	20 - 200	0.05 - 1000

Table 12: Detailed overview of parameter input of group 2.

Group 2						
Parameter	**Base case**	**Sensitivity**	**Parameter**	**Base case**	**Parameter**	**Base case**
Depth [m]	1800	800-3000	STG [sm^3/day]	4.24E+06	S_{hys} [-]	0.4
$\varphi[-]$	0.2	0.05-0.40	BHP [bar]	235	Salinity [M]	0.5
k_{ij} [mD]	100	1-1E+03	P_{res} [bar]	202	k_k [mD]	k_{ij} / 10
h [m]	100	20 - 250	T_{res} [C]	64	t_{inj} [y]	40
r [km]	2	1 - 1000	T_{inj} [C] ^{*a}	35	Z_{por} [1/kPa]	1.04E-04

*a: Only for thermal option turned on

4.4.1 Relative permeability and capillary curve

For the sensitivity study of the aquifer parameters the relative permeability curve and capillary curve from Ershadnia *et al.* (2021) are used. This study evaluates the trapping and the dynamics of the CO_2 plume in a heterogeneous fluvial system by making use of facies-dependent relative permeability and capillary curves. The curves from Ershadnia *et al.* (2021) are used so that future studies can integrate the heterogeneity model created by Ershadnia *et al.* (2021). The capillary pressure curve is fitted by the Brooks-Corey equation, see equation (35). The fitting parameters for the Corey and Brooks-Corey equations are tabulated in appendix A.

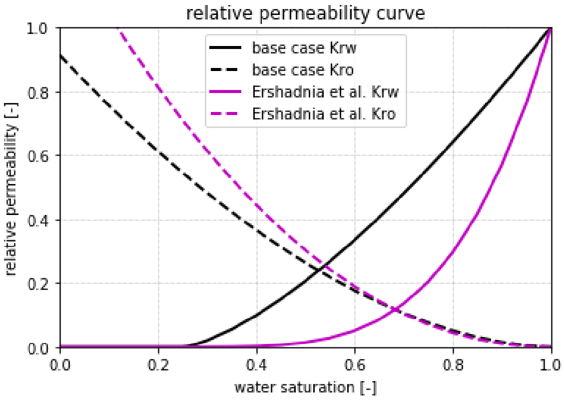

Figure 11: Two relative permeability curves used as a base cases in the relative permeability and aquifer parameter sensitivity study.

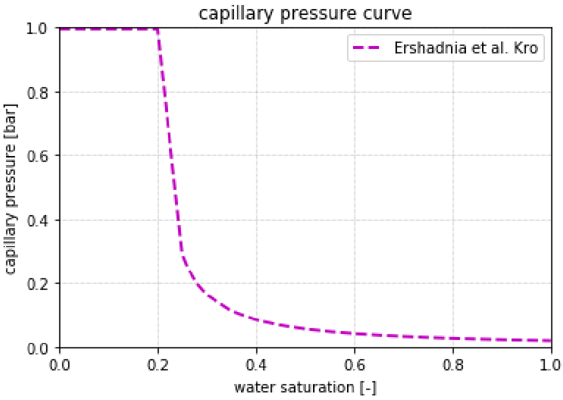

Figure 12: Capillary curve from Ershadnia *et al.* (2021) is used in the sensitivity study.

4.4.2 Efficiency factor

The result of the sensitivity study will be quantified by studying the effect of the reservoir parameters on the efficiency factor (E). The simple USDOE (2007b) storage capacity formula, see equation (1), can be rewritten to equation (47). In this equation the efficiency factor multiplied by the density of the CO_2 results from the ratio of the stored CO_2 (M_{CO_2}) to the reservoir pore volume (V_p), i.e.

$$M_{CO_2} = E * \rho_{CO_2} * \varphi * h * A = E * \rho_{CO_2} * V_p \tag{1}$$

which can be rewritten as

$$E\,\rho_{CO_2} = \frac{M_{CO_2}}{\varphi * h * A} = \frac{M_{CO_2}}{V_p}. \tag{47}$$

The formula can be simplified due to the fact that the density of the CO_2 remains relatively constant under reservoir conditions when increasing the depth from 800 to 3200 meters, see figure 2. The relatively constant CO_2 density over depth results from the combination of the geothermal and pressure gradient. Because of the relatively constant CO_2 density, the results from the sensitivity study can be quantified on the basis of the efficiency factor E.

When calculating the mass of CO_2 with the rule-of-thumb, both for volume limited and rate limited storage capacities, for simplicity it can be assumed that the density of the CO_2 is 695.4 kg/m^3. There the efficiency factor can be calculated with

$$E = \frac{M_{CO_2}}{\rho_{CO_2} * \varphi * h * A} = \frac{M_{CO_2}}{\rho_{CO_2} * V_p}. \tag{48}$$

4.5 Case study

4.5.1 Example aquifers Dutch offshore

The feasibility study of large scale CO_2 storage by TNO in 2021 [17] identified five saline formation which are considered to be the best candidates of the Early Cretaceous sandstone. TNO (2021) estimated the pore volume of these five saline formations, which is very useful for application of this study.

TNO (2012) did not estimate the storage potential. Therefore, the storage potential obtained by the rule-of-thumb from this study will be compared to the volumetric calculation TNO has used in their screening on high-capacity CO_2 storage sites in 2012 [28]. Their calculation is similar to equation (1), with an efficiency factor of E=2%. The input parameters that are used to estimate the storage capacity of the potential CO_2 storage formations are given in table 13. These parameters are based on the table provided by TNO in their 2021 report: *Table 2-1: Summary of features and properties of offshore CO_2 storage locations considered in this study*. The efficiency factor is calculated with

$$M_{CO_2} = E * \rho_{CO_2} * \varphi * h * A = E * \rho_{CO_2} * V_p. \tag{1}$$

Table 13: Input parameters which are used to estimate the storage capacity with the rule-of-thumb from this study. The data is based on the table from the TNO (2021) report, which contains features and properties of offshore CO_2 storage locations considered in their study.

	z [m]	**φ [-]**	**k [mD]**	**L [km]**	**W [km]**	**h [m]**	**V_p [m^3]**
Offshore Vlieland	1900	0.25	1000	51	51	21	5.62E+09
P18 North KN	2425	0.25	1000	12	12	130	7.80E+08
P18 South KN	2435	0.25	1000	13	13	130	8.45E+08
P18-04 dome	2163	0.25	1000	4	4	130	2.60E+08
P18-02 dome	2200	0.25	1000	4	4	130	2.60E+08

4.5.2 Mt. Simon

The Mt. Simon sandstone reservoir is located in the Illinois Basin, America. It is commonly used for natural gas storage, due to its good permeability and porosity. However, it also considered for CO_2 storage in saline formations.

The storage capacity of the Mt. Simon saline formation has previously been published by the National Energy Technology laboratoy (NETL), Birkholzer (2008) and Szulcsewsk *et al.* (2012). The NETL and Szulcsewsk *et al.* (2012) calculate the storage capacity with a migration limited method. This method models includes CO_2 migration due to the aquifer slope and static head gradient. Moreover, it includes residual and solubility trapping [38].

Another method is applied to estimate the storage capacity of the Mt. Simon saline formation by Birkholzer (2008) and Sculczewski *et al.* (2012). They estimate the storage capacity with a pressure limited method [4, 38]. This method calculates the total amount of CO_2 that can be injection over a time duration without causing tensile fractures in the caprock.

The published storage capacities will be compared with the storage capacity obtained with the rule-of-thumb from this study. The input parameters for the calculation of the storage capacity with the rule-of-thumb can be found in table 14. The input parameters are based on the data provided in the Birkholzer (2008) study.

Table 14: Input parameters to estimated the storage capacity with the rule-of-thumb. The input parameters are based on the data provided in the Birkholzer (2008) study.

	z [m]	**φ [-]**	**k [mD]**	**V_p [m^3]**
Mt. Simon	1600	0.20	100	1.5E+12

5 Results

5.0.1 Base case and sensitivity range

In most studies only one base case is chosen when investigating the sensitivity of geologic parameters on the storage capacity. However, the acquired geologic data shows a wide range in porosity, permeability and depth between the 17 considered CO_2 storage formations. Therefore a grouping system is applied in order to cover all unique combinations. This ensures that there is a representative base case for every formation with a corresponding sensitivity range.

The thickness of the considered formations all vary between 20 and 250 meter thickness. Therefore the grouping system is not taking into account the thickness, instead all base cases have an aquifer thickness of 100 meters.
For the porosity two main ranges are distinguished, from 5% to 25% and from 5% to 40%. The corresponding base case porosity values are 10% and 20%.
For the permeability four ranges are distinguished, from 1 mD to 100, 1E+03, 1E+04 and 1E+05 mD. The corresponding base case permeability values are 10, 50, 100 and 500 mD.
Last, for the aquifer top depth two ranges are distinguished. From 500 to 3000 meters and from 500 to 5600 meters. The corresponding base cases for the aquifer top depth are 1800 and 3000 meters.
The lower limit of the sensitivity range is set at 800 meters, because the CO_2 will be in gas phase at depths shallower than 800 meters. The upper limit is set a 3200 meters, because the bottomhole pressure (BHP) intersects with the hydrostatic reservoir pressure at this depth (see section 5.0.2). With the assumptions made in this study, injection after this depth is not possible because the relative injection pressure reaches zero. With the above mentioned parameters, nine unique groups are obtained from the geologic data, see figure 13. Each group has a unique base case and corresponding sensitivity range.

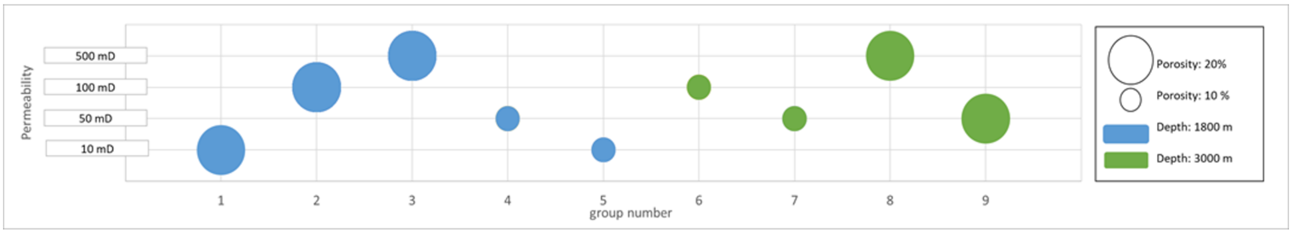

Figure 13: Base case of nine unique groups representing the considered geologic formations in this study.

5.0.2 Operating constraints: BHP and STG

Both the bottomhole pressure (BHP) and the maximum surface gas rate (STG) are taken to be a function of the reservoir depth. In order to execute the sensitivity simulations at different depths, the corresponding BHP and STG have to be implemented. First the bottomhole pressure will be explained, followed by the maximum allowed injection rate.

The BHP is either determined by the leak-off pressure or by the density of the CO_2 column. To determine the maximum allowed bottomhole pressure from the leak-off pressure, a fitted curve is constructed from the leak-off pressure data as a function of depth, see appendix B.
The bottomhole pressure is calculated with the fitted curve from the CO_2 density in the well, which is also a function of depth due to increasing weight of the CO_2 column.

The BHP is taken equal to the maximum allowed pressure, which is depending on the depth, either determined by the leak-off pressure (LOP) or by the pressure exerted by the CO_2 column, see figure 14. The intersection between the LOP and the pressure from the CO_2 column is located at 1600 meters depth. Therefore, aquifers located shallower than 1600 meters have a BHP determined by the leak-off pressure. Whereas, aquifers located deeper than 1600 meters depth have a BHP determined by the pressure exerted by the CO_2 column.

Moreover, with a tophole condition of 90 bar, the largest relative injection pressure (ΔP) occurs at 1600 meters. At this depth the LOP and the pressure from the CO_2 column intersect, see figure 14.

The hydrostatic pressure and the BHP (from the CO_2 column) cross at 3200 meters depth, which means that the relative injection pressure is zero at this intersection. Because a positive relative injection pressure is necessary in order to inject CO_2 into the subsurface, the intersection indicates that with a tophole pressure of 90 bar, CO_2 cannot be injected at depths greater than approximately 3200 meters.

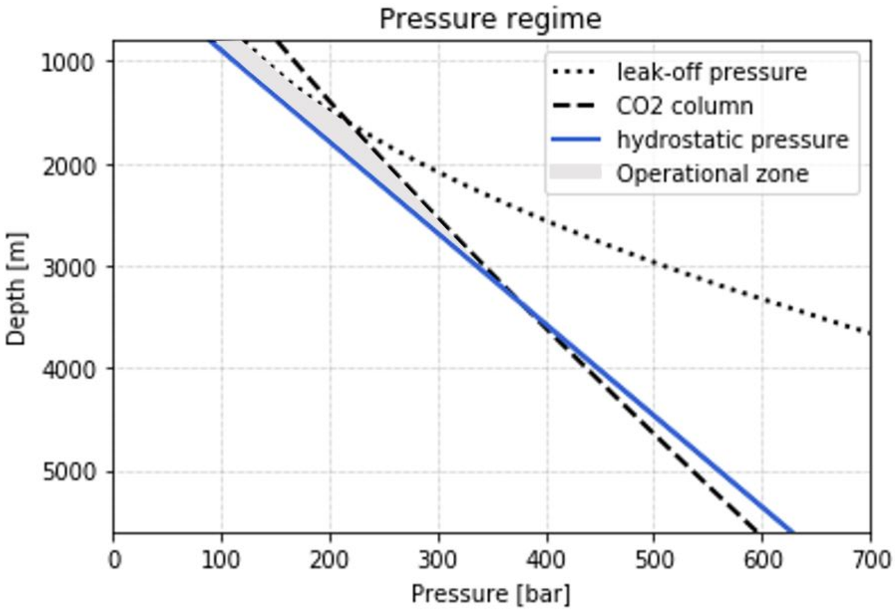

Figure 14: Hydrostatic reservoir pressure versus bottomhole pressure resulting from the leak-off pressure and the pressure exerted by the CO_2 column. The grey area depicts the possible operating window under the assumptions in this study.

Table 15: The bottomhole pressure and the maximum gas rate per reservoir depth.

Depth [m]	**BHP leak-off [bar]**	**BHP CO column [bar]**	**Reservoir pressure [bar]**	**ΔP bar**	**STG [sm^3/day]**
800	121	-	90	31	4.56E+06
1000	140	-	112	28	4.47E+06
1200	163	-	134	29	4.39E+06
1400	188	-	157	31	4.33E+06
1600	217	-	179	38	4.27E+06
1800	-	235	202	33	4.24E+06
2000	-	253	224	29	4.21E+06
2200	-	270	246	24	4.19E+06
2400	-	288	269	19	4.16E+06
2600	-	306	291	15	4.14E+06
2800	-	325	314	11	4.13E+06
3000	-	343	336	7	4.11E+06
3200	-	362	358	3	4.09E+06

The values in table 15 are used to construct several functions to determine the relative injection pressure and the maximum gas rate from the reservoir depth. The relative injection pressure is the difference between the BHP and the reservoir pressure. Depending on the reservoir depth, the BHP is either determined by the leak-off pressure or the CO_2 column, see equations (49) and (51). The relative injection pressure is approximated with a linear fit valid for a depth between 800 and 3200 meters, i.e,

$$\Delta p_{leak-off} = p_{BHP_{leak-off}} - P_{res} \tag{49}$$

if

$$800 < z <= 1600 : \ \Delta P_{leak-off} = -0.12z + 22.09 \tag{50}$$

and

$$\Delta p_{CO_2} = p_{BHP_{CO_2}} - P_{res} \tag{51}$$

if

$$1600 < z <= 3200 : \ \Delta P_{CO_2} = -0.0242z + 78.553 \tag{52}$$

The maximum allowed injection rate (STG) is a function of CO_2 density in the well. In this study the CO_2 density in the well results from the tophole pressure (THP), the bottomhole pressure (BHP) and the temperature in the well, which is assumed to be 35 ° C. The BHP is a function of depth, and consequently the CO_2 density and maximum injection rate as well.
To estimate the maximum allowed injection rate as a function of depth, a linear fit is constructed from the points in table 15. The figures of the fitted curves can be found in appendix B. The maximum injection rate at any reservoir depth between 800 and 3200 meters can be expressed as function of depth, i.e,

$$Q_{STG} = 0.0825z^2 - 520.14z + \ 5E{+}06 \tag{53}$$

The unit of the maximum allowed injection rate of the above mentioned equations is m^3/day. For simplicity, the maximum allowed injection rate can also be expressed in Mt/y. Which can be calculated with

$$Q_{STG} = 6E\text{-}08\ z^2 - 0.0004z + 3.54. \tag{54}$$

However, it must be noted that this equation only holds for the well conditions set in this study. The maximum allowed gas rate is a function of CO_2 density in the well. Which, in this study is a results of the tophole pressure (THP), the bottomhole pressure (BHP) and the temperature in the well, which is assumed to be 35 ° C. Therefore, if the the well conditions in a project are significantly different from this study, this equation might not be the best approximation of the maximum allowed injection rate. In that case, it is best to approximate the maximum allowed injection rate directly from the density of the CO_2 from the well conditions, i,e,

$$Q_{STG} = \frac{CA_{tubing}}{\sqrt{\rho_{CO_2}}} = \frac{350A_{tubing}}{\sqrt{\rho_{CO_2}}} \tag{46}$$

5.1 Preliminary sensitivity study

5.1.1 Relative permeability

The preliminary sensitivity study of the relative permeability curve is tested on group 2. Changing the capillary number and wettability of the relative permeability curve affects the injection rate, see figure 15. The relative permeability curve for a low capillary number results into a lower injection rate compared to the base case. The injection rate of the other three cases, weak wetting, strong wetting and a high capillary number, result into a higher injection rate compared to the base case.
For the case with a high capillary number, the effect is limited in the first seven years of injection by the maximum allowed gas rate, which is set an operating constraint, see figure 15.
Moreover, the effect of the relative permeability curve mostly takes place in the first 20 years of injection. After 20 years of injection, the effect of relative permeability curve on the injection rate seems to even out.

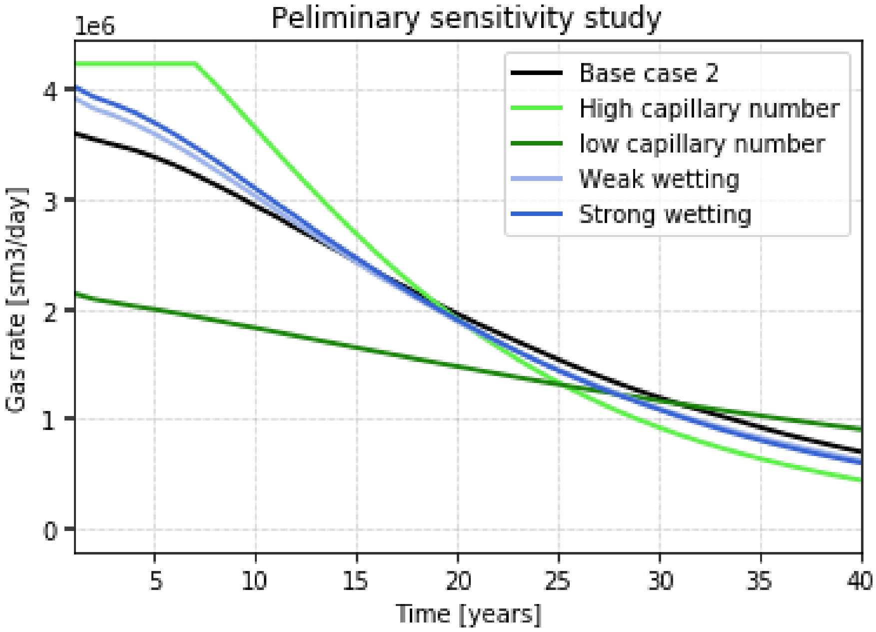

Figure 15: Effect of the relative permeability curve on the injection rate

Because the relative permeability curve with a high capillary number results into the largest positive effect on the injection rate, the high capillary number is also tested for a permeability of 1 mD. This is done to see the effect of the relative permeability curve if the reservoir permeability is low. The test case has a permeability of 1 mD, which is much smaller compared to the permeability of base case 2, which is 100 mD. All other input parameters are kept the same.
At 10 years of injection the relative permeability curve with a high capillary number results into 24.0% and 43.3% higher injection rate compared to the base case, for 100 mD and 1 mD respectively.
At 40 years of injection the relative permeability curve with a high capillary number results into a 36.7% lower injection rate compared to the base case with a permeability of 100 mD. Whereas, the relative permeability curve with a high capillary number results into a 41.4% higher injection rate compared to the base case with a permeability 1 of mD. As can be seen in table 16 and figure 16.
So, considering 10 years of injection, the relative permeability curve can result into a higher injection rate for a reservoir with a low permeability, compared to a reservoir with a higher permeability. However, this difference in injection rate seems to even out with time.

Table 16: Effect of the relative permeability curve with a high capillary number tested for a permeability of 1 mD and 100 mD.

		t = 10 years		t = 40 years	
Test	**Permeability [mD]**	**Injection rate [sm^3/day]**	%	**Injection rate [sm^3/day]**	%
Base case 2	100	2.94E+06	-	7.02E+05	-
High capillary number	100	3.65E+06	24.0	4.45E+05	36.7
Base case 2*	1	3.85E+04	-	3.70E+04	-
High capillary number	1	5.52E+04	43.3	5.23E+04	41.4

* permeability of base case 2 is changed to 1 mD instead of 100 mD

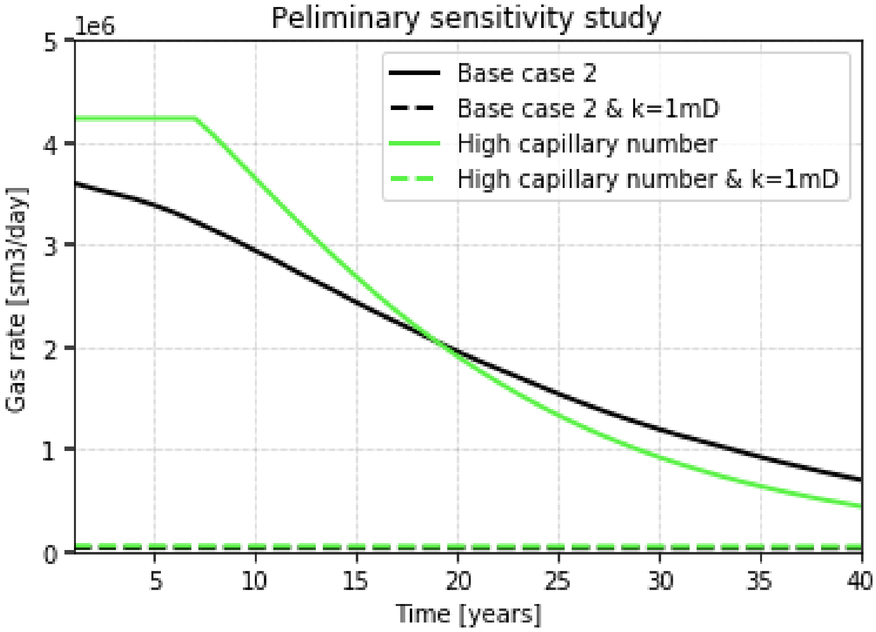

Figure 16: Effect of the relative permeability curve on the injection rate for a reservoir with a considerable low permeability of 1 mD

Even though the relative permeability does have an effect on the injection rate, all simulations in the sensitivity study are performed with only one relative permeability curve. This is mostly done because the sensitivity study already contains many runs. Adding the effect of the relative permeability curve would at least double the amount of runs, which will increase the running time significantly. However, it is good to take into account that the injection rate can be effected by the relative permeability curve that is used in the simulation, especially for shorter injection times.

5.1.2 Thermal mode

The thermal mode is tested on two different depths (1200 and 3000 m) and with two different permeabilities (10 and 1E+03 mD). Taking into account an injection temperature of 35 °C into a hotter reservoir, barely impacts the injection rate, see table 17. The injection rates are compared at 10 years of injection, and not at the usual 40 years of injection due to the early termination of these simulation. Termination of a simulation can occur due to the many timestep that the thermal mode requires, therefore longer simulation times can not be reached with the maximum number of timesteps set.

The simulation with a permeability of 10 mD result into a very small difference in injection rate for thermal mode on and thermal mode off. The difference is approximately 3%, where the higher injection rate is obtained for the simulation with the thermal mode off.

For a permeability of 1E+03 mD there is no difference in injection rate, due to constraint set on the maximum allowed injection rate.

For a depth of 1200 meters there is no difference in injection rate, whereas for a depth of 3000 meters the injection rate differs with 17%. These differences in injection rate with thermal mode on and off are considered insignificant. In combination with long computation times and early termination, all other simulations are performed without taking into account the thermal mode.

Table 17: Injection rate for thermal mode on and off.

	Injection rate [sm^3/day] at t = 10 years		
Test	**Thermal mode on**	**Thermal mode off**	%
Depth 1200 [m]	3.36E+06	3.36E+06	100
Depth 3000 [m]	8.36E+05	7.12E+05	117
Permeability 10 [mD]	6.92E+05	7.13E+05	97
Permeability 1E+03 [mD]	3.23E+06	3.23E+06	100

5.2 Sensitivity study

5.2.1 Base case

The base cases have a different injection rate during the 40 years of injection. Only two base cases, base case 1 and base case 5, can sustain the plateau rate for 40 years. In both cases the plateau rate is between 3.81E+05 and 3.88E+05 sm^3/day. After 40 years of injection this roughly result into a in-situ cumulative gas mass of 9.50 to 9.86 Mt.

The other base cases experience a decrease in injection rate over time. For these base cases the plateau rate lies between 3.07E+05 and 4.24E+06 sm^3/day. The plateau rate can only be sustained for a short amount of time, ranging between 2 to 20 years. Table 51 shows the plateau rate and plateau time for each base case.

Table 18: Plateau rate, plateau time and cumulative gas mass after 40 years of injection for all nine base cases.

Group	Plateau rate [sm^3/day]	Plateau time [years]	Cumulative gas mass t=40 years [Mt]	Volume or rate limited at t=40 years
1	3.88E+05	86	9.86	Rate limited
2	3.64E+06	10	56.86	Volume limited
3	4.24E+06	20	66.19	Volume limited
4	1.82E+06	10	28.45	Volume limited
5	3.81E+05	46	9.50	Rate limited
6	6.03E+05	5	5.79	Volume limited
7	3.07E+05	9	4.74	Volume limited
8	2.77E+06	2	12.82	Volume limited
9	3.13E+05	17	6.52	Volume limited

For the different base cases the injection rate develops different over time. For base case 3 the injection rate experiences a sharp decrease after 20 years of injecting at plateau rate, see figure 17. In the same figure, it can also be seen that base case 2 and 3 experience a much more steady decrease in injection rate. Whereas, the injection rate of base case 8 experiences an immediate sharp decrease, see figure 18.

Also, it must be noted that in figure 18 it appears that base case 7 and 9 inject at plateau rate. However, this results from the low injection rate compared to the scale. Both base cases have an inject rate which is approximately 5% to 7% compared to the first year of injection and are therefore volume limited, see 51.

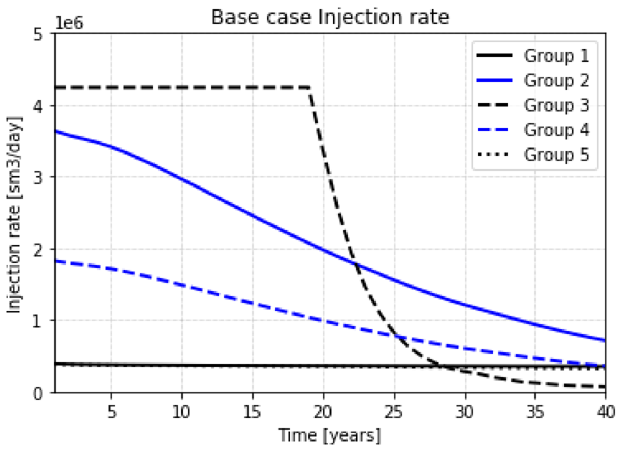

Figure 17: Injection rate for the base case of group number 1 to 5.

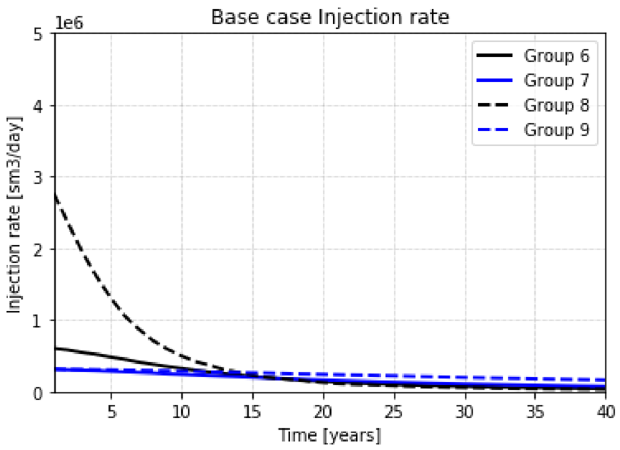

Figure 18: Injection rate for the case of group number 6 to 9.

Gas saturation

After injection the CO_2 migrates upwards due to buoyant forces resulting from the difference in density of the CO_2 and the brine. In combination with a no flow upper boundary, this results into the formation of a CO_2 plume. The evolution of the CO_2 plume for base case 1 and 2 can be seen in figure 19 to 22. In the figure the gas saturation is plotted. The green color represents brine, or a low CO_2 saturation. The red to yellow colour represents a high CO_2 saturation.

In base case 1 the CO_2 plume does not intrude very far from the well into the aquifer and no clear CO_2 plume forming can be seen. Whereas for base case 2 the CO_2 plume can clearly be seen, see figure 22. At 40 years of injection almost six times more CO_2 has been injected in base case 2 than in base case 1.

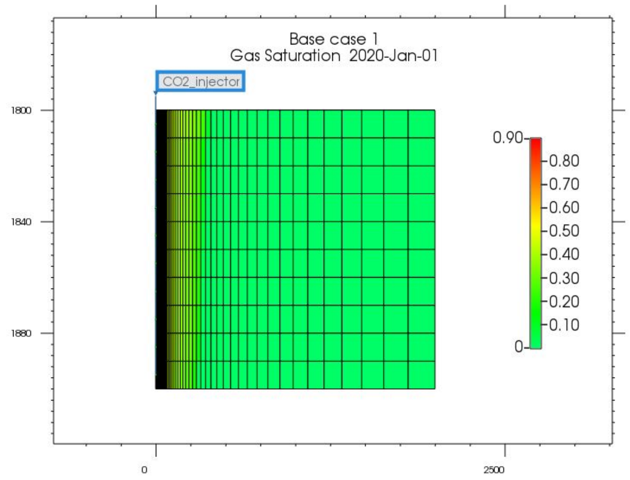

Figure 19: CO_2 plume evolution after 20 years of injection for base case 1.

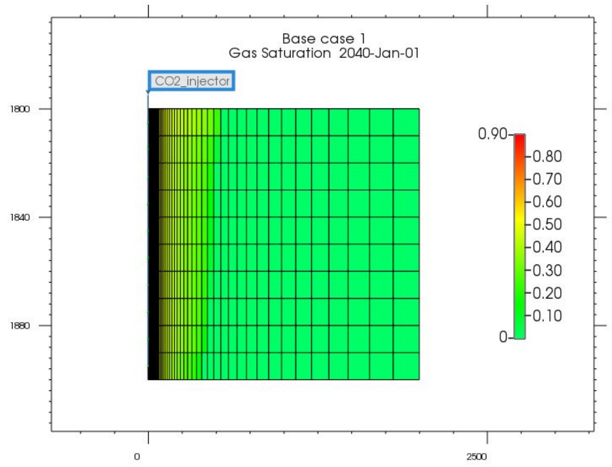

Figure 20: CO_2 plume evolution after 40 years of injection for base case 1.

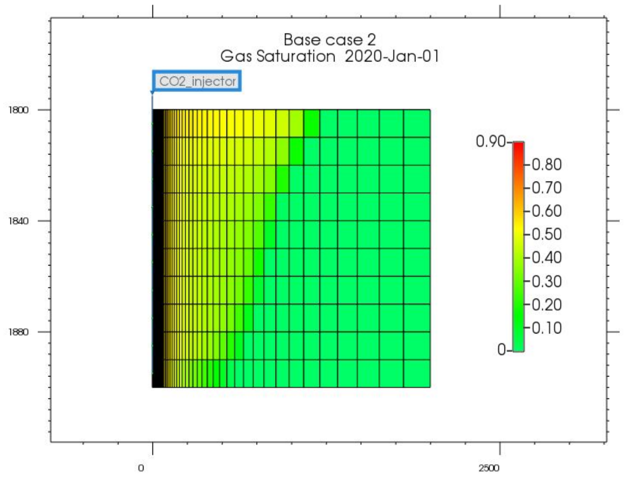

Figure 21: CO_2 plume evolution after 20 years of injection for base case 2.

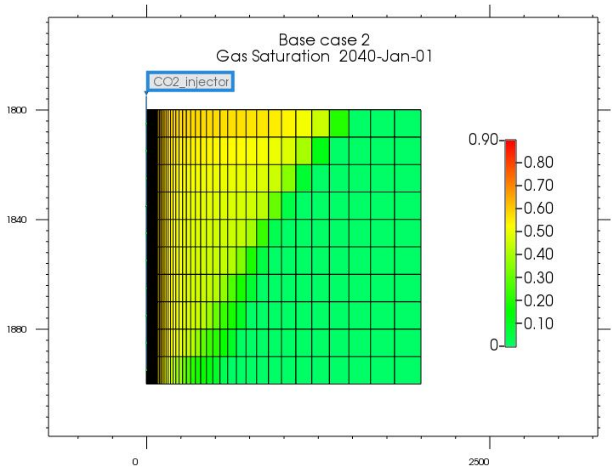

Figure 22: CO_2 plume evolution after 40 years of injection for base case 2.

Reservoir pressure and injection rate

The injection of the CO_2 in combination with the no-flow boundary can cause an increase in reservoir pressure. In base case 1 this increase in reservoir pressure is relatively small compared to the initial reservoir pressure, see figure 23. Whereas in base case 2 the increase in reservoir is significant compared the original reservoir pressure.

The BHP remains constant over time, therefore in base case 2 the relative injection pressure (ΔP) decreases over time. As a result the injection rate decreases as well. In base case 1 the relative injection pressure does not decrease over time, resulting into a constant injection rate. Figure 24 and 25 show a cross section of the reservoir pressure at 40 years of injection.

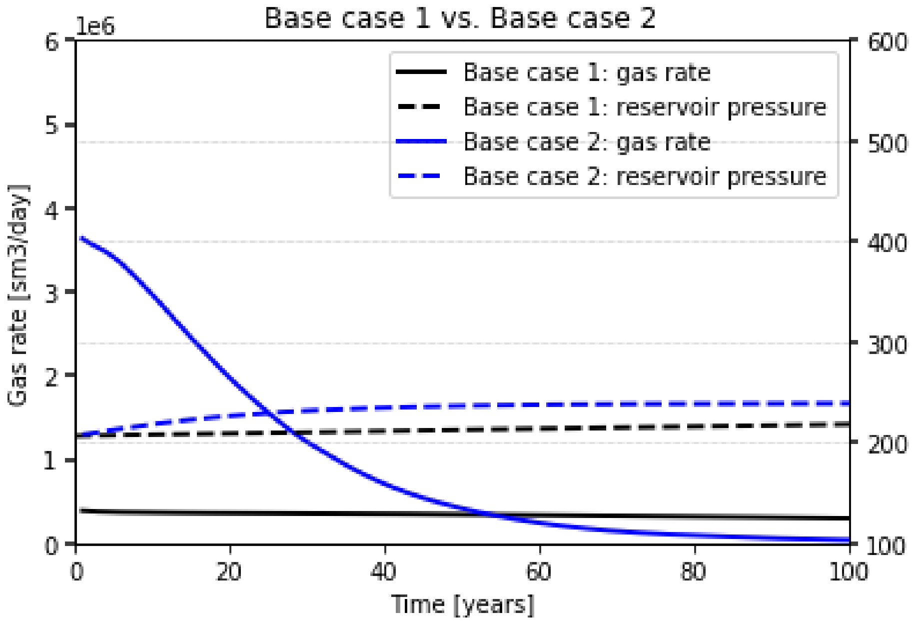

Figure 23: Injection rate and reservoir pressure for base case 1 and 2

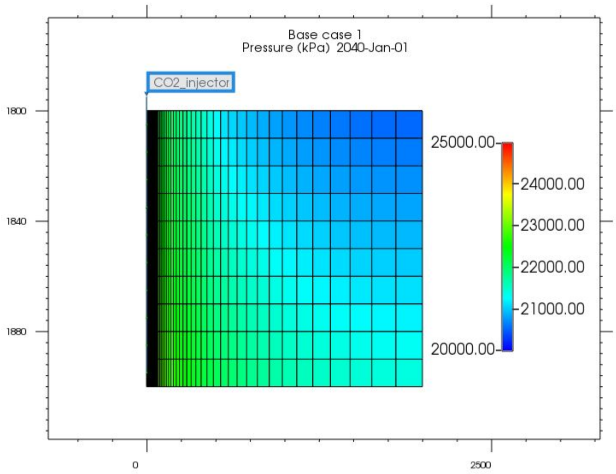

Figure 24: CO_2 plume evolution after 20 years of injection for base case 1.

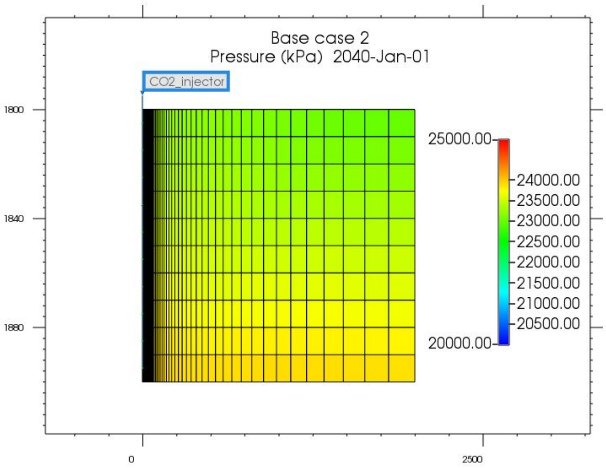

Figure 25: CO_2 plume evolution after 40 years of injection for base case 2.

5.2.2 Volume vs rate limited storage capacity

Estimation of the storage potential can be subdivided into three storage mechanism categories: volume limited storage capacity, rate limited storage capacity and something in between, which we call the transition zone. In figure 26 the three categories can be distinguished. This categorization is based on whether the pore volume or the injection rate is related to the mass of CO_2 that can be stored in a certain amount of time.

In the case of a volume limited storage capacity, the mass that can be stored is linearly related to the pore volume. The reservoir pressure increases significantly during CO_2 injection because of the limited amount of pore volume and the no-flow boundary. As the reservoir pressure increases, the relative injection pressure (ΔP) decreases because during injection a constant BHP is maintained. This results into a decrease in injection rate over time, see figure 5.2.2. A volume limited storage capacity can be estimated by a linear equation relating the storage capacity with the pore volume, including an storage efficiency factor E.

In the case of a rate limited storage capacity the pore volume is large enough for keeping the reservoir pressure constant during CO_2 injection. Since the BHP is maintained constant, the relative injection pressure remains constant, and therefore the injection can be sustained at a plateau rate. Rate limited storage capacity can not be estimated with a volumetric calculation, because the mass of CO_2 that can be stored is not related to the pore volume. However, the storage capacity is easily estimated by multiplying the plateau rate with the total time of injection.

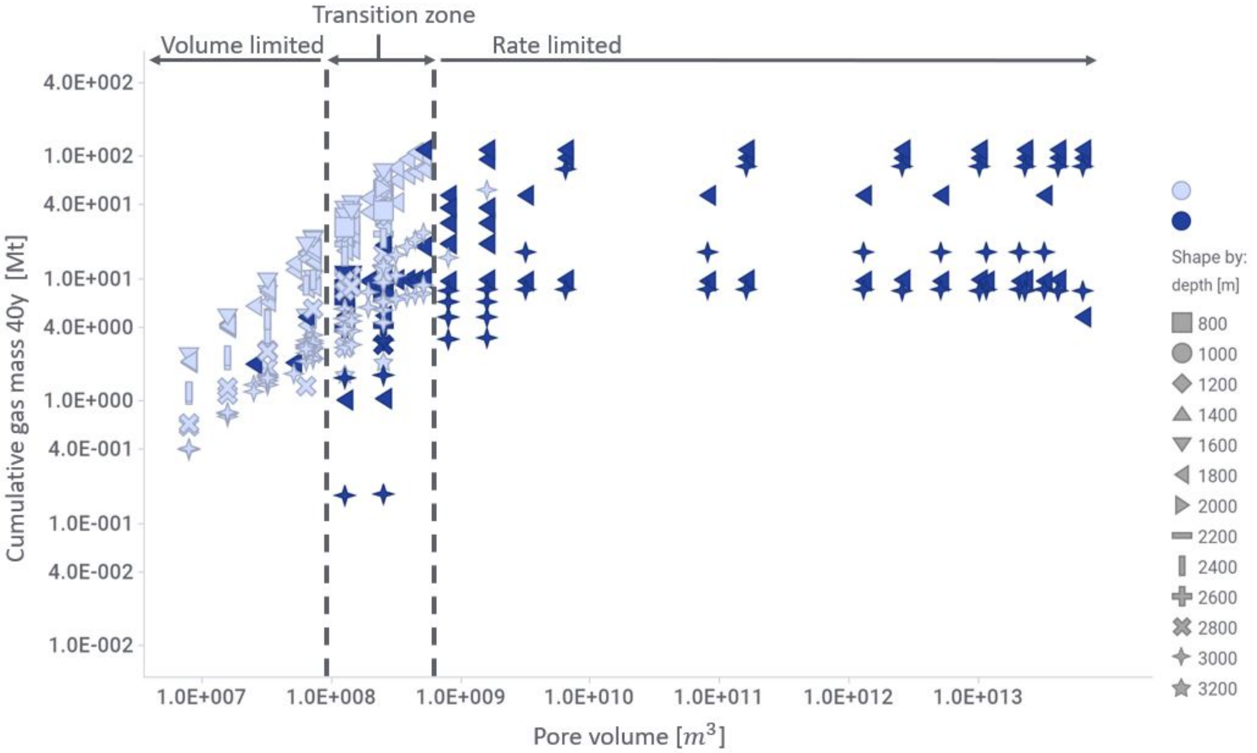

Figure 26: Mass of CO_2 injected versus pore volume at 40 years of injection. In this graph three storage mechanism categories can be distinguished.

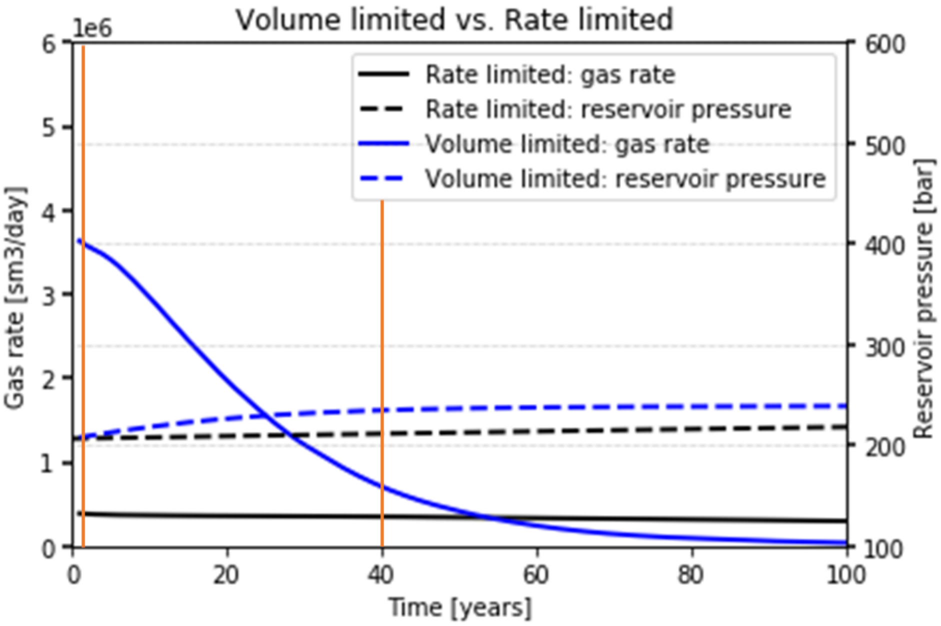

Figure 27: Gas rate and average reservoir pressure for a volume limited and rate limited storage capacity.

Since the volume limited and rate limited storage capacity estimations are related to different attributes, a rule-of-thumb should be investigated for both storage mechanism categories. Therefore, it is important to select the appropriate sensitivity runs that fall either under the volume limited or rate limited category when constructing the rule-of-thumb. In order to categorize the sensitivity runs into the volume limited or rate limited category, a proper definition of volume limited and rate limited category is needed. For this study, the boundary was arbitrarily set as follows: the injection rate at 40 years is compared to the first year of injection, see figure 19 . If the injection rate at 40 years is 20% lower than the injection rate in the first year, the storage potential is categorized as volume limited. The storage potential is categorized as rate limited, if the injection rate decreased with less than 20%.

Between the volume and rate limited storage capacity the transition zone is present. The transition zone is a range in pore volume where the storage capacity is not pure volume or pure rate limited. Instead, an aquifer with a pore volume that falls within the transition zone slowly starts to feel the boundary of the reservoir. Therefore, the storage capacity is transitioning from rate to volume limited. The simulation results that are transitioning are nonetheless categorized as either volume or rate limited based on their injection rate. Therefore, in figure 26 the transition zone exists of aquifers with either a volume or rate limited storage capacity.

With the method described above, where the injection rate defines whether a simulation is volume limited or rate limited, the pore volume at which an aquifer is pure volume limited, pure rate limited or in the transition zone can be distinguished, see table 19.

Table 19: Pore volume that defines whether the storage capacity is volume limited, rate limited or in the transition zone.

	Volume limited	**Transition zone**	**Rate limited**
Time [y]	**Pore volume [m^3]**	**Pore volume [m^3]**	**Pore volume [m^3]**
20	$Vp < 6.3E+07$	$6.3E+07 \leq Vp \leq 3.1E+08$	$Vp > 3.10E+08$
40	$Vp < 1.3E+08$	$1.3E+08 \leq Vp \leq 5.0E+08$	$Vp > 5.0E+08$
100	$Vp < 1.9E+08$	$1.9E+08 \leq Vp \leq 7.9E+08$	$Vp > 7.9E+08$

Of the total of 448 simulation, 114 results are categorized as clearly volume limited and 89 results as clearly rate limited (at time = 40 years). The remaining 245 results fall in the transition zone, of which 117 are categorized as volume limited and 68 are categorized as rate limited, see table 20.
An amount of pore volume can be categorized as pure volume or pure rate limited if not more than two outliers are present, which can be observed in figure 26. For instance, the pore volume of 6.3E+07 m^3 contains no more than two outliers, so therefore simulations with this pore volume belong to the volume limited category.
Simulation are categorized to fall in the transition zone if more than two outliers are present.

Table 20: Number of simulations per category. The transition zone is subdivided in points which are categorized as volume limited + rate limited.

Number of simulations			
Time [y]	**Pure volume limited**	**Pure rate limited**	**Transition zone**
20	73	103	193 + 98
40	116	89	177 + 68
100	169	72	83 + 23

6 Results: Volume limited storage capacity

For a volume limited storage capacity the pore volume of the reservoir is the limiting factor. Due to the relatively small pore volume and the no-flow boundary, the reservoir pressure increases. During injection a constant BHP will be maintained, therefore the relative injection pressure (ΔP) decreases and consequently the injection rate decreases over time. In the case of a volume limited storage capacity the pore volume is related to the mass of CO_2 that can be stored. Therefore, the storage capacity can be estimated with a volumetric calculation, which includes the efficiency factor E, stated as

$$M_{CO_2} = E * \rho_{CO_2} * V_p. \tag{1}$$

6.1 Efficiency factor

The efficiency factor (E) is quantified over a wide range of geologic and operational parameters at 40 years of injection. This allows for studying the effect of reservoir attributes on the efficiency factor and constructing a rule-of-thumb for the efficiency factor. The rule-of-thumb will help to select an appropriate efficiency factor when estimating the volume limited storage capacity of one or more aquifer(s). The following paragraphs will discus the effect of several reservoir characteristics.

6.1.1 Depth

In figure 28 it can be seen that the efficiency factor is significantly impacted by the reservoir depth, which is visualised by the symbols in the figure. The efficiency factors of several simulations with the same reservoir depth all cluster at a maximum efficiency factor. Every reservoir depth has a corresponding maximum achievable efficiency factor. The largest maximum efficiency factor of 0.45 is achieved at 1600 meters and the smallest maximum efficiency factor of 0.08 is achieved at 3000 meters. The other maximum efficiency factors for the remaining depths lie in between 0.08 and 0.45, see table 21.

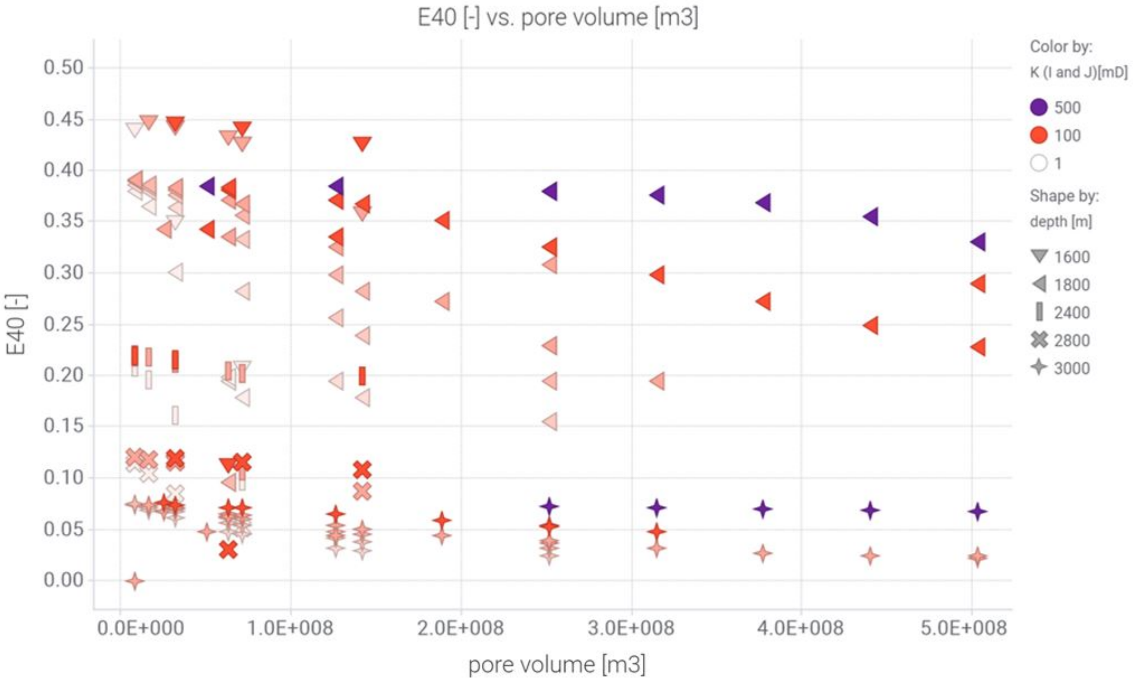

Figure 28: Effect of the reservoir depth on the efficiency factor. The color indicates the permeability and the symbol the depth.

The pore volume, which results from the reservoir thickness, radius and porosity, is plotted on the x-axis in figure 28 and the permeability is visualized by the colouring. So, in figure 28 all parameters that are tested in the sensitivity study are visualised. The first thing that can be noticed is that the main effect on the efficiency factor is the reservoir depth.

The main parameter that changes with reservoir depth is the relative injection pressure (ΔP). In this study the relative injection pressure results from the bottomhole pressure (BHP), which has been set as an operating constraint, and the reservoir pressure (P_{res}). The BHP and reservoir pressure have been theoretically constructed as a function of reservoir depth. Therefore, the relative injection pressure is also a function of reservoir depth. So even though it appears that the efficiency factor is mainly effected by the reservoir depth, the main driver behind this trend is the relative injection pressure, resulting from the BHP and reservoir pressure.

The largest efficiency factor of 0.45 at 1600 meters depth corresponds to the largest relative injection pressure obtained in this study. Also, the smallest efficiency factor of 0.08 at 3000 meters depth corresponds to the smallest relative injection pressure obtained in this study.

Table 21: Maximum achieved efficiency factor for various depths at 40 years of injection.

Depth [m]	1600	1800	2400	2800	3000
Maximum E [-]	0.45	0.39	0.22	0.12	0.08

6.1.2 Permeability

For volume limited storage capacity the pore volume is the (only) limiting factor. Therefore, the permeability of the reservoir does not influence the mass of CO_2 that can be stored. This means that with increasing the permeability the efficiency factor remains constant.
However, in figure 30 the efficiency factor it not constant, but converging with increasing permeability. The flow rate in the reservoir is relatively low for simulations with a low permeability, and therefore the pore volume is not limiting the mass of CO_2 that can be stored. The simulation with a low permeabilities are not pure volume limited and therefore experience an increase in injected CO_2 mass with increasing permeability, which consequently result into a higher efficiency factor, see figures 29 and 30.
However, the convergence of the efficiency factor shows that when simulations are pure volume limited, the permeability does not effect the efficiency factor. For volume limited storage, the pore volume is the (only) limiting factor. Therefore, increasing the permeability might result into faster flow rate in the reservoir, however the total mass of CO_2 that can be stored is limited by the pore volume.
The total mass of CO_2 that can stored and thereby the final efficiency factor are not influenced by the permeability. However, a higher permeability results into a higher injection rate in the reservoir. Therefore, the boundaries of the reservoir will be felt earlier in time. This means that the pore volume becomes limited earlier in time and changes into a volume limited storage capacity

Also, larger efficiency factors are achieved for reservoirs at 1800 meters depth compared to reservoirs at 3000 meters depth. As seen in the previous subchapter this results from the larger relative injection pressure at 1800 meter depth.

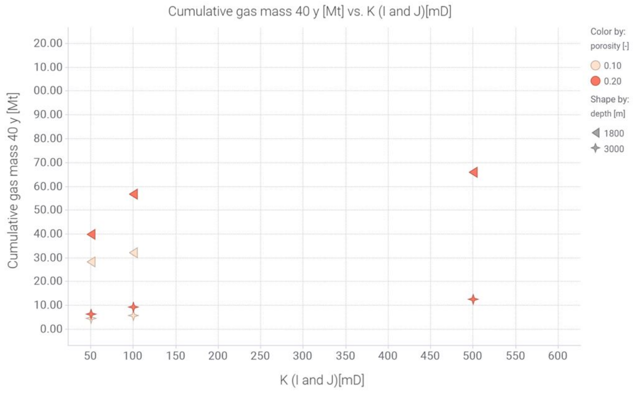

Figure 29: Effect of the reservoir permeability on the CO_2 mass stored.

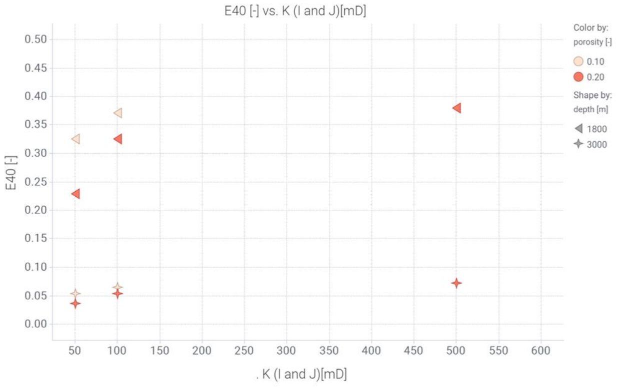

Figure 30: Effect of the reservoir permeability on the efficiency factor.

6.1.3 Thickness

The reservoir thickness does not influence the efficiency factor significantly, see figure 32. In the figure and in table 22 it can be seen that increasing the reservoir thickness from 20 tot 200 meters, results in a slight decrease in efficiency factor.

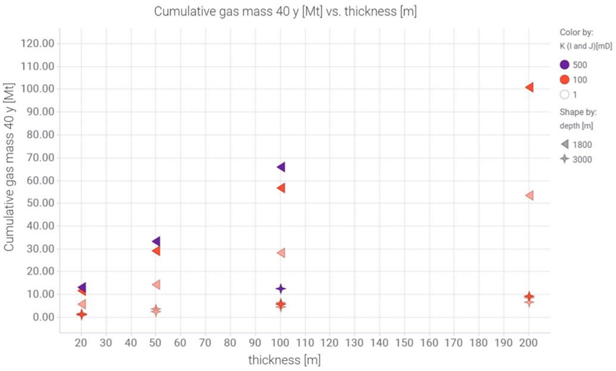

Figure 31: Effect of the reservoir thickness on the CO_2 mass stored.

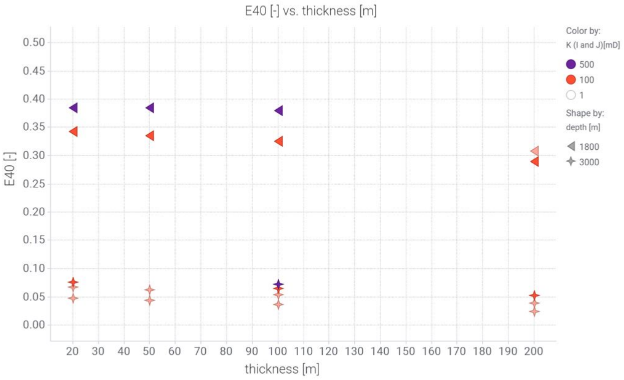

Figure 32: Effect of the reservoir thickness on the efficiency factor.

Table 22: Effect of the reservoir thickness on the efficiency factor at 40 years of injection at different depths.

k [mD]	**Depth [m]**	**h_{50m}**	**h_{100m}**
100	**1800**	E = 0.34	E = 0.33
100	**3000**	E = 0.063	E = 0.054

Note that this might seem counter intuitive, since increasing the thickness increases the pore volume, therefore a linear relationship could be expected. However, increasing the thickness also increases the rate in a linear fashion. Therefore, by increasing the thickness, the total amount of stored CO_2 will increase, see figure 31. However, the efficiency factor is not effected by the increase in reservoir thickness, see figure 32. The fact that E decreases slightly is due to secondary effects.

In equation (26) and (27) it can be seen that when doubling the reservoir thickness, the injection rate (Q) doubles as well. By doubling the injection rate, the injected CO_2 mass (M_{CO_2}) doubles. The doubling of both the reservoir thickness and the injected CO_2 mass cancels out when calculating the efficiency factor, such that

$$Q \propto kh\,\Delta P \tag{55}$$

and

$$2Q \propto k\, *\, 2h\,\Delta P, \tag{56}$$

The corresponding efficiency factors can be calculated with

$$E = \frac{M_{CO_2}}{\rho_{CO_2}\,\varphi\,h\,A} = \frac{Q_{CO_2}\,t}{\rho_{CO_2}\,\varphi\,h\,A} \tag{57}$$

and

$$E = \frac{2Q_{CO_2}\,t}{\rho_{CO_2}\,\varphi\,2h\,A}. \tag{58}$$

6.1.4 Porosity

For a volume limited storage capacity the pore volume is the (only) limiting factor. The reservoir porosity effects the amount of pore volume available for CO_2 storage. Both the efficiency factor and the stored CO_2 mass are linearly related to the porosity. Increasing the reservoir porosity results into an absolute increase in stored CO_2 mass, see figure 33. However, the efficiency factor takes into account the relative pore volume occupied by CO_2 compared to the total reservoir pore volume. If the efficiency factor remains constant when increasing the porosity, then all of the extra pore volume is filled with CO_2. Which indicates that the pore volume is the (only) limiting factor and therefore the storage capacity of these simulations are pure volume limited. However, if the efficiency factor decreases, then not all of the extra pore volume is filled with CO_2, see figure 34. Which indicates that the pore volume is not the limiting factor, and therefore the storage capacity of these simulations is not pure volume limited.

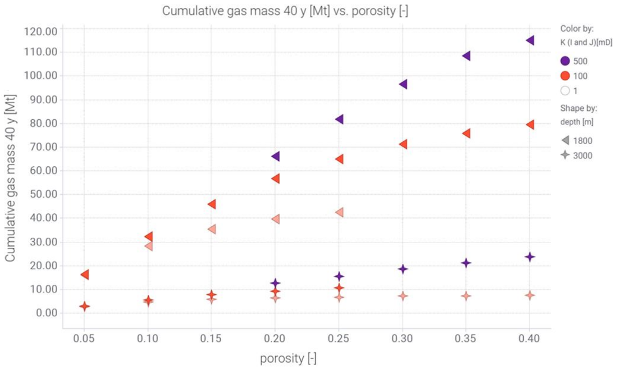

Figure 33: Effect of the reservoir porosity on the CO_2 mass stored.

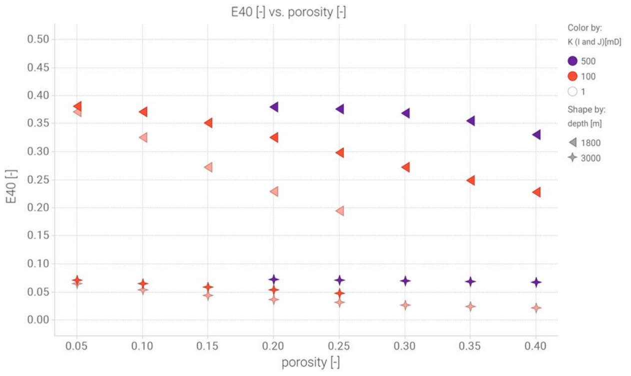

Figure 34: Effect of the reservoir porosity on the efficiency factor.

Two trends can be noticed in figure 34. As seen in the previous subchapters, larger efficiency factors are achieved for reservoirs at 1800 meters depth compared to reservoirs at 3000 meters depth. This results from the larger relative injection pressure at 1800 meters depth.

Moreover, the slope ($dE_{40}/d\varphi$) of the simulations which are not pure volume limited (where an increase in porosity results into a decrease in efficiency factor) becomes shallower with increasing permeability. This can clearly be seen for reservoir at 1800 meters depth in figure 34. As mentioned in the previous subchapter, for simulations which are not pure volume limited it holds that an increase in permeability results into an increase in injected CO_2 mass, which consequently result into a higher efficiency factor. Which can be seen for simulation at 1800 meters depth with a permeability of 10 and 100 mD. However, with a high permeability and consequently a high flow rate, the boundary of the reservoir is felt earlier in time. Therefore, the storage capacity becomes volume limited and the efficiency factor remains constant with increasing permeability. Which can more or less be seen for a reservoir at 1800 meters depth, with a permeability of 500 mD in figure 34.

6.1.5 Radius

For a volume limited storage capacity the pore volume is the (only) limiting factor. The reservoir radius effects the amount of pore volume available for CO_2 storage. Increasing the reservoir radius results into an absolute increase in stored CO_2 mass, see figure 35. However, the efficiency factor takes into account the relative pore volume occupied by CO_2 compared to the total reservoir pore volume. If the efficiency factor remains constant when increasing the reservoir radius, then all of the extra pore volume is filled with CO_2. Which indicates that the pore volume is the (only) limiting factor and therefore the storage capacity of these simulations are pure volume limited. However, if the efficiency factor decreases, then not all of the extra pore volume is filled with CO_2, see figure 36. Which indicates that the pore volume is not the limiting factor, and therefore the storage capacity of these simulations is not pure volume limited. The reservoir porosity and radius have a similar effect on the efficiency factor.

The convergence of the efficiency factor with decreasing reservoir radius, indicates that the simulations with a large reservoir radius are not pure volume limited. Therefore, an increase in reservoir radius results into a decrease in efficiency factor. Whereas, the simulations with a small reservoir radius are pure volume limited. Therefore, an increase in reservoir radius does not effect the efficiency factor, and consequently the efficiency factor converges.

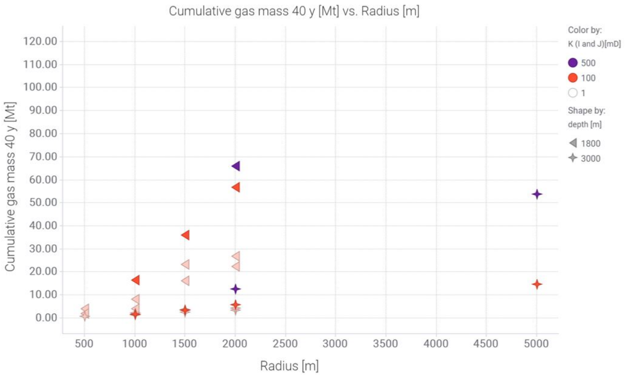

Figure 35: Effect of the reservoir radius on the CO_2 mass stored.

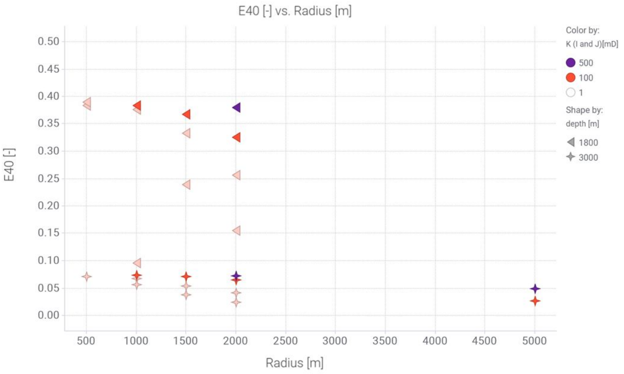

Figure 36: Effect of the reservoir radius on the efficiency factor.

6.2 Rule-of-thumb for efficiency factor E

The efficiency factor is significantly impacted by the reservoir depth, as can be seen in figure 37. However, the main parameter that changes with reservoir depth is the relative injection pressure (ΔP). So even though it appears that the efficiency factor is mainly effected by the reservoir depth, the main driver behind this trend is the relative injection pressure, resulting from the BHP and reservoir pressure. The maximum efficiency factor is linearly related to the relative injection pressure, see figure 37.

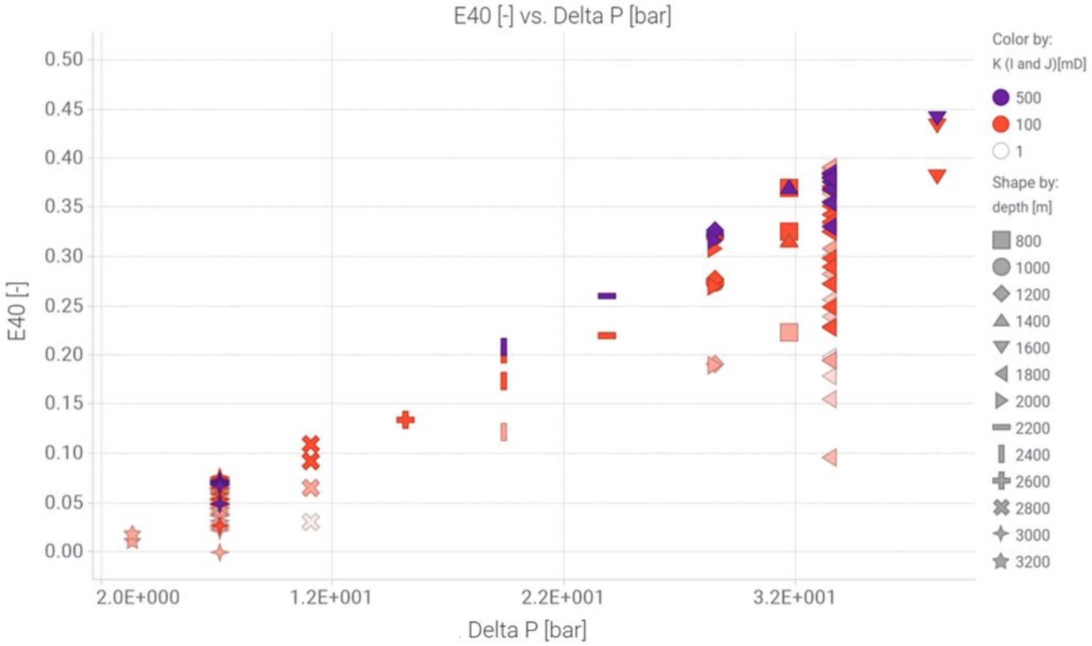

Figure 37: Linear trend between the efficiency factor (E) and the relative injection pressure (ΔP) at 40 years of injection.

The maximum efficiency factor is approximated by a linear fit, see table 23. With this equation the maximum achievable efficiency factor can be calculated as a function of relative injection pressure. This linear function is used as a rule-of-thumb to calculate the efficiency factor with the relative injection pressure or indirectly with the reservoir depth. Since, in this study the relative injection pressure is a function of depth. Equation (49) and (51) can be used to calculate the relative injection pressure. The efficiency factor can then be used to approximate the storage capacity at 20, 40 or 100 years of injection, see equation (59). Other input parameters that are needed to approximate the storage capacity, are the pore volume and the CO_2 density. The CO_2 density is relatively constant with increasing reservoir depth, which is a result of the combination of the geothermal and pressure gradient. Therefore, the density of the CO_2 can be assumed to be 695.4 kg/m^3 for simplicity. The mass of CO_2 injected can be calculated with

$$M_{CO_2,\, t\,=\,40y} = E_{40} * \rho_{CO_2} * V_p. \tag{59}$$

Table 23: Linear relation between the efficiency factor (E) and the relative injection pressure (ΔP) for an injection period of 20, 40 and 100 years.

Time [y]	Linear relation	R^2
20	E_{20} = 0.0107 ΔP	0.9969
40	E_{40} = 0.0113 ΔP	0.9961
100	E_{100} = 0.0115 ΔP	0.9980

Validation of the linear relationship with relative injection pressure

In order to validate whether the effect on the efficiency factor results from the relative injection pressure only and not from other processes influenced by the reservoir temperature and pressure, a similar relative injection pressure is tested on two different reservoir depths. An relative injection pressure of 33.41 bar, originating from a reservoir depth of 1800 meters, is applied to a reservoir depth of 3000 meters. Table 24 shows that indeed very similar efficiency factors are achieved when using equivalent injection pressures. Therefore it can be concluded that the relative injection pressure is the main driver of the efficiency factor when considering various depths.

Moreover, the linear relation between the efficiency factor and the relative injection pressure is validated. In table 24 it can be seen that multiplying the relative injection pressure by 2, leads to an efficiency factor which is multiplied by 1.9.

Table 24: Validation of the effect of the relative injection pressure on the efficiency factor at 40 years of injection.

Base case	Note	Depth [m]	ΔP [bar]	E [-]
2	Original ΔP	1800	33.41	0.33
7	ΔP from base case 2	3000	33.41	0.33
2	Original ΔP x2	1800	66.82	0.63

6.2.1 Validation of efficiency factor rule-of-thumb

In order to validate the proposed rule-of-thumb, the efficiency factor resulting from the simulations are compared to the efficiency factors calculated with the rule-of-thumb.

The base cases which fall within the volume limited storage capacity are examined. Moreover, the extremes from the sensitivity study of base case 2 are also examined, see table 25.

In table 25 some simulations are denoted with N.V., which means that at that timestep the storage capacity of the simulated reservoir is not volume limited. It is possible that a rate limited storage capacity of a reservoir turns into a volume limited storage capacity over time. With time more CO_2 is injected, and therefore it is possible that the injection rate falls off the plateau rate if the pore volume cannot sustain a constant reservoir pressure anymore. This is the case for base case 1 and 5, and it also holds for some sensitivity runs of base case 1 in table 25.

Moreover, some simulations are noted with an x. This means that the simulation terminated before this timestep. Termination of a simulation can sometimes occur with high permeabilities, which requires smaller timesteps and therefore 100 years of simulation can not be reached within the maximum set number of timesteps.

Regarding the validation of the rule-of-thumb, it can be seen in table 25 that the error for 20 years of injection lies between 71% and 5%, and the median error is 35%. For 40 years of injection the error lies between 53% and 2%, and the median error is 12%. For 100 years injection the error lies between 65% and 0%, and the median error is 6%. From these values it can be concluded that the error reduces over time. Simulations become more and more pure volume limited over time, because the expected injection rate lower and lowers over time. With an injection rate of zero, the storage capacity is completely pure volume limited. Based on this, the rule-of-thumb is assumed to be a food approximation for estimating volume limited storage capacities.

Table 25: Comparison between the efficiency factor from the simulation and the rule-of-thumb.

	Simulation			**Rule-of-thumb**			**Error [%]**		
Simulation ID	**E20**	**E40**	**E100**	**E20**	**E40**	**E100**	**E20**	**E40**	**E100**
BC1*	N.V.	N.V..	0.13	N.V.	N.V.	0.38	N.V.	N.V.	66
BC2	0.23	0.33	0.38	0.35	0.37	0.38	35	12	0
BC3	0.23	0.38	x	0.35	0.37	0.38	35	2	x
BC4	0.23	0.33	0.38	0.35	0.37	0.38	35	12	0
BC5*	N.V.	N.V.	0.38	N.V.	N.V.	0.38	N.V.	N.V.	0
BC6	0.05	0.07	x	0.07	0.08	0.08	28	17	x
BC7	0.04	0.05	0.07	0.07	0.08	0.08	51	32	16
BC8	0.07	0.07	x	0.07	0.08	0.08	9	8	x
BC9	0.02	0.04	x	0.07	0.08	0.08	71	53	x
BC2 Z_{1600m}	0.27	0.38	0.35	0.41	0.43	0.44	35	11	20
BC2 Z_{3000m}	0.04	0.05	0.07	0.07	0.08	0.08	51	32	16
BC2 $\varphi_{0.05}$	0.37	0.38	x	0.35	0.37	0.38	5	2	x
BC2 $\varphi_{0.35}$	0.15	0.25	0.36	0.35	0.37	0.38	58	33	6
BC2 $\varphi_{0.40}{}^{*}$	N.V.	0.23	0.35	N.V.	0.37	0.38	N.V.	39	8
BC2 K_{50mD}	0.13	0.23	0.35	0.35	0.37	0.38	63	39	8
BC2 K_{500mD}	0.33	0.38	x	0.35	0.37	0.38	7	2	x
BC2 H_{20m}	0.25	0.34	0.38	0.35	0.37	0.38	30	8	1
BC2 H_{200m}	0.23	0.29	0.37	0.35	0.37	0.38	65	22	4
BC2 R_{1km}	0.37	0.38	0.39	0.35	0.37	0.38	6	3	3
BC2 R_{2km}	0.23	0.33	0.38	0.35	0.37	0.38	35	13	1
BC2 $R_{5km}{}^{*}$	N.V.	N.V.	0.20	N.V..	N.V..	0.38	N.V.	N.V.	48

* = becomes volume limited with time, x = simulation termination

N.V.. = not volume limited

6.3 Conclusion for practical application

The theory obtained from the volume limited storage capacity can be applied in practice.
First of all, the injection rate cannot be sustained at plateau rate. At 40 years of injection, the injection rate decreased with at least 20% of the plateau rate. Because the plateau rate can not be sustained, it can be argued that volume limited aquifers are not the best option for CO_2 storage when considering projects where new facilities (platform and wells etc.) have to be developed. However, for projects where facilities can be re-used it might be cost-efficient to target nearby aquifers with a volume limited storage capacity. With the assumptions made in this study, even a closed aquifer with a radius of 1 km (BC2) has an efficiency factor of 0.37. This results into a possible storage capacity of 16.7 Mt. The small closed boundary aquifer can be used as an analogue for the compartmentalized aquifers resulting from the extensive fracture network in the Dutch offshore [40]. Due to the volume limited storage capacity of these small compartmentalized aquifers, it is best to utilize these aquifers when located nearby existing gas platform, where facilities can be re-used.

Moreover, the relative injection pressure (ΔP) is the main factor that impacts the efficiency factor and the possible storage capacity. The relative injection pressure results from the BHP and the reservoir pressure. Therefore, when starting a project it is important to investigate the BHP and reservoir pressure in order to optimally estimate the storage capacity. For instance, it can be the case that a reservoir is underpressured or overpressured, which consequently affects the relative injection pressure.
Moreover, the salinity of brine increases with depth [13]. This can affect the density of the brine column overlying the reservoir and consequently affects the reservoir pressure.
Moreover, the final reservoir pressure and maximum allowed BHP can depend on regulatory aspects. However, applying a conservative BHP, which is below the maximum regulatory and technical limit, directly impacts the storage capacity.

The rule-of-thumb for volume limited storage capacity can be applied in three practical ways.
First, using the rule-of-thumb to estimate the possible storage capacity, see equation (60). Here the efficiency factor E is calculated with the rule-of-thumb, which is a linear function of the relative injection pressure (ΔP). The other input parameters to calculate the storage capacity are the density of the CO_2 (ρ_{CO_2}), which can be assumed to be about 0.695 kg/m^3 under final reservoir conditions, and the reservoir pore volume(V_p). This method can be applied during screening of several aquifers to select the aquifers with the highest possible storage potential. The mass of injected CO_2 is calculated with

$$M_{CO_2} = E(\Delta P)\ \rho_{CO_2}\ V_p. \tag{60}$$

Second, the rule-of-thumb can be used to estimate the reservoir pore volume necessary when injecting a certain amount of CO_2 with a specific relative injection pressure, see equation (61). With the necessary pore volume the corresponding reservoir porosity (φ), height (h) and radius (r) can be calculated, i.e,

$$V_p = \frac{M_{CO_2}}{E(\Delta P)\ \rho_{CO_2}}. \tag{61}$$

When injecting CO_2 into a large aquifer with several wells, the minimum distance between the wells in order to prevent interference can be approximated with the plume radius, see equation (62). With the pore volume obtained from equation (61) the plume radius (r_{plume}) can be estimated, i.e,

$$D_{w1-w2} > 2r_{plume} \tag{62}$$

and

$$r_{plume} = \frac{V_p}{\varphi\ h} \tag{63}$$

7 Results: Rate limited storage capacity

For a rate limited storage capacity the injection rate in the limiting factor. Whereas for volume limited storage capacity the pore volume is the limiting factor, here the pore volume is large enough for keeping the reservoir pressure relative constant during CO_2 injection. Since the BHP is maintained constant, the relative injection pressure remains constant, and therefore the injection can be sustained at a plateau rate. A rate limited storage capacity can not be estimated with a volumetric calculation, because the mass of CO_2 that can be stored is not related to the pore volume. However, the storage capacity is easily estimated by multiplying the plateau rate with the total time of injection.

7.1 Plateau rate

The plateau rate (Q_p) is quantified over a wide range of geologic and operational parameters at 40 years of injection. This allows for studying the effect of reservoir attributes on the plateau rate and constructing a rule-of-thumb for the plateau rate. The rule-of-thumb will help to estimate the plateau rate, which can be used to approximate the rate limited storage capacity of a reservoir. The following paragraphs will discus the effect of several reservoir characteristics.

7.1.1 Depth

In figure 38 it can be seen that the efficiency factor is significantly impacted by the reservoir depth, which is visualised by the symbols in the figure. The injection rate for a reservoir located at 1800 meters depth is significantly higher compared to reservoir located at 3000 meters depth.
The simulations with a small pore volume fall off the plateau rate. For a pure rate limited storage capacity the pore volume is large enough for keeping the reservoir pressure constant during CO_2 injection, and therefore the injection can be sustained at a plateau rate. Therefore, the simulations with a small pore volume that fall off the plateau rate are not pure rate limited.

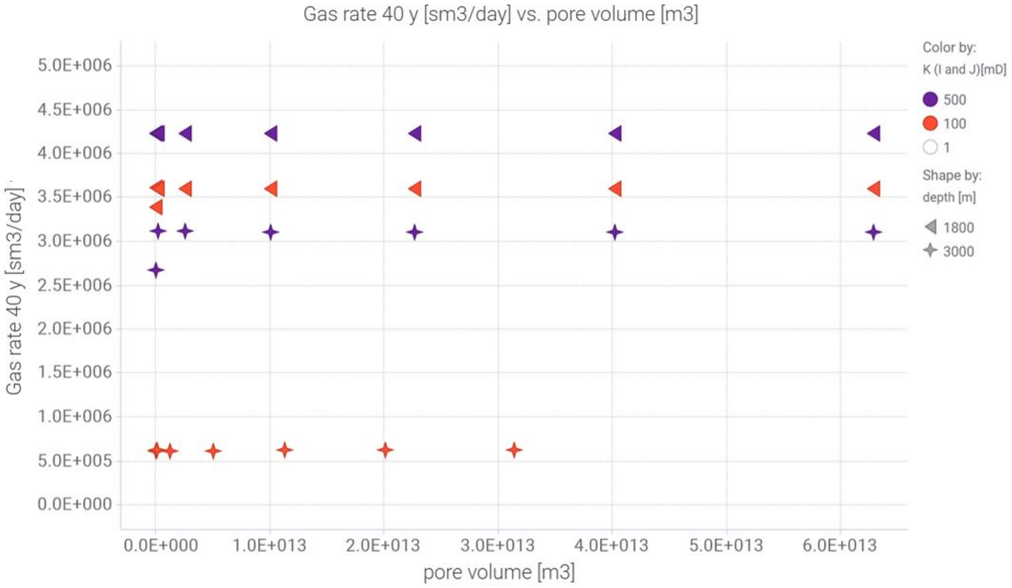

Figure 38: Effect of the reservoir radius on the injection rate at 40 years of injection.

The main parameter that changes with reservoir depth is the relative injection pressure (ΔP). In this study the relative injection pressure results from the bottomhole pressure (BHP), which has been set as an operating constraint, and the reservoir pressure (P_{res}). The BHP and reservoir pressure have been theoretically constructed as a function of reservoir depth. Therefore, the relative injection pressure is also a function of reservoir depth. So even though it appears that the efficiency factor is mainly effected by the reservoir depth, the main driver behind this trend is the relative injection pressure.

In figure 38 all parameters that are tested in the sensitivity study are visualised. On the x-axis the pore volume is plotted, which consists of the reservoir thickness, porosity and radius. The colour visualizes the reservoir permeability and the shape visualizes the reservoir depth. What can be noticed is that the injection rate is mostly affected by the reservoir depth and reservoir permeability. Thickness is another important factor, but is kept constant for the simulation results given in the figure. Another observation is that the porosity and reservoir size, which make up the reservoir pore volume, do not effect the injection rate.

7.1.2 Permeability

The reservoir permeability significantly affects the injection rate. The injection rate is linearly related to the permeability, as can be seen in figure 38. This results from the linear relationship between permeability and injection rate of the well. The linear relationship is stated as

$$Q_{inj} \propto \mathbf{k} h \Delta P. \tag{64}$$

Doubling the reservoir permeability leads to a doubled injection rate, as can be seen for a reservoir depth of 1800 meters in table 26. For 3000 meters the ratio is a bit lower, which is due to secondary effects.

The linear trend stops at the maximum allowed injection rate. At a depth of 1800 meters the maximum allowed injection rate is 4.42E+06 sm^3/day, which is visualised by the dashed straight line. For a reservoir at 1800 meters depth, this maximum injection rate has been achieved with a permeability of 500 mD, see figure 39.

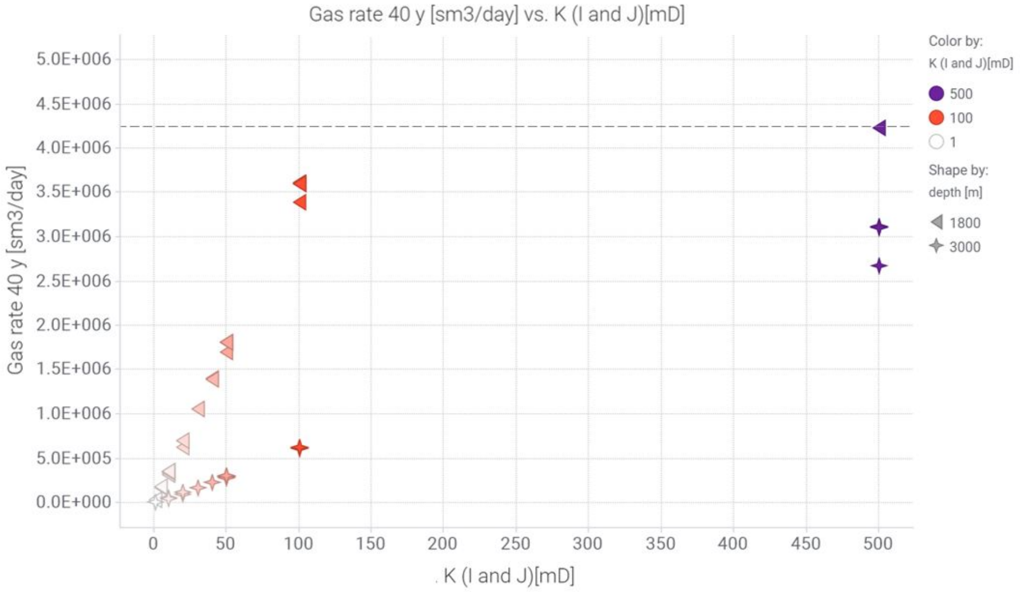

Figure 39: Effect of the reservoir permeability on the injection rate at 40 years of injection. The dashed straight line indicates the maximum injection rate at 1800 meters depth.

Table 26: Effect of the reservoir permeability on the injection rate at 40 year of injection at different depths.

Depth [m]	$\mathbf{k}_{50mD}$	$\mathbf{k}_{100mD}$	k_{100mD} / k_{50mD}
1800	Q = 1.8E+06 [sm^3/day]	Q = 3.6E+06 [sm^3/day]	2.0
3000	Q = 3.2E+05 [sm^3/day]	Q = 6.2E+05 [sm^3/day]	1.9

7.1.3 Thickness

The thickness affects the injection rate significantly. Due to the scale of figure 40, the effect of the thickness can not be clearly seen. However, the injection rate shown in table 27 does show this effect clearly. This results from the linear relation of the thickness and the injection rate, see equation (64). Increasing the thickness (h) directly impacts the the injection rate (Q). As also can be seen in table 27, a doubled thickness results roughly into a doubled injection rate. The fact that there is a slight deviation from this is due to secondary effects The injection rate proportional to

$$Q_{inj} \propto k\mathbf{h}\Delta P. \tag{64}$$

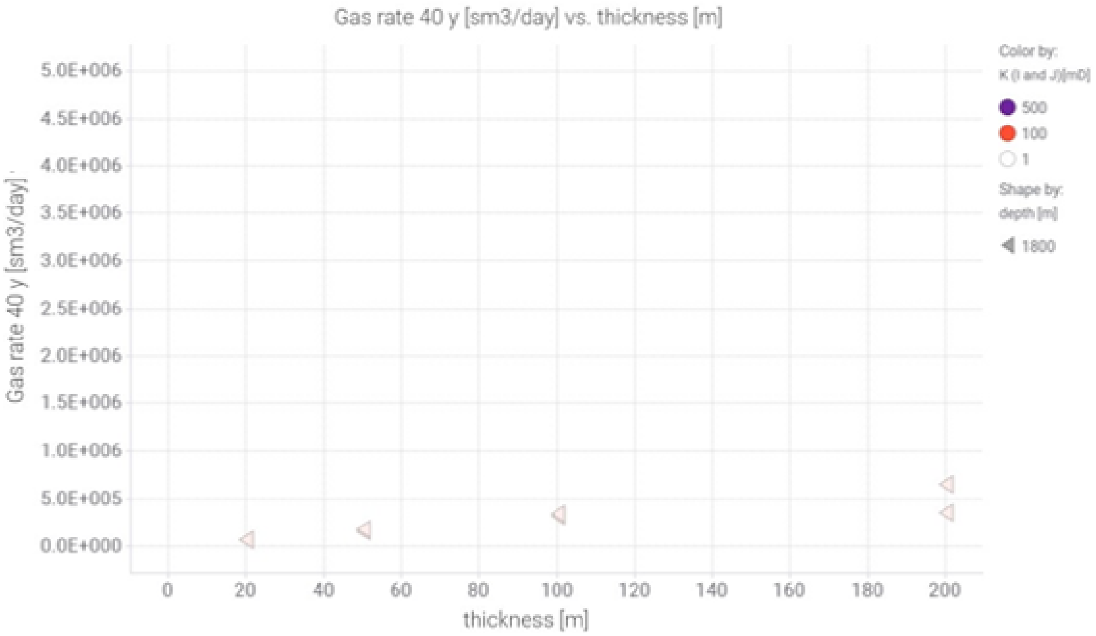

Figure 40: Effect of the reservoir thickness on the injection rate at 40 years of injection.

Table 27: Effect of the reservoir thickness on the injection rate at 40 years of injection.

k [mD]	**Depth [m]**	$\mathbf{h}_{100m}$	$\mathbf{h}_{200m}$	$\mathbf{h}_{200m}$ / $\mathbf{h}_{100m}$
10	1800	Q = 3.5E+05 [sm^3/day]	Q = 6.5E+05 [sm^3/day]	1.86

7.1.4 Porosity

The effect of the reservoir porosity on the injection rate is almost insignificant, see figure 41 and table 28. This results from the fact that for a rate limited storage capacity, the pore volume is not a limiting factor on the storage capacity. Therefore, increasing the porosity, and thereby the pore volume, does not effect the storage capacity and injection rate.
In table 28 it can be seen that a multiplication in porosity, from 10% to 20%, does not results into a significant increase in injection rate, and consequently does not increase the rate limited storage capacity significantly. The fact that there is a slight increase in injection results from secondary effects.

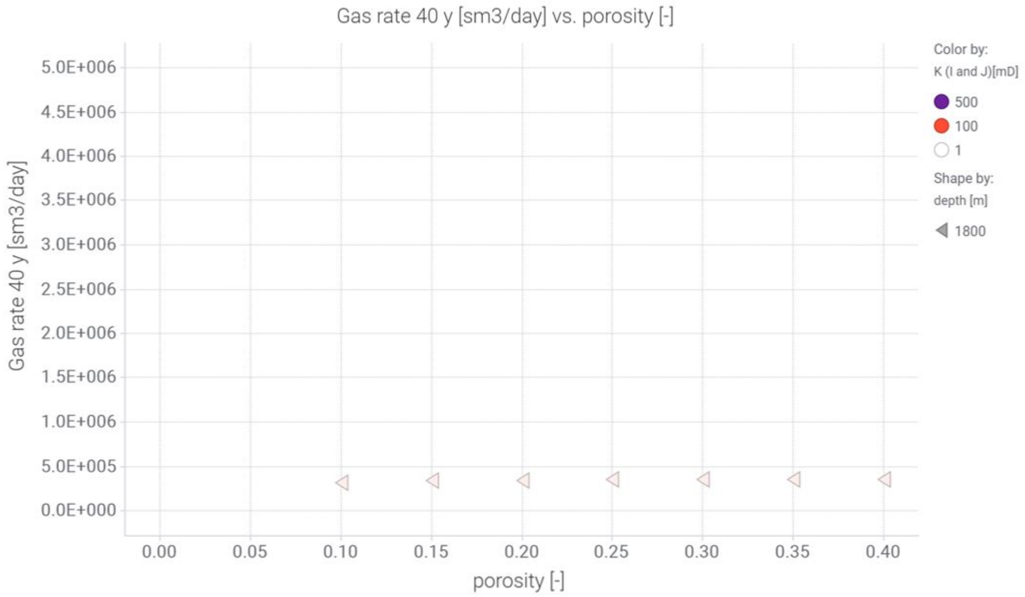

Figure 41: Effect of the reservoir porosity on the injection rate at 40 years of injection.

Table 28: Effect of the reservoir porosity on the injection rate at 40 years of injection.

k [mD]	**Depth [m]**	$\varphi_{10\%}$	$\varphi_{20\%}$
10	1800	Q = 3.2E+05 [sm^3/day]	Q = 3.5E+05 [sm^3/day]

7.1.5 Radius

The effect of the reservoir radius on the injection rate is insignificant, see figure 42 and table 29. This results from the fact that for a rate limited storage capacity, the pore volume is not a limiting factor on the storage capacity. Therefore, increasing the reservoir radius, and thereby the pore volume, does not effect the storage capacity and injection rate.

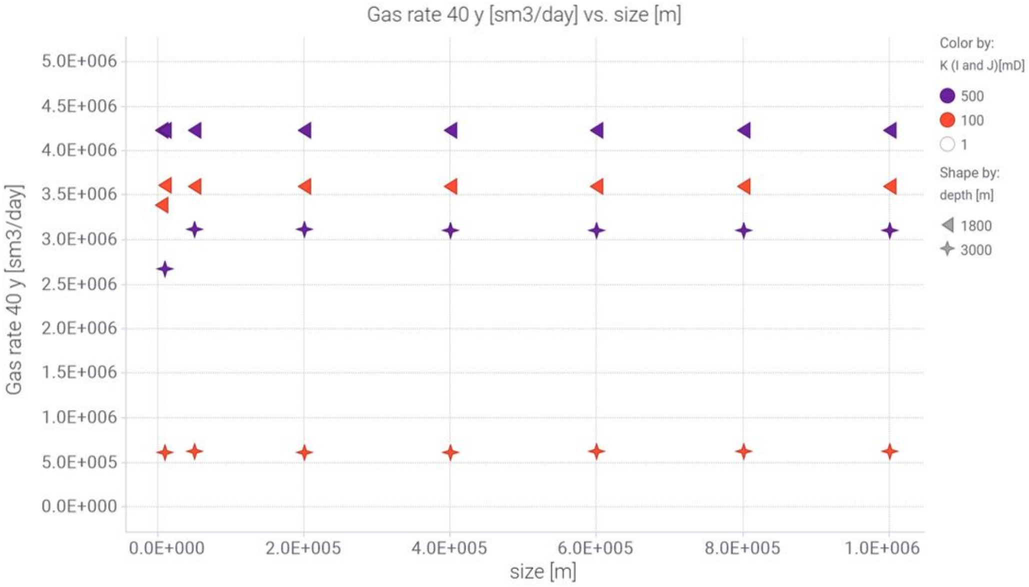

Figure 42: Effect of the reservoir radius on the injection rate at 40 years of injection.

Table 29: Effect of the reservoir radius on the injection rate at 40 years of injection.

k [mD]	Depth [m]	r_{100km}	r_{200km}	r_{200km} / r_{100km}
100	1800	Q = 3.6E+06 [sm^3/day]	Q = 3.6E+06 [sm^3/day]	1.0
100	3000	Q = 2.0E+05 [sm^3/day]	Q = 2.0E+05 [sm^3/day]	1.0

However, in figure 42 it can be seen that for smaller radii, for example 5 and 10 km, the increase in radius does influence the injection rate slightly. This results from the fact that these points are very close to the transition zone and not pure rate limited anymore, see subsection 8.3 for further information.

7.2 Rule-of-thumb for injection rate

As seen in the previous subsections and from equation (64), the reservoir permeability, thickness and relative injection pressure all effect the injection rate directly, i.e,

$$Q_{inj} \propto kh\Delta P. \tag{64}$$

The linear relation of the injection rate (Q) with these parameters can be seen in figure 43. In this figure the injection rate divided by the relative injection pressure (Q/ΔP), is plotted against the reservoir injectivity (kh). So, here the operational parameters on the y-axis are plotted against the reservoir parameters on the x-axis. Note that the points that do not fall on the linear trend have been constrained by the maximum rate constraint. The injection rate divided by the relative injection pressure is approximated with a linear fit, see table 30.

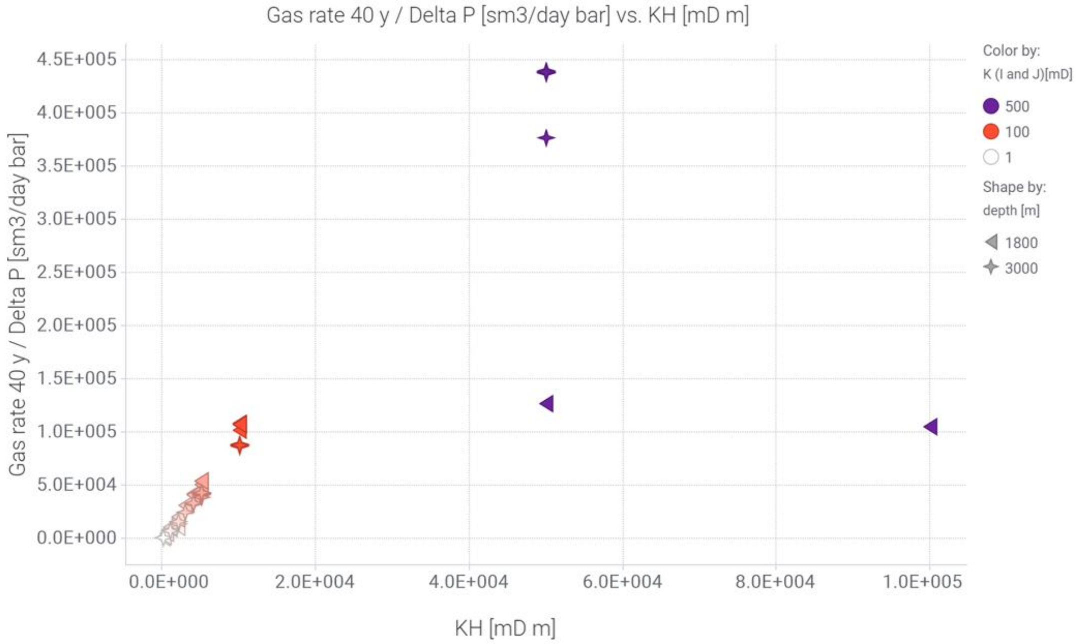

Figure 43: Rate limited points display a linear relation of the injection rate divided by the relative injection pressure (Q/ΔP) as a function of the reservoir injectivity (kh).

Table 30: Linear relation of the injection rate divided by the relative injection pressure (Q / ΔP) as a function of the reservoir thickness and permeability (kh).

Time [y]	**Linear relation** [sm3 / bar day]	**Linear relation** [Mt / bar y]	**R^2** [-]
20	$Q_p/\Delta P$ = 8.7163 kh	$Q_p/\Delta P$ = 6.2993E-06 kh	0.9967
40	$Q_p/\Delta P$ = 8.7244 kh	$Q_p/\Delta P$ = 6.3051E-06 kh	0.9947
100	$Q_p/\Delta P$ = 8.9152 kh	$Q_p/\Delta P$ = 6.4430E-06 kh	0.9968

The linear fit can be used as a rule-of-thumb to approximate the plateau rate. With this, the storage capacity can be calculated, see equation (65) and (66). To calculate the storage capacity, the injection at plateau rate [Mt/y] can simply be multiplied with the time of injection, i.e,

$$Q_{p,\, t\,=\,40y} = 6.3051E\text{-}06\ kh\ \Delta P \tag{65}$$

with

$$M_{CO_2} = Q\ t. \tag{66}$$

The relative injection pressure used in this study is a function of depth and can be calculated with equation (50) and (52). These equations can be used if the relative injection pressure of project is unknown. However, if the relative injection pressure is known, then equations (65) and (66) can be used directly. Which relative injection pressure is used depend on the reservoir depth, i.e,

$$800 < z <= 1600: \ \Delta p_{leak-off} = -0.12z + 22.09 \tag{50}$$

or

$$1600 < z <= 3200: \ \Delta p_{CO_2} = -0.0242z + 78.553. \tag{52}$$

It is important to note that the injection rate calculated with the rule-of-thumb can not exceed the maximum allowed injection rate, which is set as an operational constraint. As can be seen in figure 43 the linear trend of the injectivity stops when the plateau rate reaches the maximum gas rate constraint, which is set as an operating constraint.
Therefore, when using the rule-of-thumb it is important to check whether the calculated injection rate exceeds the maximum allowed injection rate. The maximum allowed injection rate [Mt/y] is also a function of depth, and can be calculated with equation (54).

However, it must be noted that this equation only holds for the well conditions set in this study. The maximum allowed gas rate is a function of CO_2 density in the well. Which, in this study is a results of the tophole pressure (THP), the bottomhole pressure (BHP) and the temperature in the well, which is assumed to be 35 ° C. Therefore, if the the well conditions in a project are significantly different from this study, this equation might not be the best approximation of the maximum allowed injection rate. In that case, it is best to approximate the maximum allowed injection rate directly from the density of the CO_2 from the well conditions, i.e,

$$Q_{STG} = 6E\text{-}08\ z^2 - 0.0004z + 3.54 \tag{54}$$

and

$$Q_{STG} = \frac{CA_{tubing}}{\sqrt{\rho_{CO_2}}} = \frac{350A_{tubing}}{\sqrt{\rho_{CO_2}}}, \tag{46}$$

if

$$Q_p \ < \ Q_{STG} \quad then \quad Q = Q_p \tag{67}$$

if

$$Q_p \ > \ Q_{STG} \quad then \quad Q = Q_{STG} \tag{68}$$

7.2.1 Validation of injection rate rule-of-thumb

In order to validate the rule-of-thumb, the injection rate resulting from the simulations is compared to the injection rate calculated with the rule-of-thumb. Therefore, the base cases which fall within the rate limited storage capacity are examined, which includes base case 1 and 5. Moreover, the extremes from the sensitivity study of base case 1 are examined as well, see table 31.

In table 31 some simulation are noted with N.R., which means that at that timestep the aquifer is not rate limited anymore. It is possible that for the first couple of years the pore volume is not a limiting factor for CO_2 injection and is therefore classified as rate limited. However, as more CO_2 is injected with time, it is possible that the pore volume becomes the limiting factor. Therefore over time the aquifer transitions from a rate limited aquifer to a volume limited aquifer. This occurs for some sensitivity runs of base case 1, see table 31.

In the case of the sensitivity run with 5% porosity, the pore volume is not a limiting factor in the first 20 years of injection. However with time, at 40 years of injection, the pore volume is not large enough anymore to sustain a constant injection rate and the storage capacity becomes volume limited.

In the case of the sensitivity run with 10% porosity, the transition from rate to volume limited occurs later because more pore volume is available. This trend also holds for the sensitivity runs with a radius of 1 km and 1.5 km.

On the other hand, when considering the permeability the transition from rate to volume limited occurs earlier with higher permeability, which can be seen in table 31. This is due to the fact that with a higher permeability the flow rate increases and therefore reaches the boundary of the aquifer earlier in time. So, a transition can occur from rate to volume limited storage capacity over time. This transition occurs later in time if more pore volume is available for CO_2 storage (influenced by porosity and radius) or with a lower permeability.

Regarding the validation of the rule-of-thumb, it can be seen in table 31 that the error of the rule-of-thumb compared to the simulation is smallest at 40 years of injection. At 40 years of injection the error lies between 32% and 5%, and the median error is 21%. Whereas, at 20 years of injection the error lies between 1 and 94%, and the mean error is 24%. The high outlier with an error of 94% is the sensitivity run of base case 1 with a reservoir radius of 5 km. For 100 years injection the error lies between 91% and 1%, and the mean error is 19%. The high outlier with an error of 91% is the sensitivity run of base case 1 with a reservoir thickness of 200 meters. Also the sensitivity run with a reservoir thickness of 100 meters has a high error of 90%.

It can be concluded from these number that at 40 years of injection the outliers are less significant than for 20 and 100 years of injection. Therefore the rule-of-thumb at 40 years is the best approximation.

Table 31: Comparison between the injection rate from the simulation and the rule-of-thumb.

	Simulation [sm^3/day]			**Rule-of-thumb** [sm^3/day]			**Error** [%]		
Simulation ID	**Q20**	**Q40**	**Q100**	**Q20**	**Q40**	**Q100**	**Q20**	**Q40**	**Q100**
BC1	3.6E+05	3.5E+05	3.0E+05	2.9E+05	2.9E+05	2.9E+05	25	21	1
BC5	3.5E+05	3.2E+05	2.0E+05	2.9E+05	2.9E+05	2.9E+05	21	10	32
BC1$_{\varphi_{0.05}}$*	3.2E+05	N.R.	N.R.	2.9E+05	2.9E+05	2.9E+05	10	N.R.	N.R.
BC1$_{\varphi_{0.10}}$*	3.5E+05	3.2E+05	N.R.	2.9E+05	2.9E+05	2.9E+05	21	10	N.R.
BC1$_{\varphi_{0.05}}$*	3.6E+05	3.6E+05	3.2E+05	2.9E+05	2.9E+05	2.9E+05	24	24	8
BC1$_{\varphi_{0.40}}$	3.7E+05	3.6E+05	3.4E+05	2.9E+05	2.9E+05	2.9E+05	27	25	16
BC1$_{K_{1mD}}$	3.8E+04	3.7E+04	3.6E+05	2.9E+04	2.9E+04	2.9E+04	32	30	24
BC1$_{K_{50mD}}$*	1.5E+06	N.R.	N.R.	1.4E+06	1.4E+06	1.5E+06	3	N.R.	N.R.
BC1$_{K_{10mD}}$*	3.6E+05	3.5E+05	N.R.	2.9E+05	2.9E+05	2.9E+05	25	21	N.R.
BC1$_{K_{5mD}}$*	1.8E+05	1.8E+05	1.7E+05	1.4E+05	1.4E+05	1.5E+05	27	25	16
BC1$_{r_{1km}}$*	3.2E+05	N.R.	N.R.	2.9E+05	2.9E+05	2.9E+05	12	N.R.	N.R.
BC1$_{K_{1.5km}}$*	3.6E+05	3.3E+05	N.R.	2.9E+05	2.9E+05	2.9E+05	24	14	N.R.
BC1$_{K_{5km}}$*	5.6E+05	3.5E+05	3.5E+05	2.9E+05	2.9E+05	2.9E+05	94	23	20
BC1$_{K_{1E3km}}$	3.6E+05	3.6E+05	3.5E+05	2.9E+05	2.9E+05	2.9E+05	24	24	19
BC1$_{H_{20m}}$	7.7E+04	7.6E+04	6.5E+04	5.8E+04	5.8E+04	5.9E+04	33	32	11
BC1$_{H_{200m}}$	6.8E+05	6.5E+05	5.5E+04	5.8E+05	5.8E+05	5.9E+05	17	14	91
BC1$_{Z_{1600m}}$	4.1E+05	4.0E+05	3.4E+04	3.3E+05	3.3E+05	3.4E+05	24	21	90
BC1$_{Z_{3000m}}$	6.1E+04	5.8E+04	4.8E+04	6.1E+04	6.1E+04	6.2E+04	1	5	23

* = become volume limited with time

N.R. = not rate limited

7.3 Conclusion for practical application

The theory obtained from the rate limited storage capacity can be applied in practice.
First of all, the injection rate can be sustained at plateau rate. At 20, 40 or 100 years the injection rate does not drop below 80% of the initial (plateau) rate. Because the plateau rate can be sustained on a project time-scale, it can be argued that rate limited aquifers are a good option for CO_2 storage when considering projects where new facilities (platform and wells etc.) have to be developed.
The reservoir pressure does not increase significantly during CO_2 injection, because it does not feel the boundary of the reservoir yet. Therefore, the plateau rate can be sustained. The rate limited storage capacity can be used to estimate the possible storage capacity of large open aquifers.
Moreover, the relative injection pressure (ΔP) and the reservoir injectivity (kh) are the main parameters that impact the storage potential. The relative injection pressure results from the bottomhole pressure (BHP) and the reservoir pressure. Therefore, as stated before in the practical application for volume limited storage capacity, it is important to investigate the BHP and the reservoir pressure in order to optimally estimate the storage potential, see section 6.3.

The rule-of-thumb for rate limited storage capacity can be applied in three practical ways.
First, using the rule-of-thumb to estimate the possible storage capacity, see equation (69). Here the injection rate is calculated with the rule-of-thumb, which is a function of the relative injection pressure (ΔP), reservoir permeability and height (kh). The other input parameter to calculate the storage capacity is the time of injection [y], which can be any time below 20, 40 and 100 years of injection as long as storage capacity remains rate limited. This method can be applied during screening of several aquifers to select the aquifers with the highest possible storage potential. The mass of CO_2 is calculated with

$$M_{CO_2} = Q_p(\Delta P, kh)\ t_p. \tag{69}$$

Second, the rule-of-thumb can be used to estimate the reservoir permeability and height (kh) or the relative injection pressure (ΔP) necessary when injecting CO_2 at a certain rate [Mt/y]. For instance for 20 years of injection,

$$kh = \frac{Q_p}{\Delta P\ 6.2993E{-}06} \tag{70}$$

and

$$\Delta P = \frac{Q_p}{kh\ 6.2993E{-}06}. \tag{71}$$

Last, the efficiency factor can be applied to calculate the pore volume necessary to inject CO_2 at a certain rate in the rate limited regime. Which means that the injection will remain at plateau rate. Even though the efficiency factor does not directly apply to rate limited storage capacities, below an efficiency factor of 0.012 the storage capacity is always rate limited for 40 years of injection, see table 32. This means that at a certain ratio between stored CO_2 mass and the pore volume, the storage capacity is always rate limited. The necessary pore volume can be calculated with

$$\frac{M_{CO_2}}{t_p} = \frac{E_{rate}\ \rho_{CO_2}\ V_p}{t_p} \tag{72}$$

and

$$Q_p = \frac{E_{rate}\ \rho_{CO_2}\ V_p}{t_p} \tag{73}$$

and

$$V_p = \frac{Q_p\ t_p}{E_{rate}\ \rho_{CO_2}} \tag{74}$$

Table 32: Efficiency factor at which the injection is in the rate limited regime for 20, 40 and 100 years of injection.

	20 years	**40 years**	**100 years**
$\mathbf{E}_{rate}$	0.012	0.012	0.021

8 Results: Transition zone

8.1 Pore volume

The transition zone is observed over a range of pore volumes where the storage capacity is not pure volume or pure rate limited. Instead, an aquifer with a pore volume that falls within the transition zone slowly starts to feel the boundary of the reservoir. The range in pore volume is indicated as the lower and upper limit, see figure 44.

At 40 years of injection the transition zone includes points with a pore volume of 1.3E+08 m^3 to 5.0E+08 m^3. This corresponds to a reservoir radius of 1.5 to 2 km, a thickness of a 100 meters and a porosity of 20% to 40%.

The pore volume of the transition zone changes over time, see table 19. With increasing time, from 20 to 100 years of injection, the lower limit of the pore volume in the transition zone increases. When injecting CO_2 over a long periods of time, the points present in the transition zone start to feel the boundary of the reservoir and therefore shift to a pure volume limited storage capacity.

Also, the upper limit of the pore volume in the transition zone increases with time. Due to the continuous CO_2 injection, the pure rate limited storage capacity with a relatively small pore volume transitions into the transition zone. Because with increasing time, larger pore volumes are required to sustain the continuous CO_2 injection.

Table 33: Pore volume that defines whether the storage capacity is volume limited, rate limited or in the transition zone.

	Volume limited	**Transition zone**	**Rate limited**
Time [y]	**Pore volume [m^3]**	**Pore volume [m^3]**	**Pore volume [m^3]**
20	$Vp < 6.3E+07$	$6.3E+07 \leq Vp \leq 3.1E+08$	$Vp > 3.10E+08$
40	$Vp < 1.3E+08$	$1.3E+08 \leq Vp \leq 5.0E+08$	$Vp > 5.0E+08$
100	$Vp < 1.9E+08$	$1.9E+08 \leq Vp \leq 7.9E+08$	$Vp > 7.9E+08$

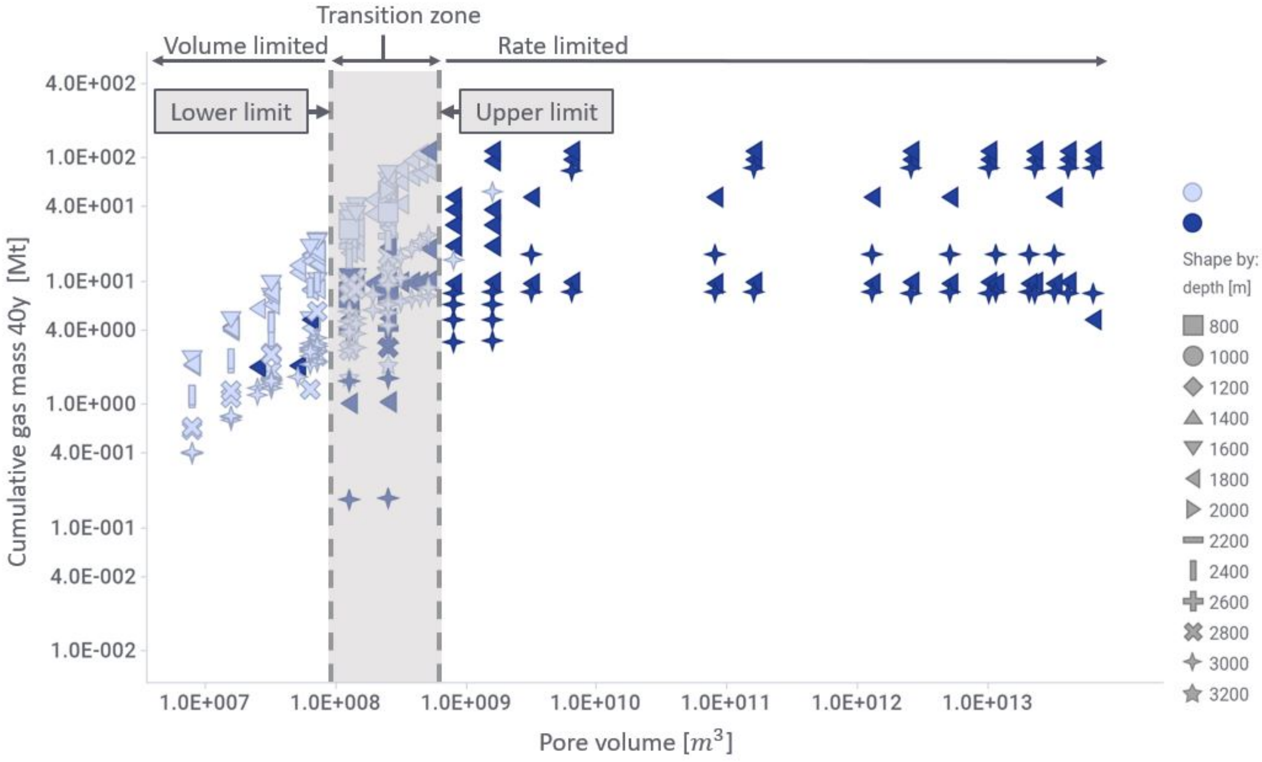

Figure 44: Lower and upper limit of the pore volume in the transition zone.

8.2 Storage capacity estimation

If a pore volume falls within the transition zone, it is not possible to estimate the storage capacity with the volume or rate limited rule-of-thumb. Because, strictly speaking the storage capacity is not pure volume or pure rate limited. With the current knowledge it is not possible to define a rule-of-thumb for the storage capacity if the pore volume falls within the transition zone. Or to estimate, based on the geologic reservoir parameters, whether the pore volume in the transition zone has a storage capacity which is more volume or more rate limited. Therefore, two other methods can be applied to estimate the storage capacity when the pore volume falls within the transition zone.
First, the storage capacity can be calculated with the volume limited and rate limited rule-of-thumb. These estimations can be regarded as a minimum and maximum storage capacity.
Second, a look-up table is created from the simulations at 20, 40 and 100 years of injection. The table is sorted first by pore volume, then by reservoir depth, followed by kh. The table is based on these reservoir parameters because they turned out to be the most important for the volume limited and rate limited storage capacity. The table also includes the storage capacity and the injection rate of the simulations. So, with the reservoir parameters the storage capacity of an aquifer with a pore volume in the transition zone can be approximated by finding the simulation that most resembles the case specific aquifer. The look up table for 20, 40 and 100 years of injection can be found in appendix C (tables 52, 53 and 54).

8.3 Outliers

In some of the volume and rate limited results it can be noticed that some points are categorized as rate or volume limited, however they are not in line with pure volume or pure rate limited trends. Their pore volume falls within the transition zone, which means that they slowly start to feel the boundary of the reservoir.
A good example is figure 45 from chapter 6, where the efficiency factor versus the relative injection pressure is plotted. This plot represents the rule-of-thumb for the volume limited storage capacity. All pure volume limited points are expected to lie on the linear line, which represents the maximum efficiency factor. However, some points fall below this linear line.

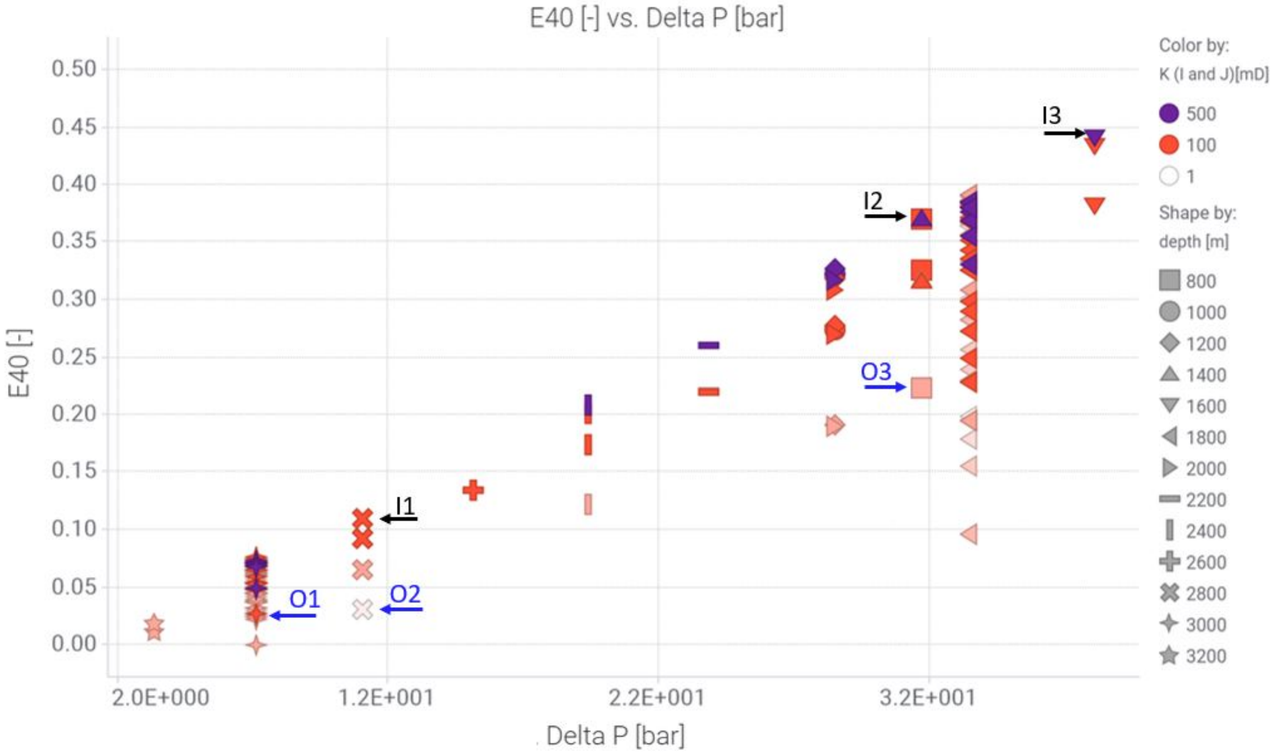

Figure 45: Outliers (O) and inliers (I) on the plot which represents the rule-of-thumb for the volume limited storage capacity.

These outliers are not pure volume limited, but are in transition. Therefore, they are out of line with the pure volume limited trend. That the points are not pure volume limited yet can be seen in figure 46 and table 34. The injection rate of the outliers is just below the 80% threshold, which is used to define whether a point is volume or rate limited. Therefore, these point are not pure rate limited anymore and are also not pure volume limited yet. However, these points are in transition. Whereas, the points that are inline with the pure volume limited trend in figure 45 indeed show an injection rate which is significantly lower than the 80% used as a threshold. From the injection rate it can be concluded that these points are indeed pure volume limited.

Table 34: Injection rate for the inliers and outliers at 40 years of injection compared to the first year of injection.

Point	**Injection rate [sm^3/day]**	**Percentage of first year [%]**	**Note**
Inlier 1	4.78E+04	4.5	Pure volume limited
Inlier 2	2.22E+05	7.3	Pure volume limited
Inlier 3	1.33E+05	3.1	Pure volume limited
Outlier 1	2.61E+05	79.4	Not pure volume limited
Outlier 2	8.93E+04	79.8	Not pure volume limited
Outlier 3	9.80E+05	62.4	Not pure volume limited

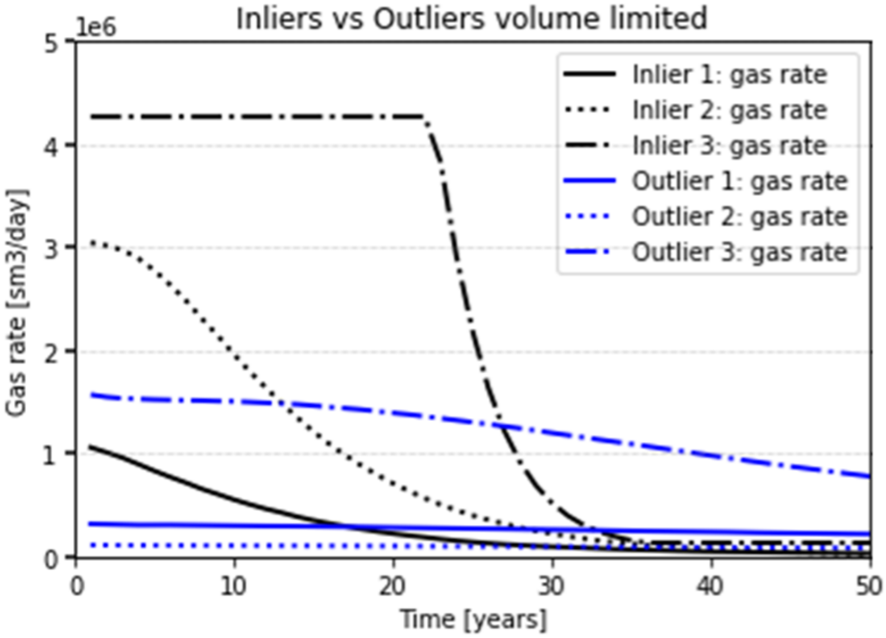

Figure 46: Injection rate of the outliers (O) and inliers (I) from figure 45.

Another example is figure 47 from chapter 7, where the injection rate versus the reservoir radius is plotted for rate limited storage capacity. Here the points for a small radius of 5 and 10 km deflect from the points with a larger radius. The points with a radius of 5 and 10 km are not pure rate limited, because they slowly start to feel the reservoir boundary as a result of continuous CO_2 injection. Therefore the points deflects from the pure rate limited trend.

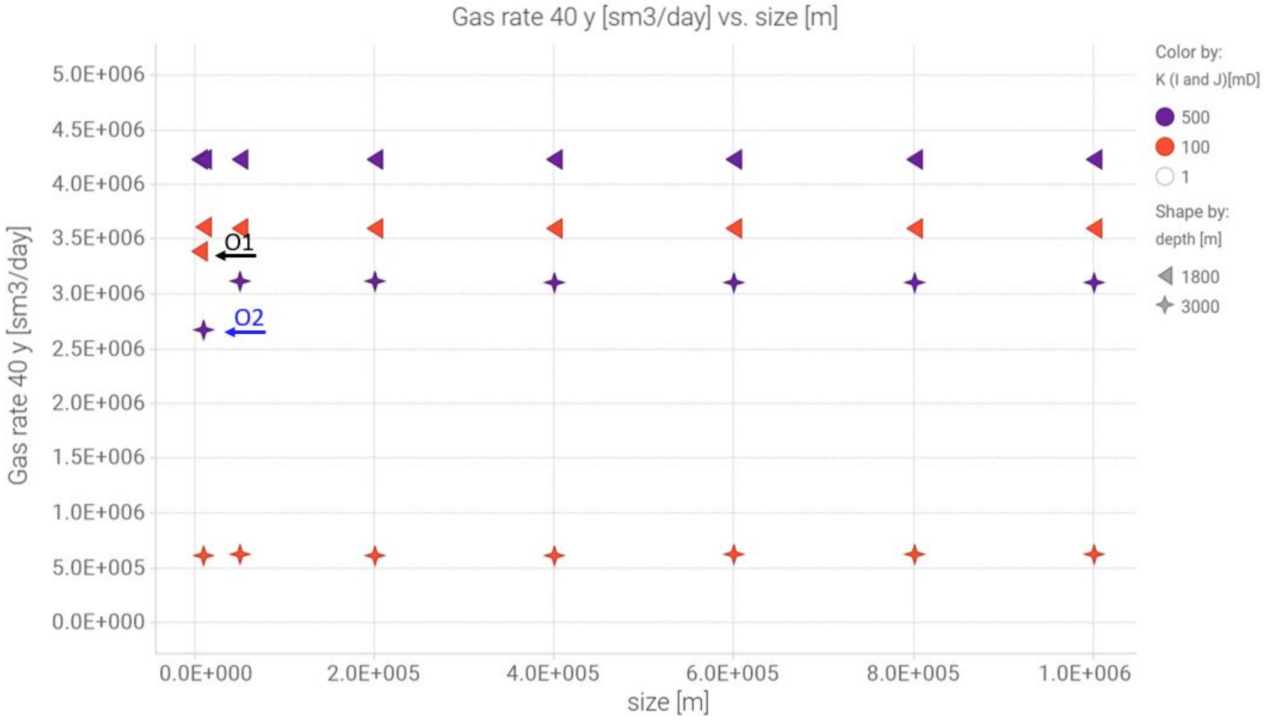

Figure 47: Outliers (O) on the plot for the rate limited storage capacity

From figure 48 it can indeed be seen that the outliers of 5 km (O1) and 10 km (O2) have a slight decrease in injection rate and a slight increase in reservoir pressure. The injection rate decreased approximately 7% to 10% after 40 years of injection. The reservoir pressure increased approximately 0.5% to 4%, see table 35. Therefore, it can be concluded that these points are strictly speaking not pure rate limited anymore, but slowly start to feel the reservoir boundaries.

Table 35: Injection rate and increase in reservoir pressure for the outliers at 40 years of injection compared to the first year of injection.

Point	**Injection rate** [sm^3/day]	**Percentage of first year** [%]	**Increase in reservoir pressure** [%]
Outlier 1	3.40E+06	93.6	3.7
Outlier 2	2.67E+06	90.9	0.5

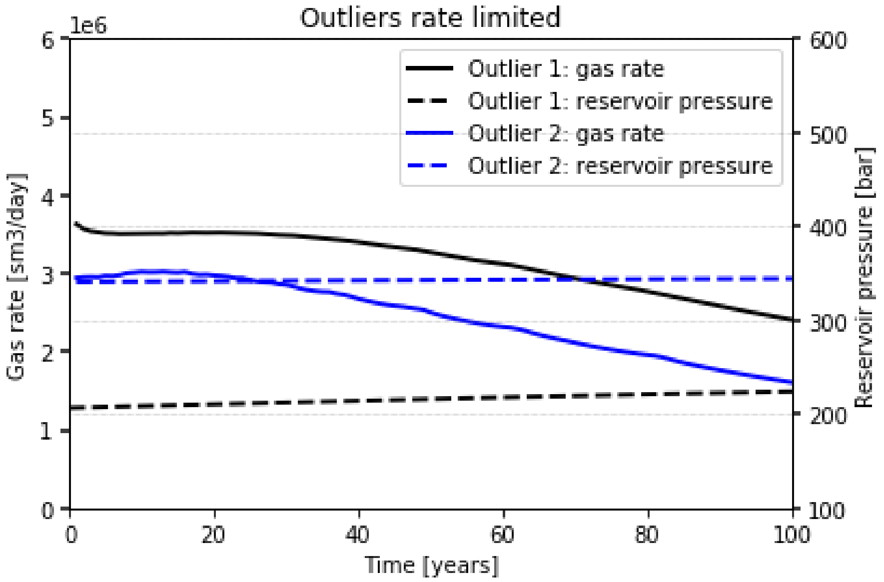

Figure 48: Injection rate and reservoir pressure for the outliers (O) of the rate limited storage capacity from figure 47

9 Workflow

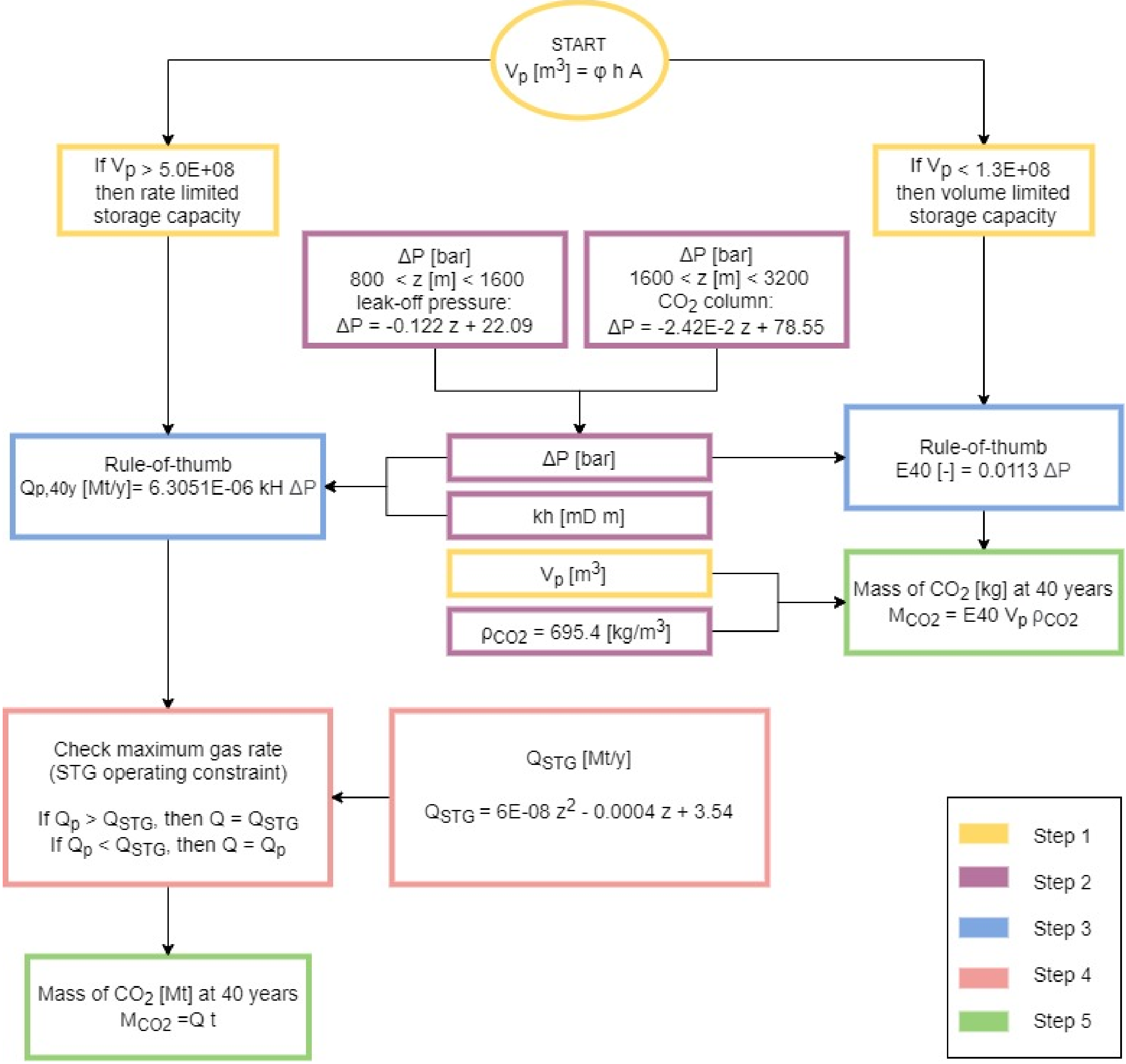

Figure 49: Flowchart to estimate the storage capacity for volume and rate limited aquifers. Rule-of-thumb for 40 years of injection is used as an example.

The workflow shown in figure 49 is an example for 40 years of injection. In the case the storage potential is calculated for 20 or 100 years of injection, step 1 and step 3 have to be adapted. For step 1, check table 19, and for step 3, check table 23 and 30 for the volume limited and rate limited rule-of-thumb.

Step 1:
The first step is to categorize whether the storage capacity of the aquifer is rate or volume limited based on the pore volume, see table 19 in chapter 5. To calculate the pore volume the average reservoir height, area and porosity have to be multiplied. In the case that the pore volume of the aquifer falls in the transition zone, both the volume and rate limited storage capacities can be calculated. These estimations can be used as a minimum and maximum storage capacity.

Step 2:
For both the rate limited and volume limited storage capacity, the input parameters of the rule-of-thumb have to be known. In both cases the relative injection pressure (ΔP) and the pore volume (V_p) are required in order to estimate the storage potential. In the case of a rate limited storage capacity, the reservoir injectivity (kh) is also required.
Depending on the reservoir depth, the relative injection pressure must either be calculated with the leak-off pressure or with the pressure from the weight of the CO_2 column. Because the relative injection pressure directly influences the storage potential, it is also possible to insert a case specific relative injection pressure. Section 5.0.2 shows the calculation of the relative injection pressure in detail.

Step 3:
Use the rule-of-thumb to estimate the injection rate for the rate limited storage capacity. Or use the rule-of-thumb to estimate the efficiency factor for volume limited storage capacity.

Step 4:
This step only has to be considered for a rate limited storage capacity. The injection rate calculated with the rule-of-thumb has to be checked. Because, it is not possible to inject at a higher rate than the maximum injection rate, which is set as an operating constraint to prevent erosion of the pipeline. If the injection rate from the rule-of-thumb (Q_p) is higher than the maximum injection rate (Q_{STG}), then the storage capacity has to be calculated with the maximum injection rate. If the injection rate from the rule-of-thumb (Q_p) is lower than the maximum injection rate (Q_{STG}), then the storage capacity has to be calculated with the injection rate calculated with the rule-of-thumb.
See section 5.0.2 for a detailed calculation of the maximum injection rate.

Step 5:
With the rule-of-thumb the volume and rate limited storage potential can be calculated. With the volume limited rule-of-thumb the storage capacity at 20, 40 and 100 years of injection can be calculated with the efficiency factor. With the rate limited rule-of-thumb the storage capacity at 20, 40 and 100 years of injection can be calculated with the injection rate.

10 Case studies

10.1 Example aquifers Dutch Offshore

The rule-of-thumbs constructed in this study are used to estimate the storage potential at 20 years of injection of five saline storage formations selected by TNO, which is close to the typical project time. The estimated storage capacities are compared to the volumetric calculation by TNO, which they have used in their screening on high-capacity CO_2 storage sites in 2012 [28]. Their calculation is similar to equation (1), with an efficiency factor of 2%.

The pore volume of the offshore Vlieland area falls within the rate limited storage capacity, whereas the pore volume of the other four areas (P18 North KN, P18 South KN, P18-04 dome and P18-02 dome) fall within the transition zone. Therefore, for the latter four the volume and rate limited storage capacities are estimated.

The volume limited storage capacities for the four reservoirs are estimated, given in table 36. What can be noticed is that the estimation with the volumetric approach done by TNO is much smaller than the estimation from this study. The estimation from the TNO study is only 10% of the storage capacity estimated in this study. This mainly results from the fact that TNO (2012) is applying an efficiency factor of 2%, regardless of the reservoir pore volume. This 2% does not represent the pore volume that is actually used for CO_2 storage under assumed pressure conditions.

Table 36: Volume limited storage capacity estimation at 20 years of injection for the TNO (2021) saline formations.

Area	**ΔP [bar]**	**ρ_{CO_2} [kg/m^3]**	**E20 [-]**	**M$_{CO_2}$ [Mt]**	**TNO M$_{CO_2}$ [Mt]**	**Error [%]**
P18 North KN	20	695	0.21	115.3	10.9	90.5
P18 South KN	20	695	0.21	124.9	11.8	90.5
P18-04 dome	26	695	0.28	38.4	3.6	90.5
P18-02 dome	25	695	0.27	38.4	3.6	90.5

The rate limited storage capacity is estimated for all five potential storage formations, see table 37. For all five reservoirs, the estimated plateau rate (Q_p) is higher than the maximum allowed injection rate (Q_{STG}), which is set as an operating constraint. Therefore, the maximum allowed injection rate is used to calculate the cumulative mass of CO_2 at 20 years of injection.

The storage capacity estimation by TNO for the Offshore Vlieland area has a relatively small error (25.8%) compared to the other four areas, which have an error varying between 80% to 94%. Only the storage capacity estimated by TNO for the Offshore Vlieland area is estimated higher than by this study. Finally, note that this comparison is all based on 1 well per reservoir. Since TNO uses a volumetric storage capacity approach, it can also be assumed that the complete pore volume of the Offshore Vlieland area is utilized by placing several wells. Comparing the total pore volume of the Offshore Vlieland area with the injection rate calculated with the rule-of-thumb from this study, approximately 62 wells are needed to utilize the total pore volume of the reservoir in 20 years. Whereas, only one well is needed to utilize the pore volume estimated with the 2% efficiency factor by TNO.

Table 37: Rate limited storage capacity estimation for TNO (2021) saline formations for 20 years of injection.

Area	**ΔP [bar]**	**ρ_{CO_2} [kg/m^3]**	**Q$_p$ [sm^3/day]**	**Q$_{STG}$ [sm^3/day]**	**M$_{CO_2}$ [Mt]**	**TNO M$_{CO_2}$ [Mt]**	**Error [%]**
Offshore Vlieland	33	695	5.96E+06	4.33E+06	62.6	78.7	25.8
P18 North KN	20	695	2.25E+07	4.25E+06	61.4	10.9	82.2
P18 South KN	20	695	2.22E+07	4.25E+06	61.4	11.8	80.7
P18-04 dome	26	695	2.97E+07	4.28E+06	61.9	3.6	94.1
P18-02 dome	25	695	2.87E+07	4.28E+06	61.8	3.6	94.1

10.2 Mt. Simon

Due to the large pore volume of the Mt. Simon aquifer, the storage capacity should be calculated with the rate limited storage capacity. The input parameters that are used to calculate the injection rate and storage capacity with the rate limited method can be seen in table 38. The injection rate which is estimated with the rule-of-thumb does not exceed the maximum allowed injection rate (Q_{STG}), which is set as an operating constraint. Therefore the plateau rate (Q_p) is used to calculate the mass of CO_2 stored at 20, 40 and 100 years of injection. With the rule-of-thumb the injection rate is estimated to be 3.0 Mt/y, which results into a storage capacity of roughly 120 Mt per well after 40 years of injection.

Table 38: Input parameters which are used to calculate the rate limited storage capacity and injection rate.

Area	**ΔP [bar]**	**ρ_{CO_2} [kg/m^3]**	**Q_{STG} [sm^3/day]**	**kh [mD m]**
Mt Simon	79	695	4.39E+06	6000

Table 39: Rate limited storage potential per well estimated by the rule-of-thumb.

	t = 20 years	**t = 40 years**	**t = 100 years**
Storage Capacity [Mt]	59.4	118.9	303.67
Injection rate [sm^3/y]	4.11E+06	4.11E+06	4.20E+06
Injection rate [Mt/y]	3.0	3.0	3.04

The estimated storage capacity for one well from this study is significantly lower than the storage capacity previously estimated by the National Energy Technology laboratoy (NETL), Birkholzer (2008) and Szulcsewsk *et al.* (2012), see table 40 and **??**. With the migration limited method, NETL estimated a storage capacity of 11-151 (average of 75.5) Gt, whereas Szulcsewsk *et al.* estimated a storage capacity of 88 Gt. With the pressure limited method Birkholzer (2008) and Sculczewski *et al.* (2012) estimated a storage capacity of 13 and 15 Gt respectively, per 50 years [4,38].

To reach these estimates with the method proposed by this study, 87 to 101 wells are necessary to achieve the injection rate estimated by Birkholzer (2008) and Sculczewski *et al.* (2012). To reach the storage capacity estimated with the method proposed by this study, 629 and 733 wells are neccesarry to achieve to storage capacity estimated by NETL and Sculczewski *et al.* (2012).

Table 40: Comparison of the injection rate from this study with published estimates

Study	**Injection rate** [Mt/y]	**Comparison t =40 years** [%]	**Number of wells** [-]
NETL	1888	0.16	629
Sculczewski *et al.* (2012)	2200	0.14	733
Birkholzer (2008)	260	1.2	87
Sculczewski *et al.* (2012)	300	1.0	101

11 Discussion

11.1 Model simplifications

The simplifications applied to the reservoir model leads to optimal conditions for CO_2 storage. First of all, the radial model results into optimal placement of the well with respect to the no-flow boundary. Because everywhere the boundary is at the same distance from the well, the pressure gradient will be optimal. The reservoir pressure is of significant importance for the volume limited and rate limited storage capacity. The optimal pressure gradient results into an overestimation of the storage capacity. If the well would be positioned in a Cartesian grid, the pressure gradient throughout the reservoir will not be optimal, and consequently result into a lower storage capacity for the same reservoir pore volume.

Another simplification applied to the model is the anisotropic permeability in i and j direction, which leads to a perfect CO_2 displacement and plume evolution. Implementing layered permeability in order to create a better analogue for real life aquifers might impact the CO_2 migration and storage.
Adding layered permeability, but keeping the overall permeability similar to a homogeneous model, can result into a larger area being invaded by the CO_2. Which consequently can result into more CO_2 stored by residual trapping [15]. Whereas, in the simplified homogeneous model all CO_2 migrates upwards due to the buoyant forces and therefore a smaller area is swept by the CO_2 plume, which consequently results into less CO_2 stored by residual trapping.
Better distribution of the CO_2 resulting from layered permeability might impact the storage capacity for volume limited aquifers. For volume limited aquifers, a significant section of the reservoir is filled with brine because all the CO_2 migrates upwards, see figure 22. Adding layered permeability could improve the lateral distribution of the CO_2 and thereby result into a higher storage capacity.
In case of a rate limited aquifer, it is not expected that adding layered permeability significantly effects the storage capacity. Because enough pore volume is present, a better CO_2 distribution is not expected to increase the storage capacity.
Moreover, the effect of the reservoir boundaries will be felt earlier in time if high permeable layers are added to a model which has a rate limited storage capacity compared to a homogeneous model (again, keeping the overall permeability the same). This effect results from the faster flow rate in the high permeable layers, and therefore reach the reservoir boundaries earlier in time compared to a homogeneous model. Whereas, the effect well be felt later in time if low permeable layers are added to the model.

11.2 Operating constraint

The bottomhole pressure (BHP) operating constraint is of significant importance when estimating the storage capacity for volume and rate limited aquifers. The relative injection pressure, which results from the reservoir pressure and the BHP, directly impacts the storage potential. Therefore it is important that the BHP is not set too conservative because this directly decreases the efficiency factor (for volume limited aquifers) and the injection rate (for rate limited aquifers).
Because the relative injection pressure directly impacts the storage potential, it is important to note the initial conditions that have been set in this study. The aquifer is assumed to be at hydrostatic pressure and the tophole pressure of the injection well is assumed to be 90 bar. With these conditions the largest relative injection pressure can be achieved at approximately 1600 meters depth, which is where the leak-off pressure and CO_2 pressure intersect. Moreover, the maximum injection depth is located at approximately 3200 meters. At this depth the relative injection pressure is zero and therefore injection of CO_2 into the subsurface at greater depths is not possible.
Regarding the hydrostatic pressure, in reality it is possible that an aquifer is overpressured or underpressured, which leads to a higher or lower pressure in the reservoir than expected with the hydrostatic gradient. Moreover, the brine salinity increases with depth [13], which increases the density of the overlying brine column and consequently increases the reservoir pressure. An increase in reservoir pressure, in combinations with the bottomhole pressure applied in this study, will result into a lower maximum injection depth. In this study a gradient of 0.112 bar/m is used for brine and

0.0654 bar/m for CO_2. When instead using an increased brine gradient of 0.120 bar/m, the maximum injection depth shifts from 3200 meters towards approximately 2400 meters. The maximum relative injection pressure remains at 1600 meters depth. Because the maximum relative injection pressure does not depend on the hydrostatic gradient, but on the intersection between the leak-off pressure and the pressure from the CO_2 column.

Also, the tophole pressure directly impacts the maximum relative injection pressure, which directly effects the storage potential and the maximum injection depth.
Increasing or decreasing the tophole pressure results into a shallower or deeper maximum injection depth. Assuming the hydrostatic brine and CO_2 gradient from this study, the gradient that has to be overcome in order to inject CO_2 into the subsurface is 0.0466 bar/m (0.112 - 0.0654 bar/m). Therefore every bar added to the tophole pressure results into an increase in maximum injection depth with 21.5 meters.

Moreover, the density of the CO_2, which is used to calculate the BHP at depths greater than 1600 meters, is currently estimated with a look-up table from a vertical lift profile calculation (VLP). The estimation of the CO_2 density along the well could be refined.
Last, in this study the BHP has been set based on the technical limitations. However, the maximum relative injection pressure and maximum rise in reservoir pressure can also be regulated by national legislation.

11.3 Storage capacity vs Injection rate

The case studies of TNO and Mt. Simon show the importance of categorizing the possible storage capacity into volume and rate limited. Moreover, it shows the importance of consistent terminology. Many studies, including the study by TNO and Mt. Simon, use the term storage capacity. However they do not take operational limitations into account. Therefore, their estimation should actually be considered to be a static subsurface volume estimation.

The small scale feasibility study by TNO shows that applying a volumetric calculation with an efficiency factor of 2% for aquifers with a small pore volume, results into a much smaller storage capacity compared to the storage capacity achieved in this study. Therefore, it is very likely that during screening of geologic structures the storage potential of small aquifers is consistently underestimated.
The compartmentalized geologic structures in the Dutch offshore [40] have the potential to host many small, closed-boundary aquifers. With the current methodology applied in many studies, those type of aquifers are underestimated in their possible storage potential and might be wrongly disregarded on project scale. Moreover, these small scale structures might be cost-efficient when combining the CO_2 storage with existing projects. The infrastructure from offshore gas platforms could be re-used to target small near-by aquifer structures.

The Mt. Simon case study shows that the possible storage potential can also be overestimated when the injection rate of CO_2 into the aquifer is disregarded. The large pore volume of the Mt. Simon aquifer falls within the rate limited storage capacity. However, in previous studies the limitation on the injection rate is not taken into account. Therefore, the estimation result into an extremely high and unrealistic storage capacity.
With the rule-of-thumb from this study 87 to a 101 wells are needed to achieve the proposed storage capacity. Moreover, it must be noted that these wells at least need a spacing of 4 kilometer (two times the plume radius) in order to prevent interference. This spacing and number of wells seems very unlikely on project scale and therefore the storage capacity is highly overestimated.

11.4 Transition zone

The transition zone is a range in pore volumes where both volume limited and rate limited storage capacities are present. With the current knowledge it is not possible to define a rule-of-thumb for the transition zone. Therefore, the storage capacity can be estimated with the volume limited and rate limited rule-of-thumb, which can be regarded as a minimum and maximum storage capacity. Also, a look-up table from the sensitivity simulations is created.

However, these methods are both not optimal. The TNO case study shows that the volume limited and rate limited storage capacities differ significantly. For the P18 North and South KN case studies, the volume limited storage capacity is estimated to approximately 10 Mt. Whereas, the rate limited storage capacity is estimated to be approximately 60 Mt. The same holds for the P18-04 and P18-02 dome, where the volume limited storage capacity is estimated to be approximately 4 Mt. Whereas, the rate limited storage capacity is estimated to be 60 Mt.
The look-up table might come in handy in some cases, but is not very user-friendly. For instance, the look-up table for 40 years of injection contains 150 rows with unique reservoir parameters and corresponding storage capacity and injection rate. Also, in some cases similar reservoir parameters in the look-up table result into slightly different storage capacities at a certain time, due to historic injection rates. Again, these could be regarded as a minimum and maximum storage capacity.
Moreover, it is possible that the case specific reservoir parameters are not present in the look-up table. To find an approximate storage capacity, reservoir parameters in the look-up table should be chosen that resemble the case specific parameters the most. The table is ordered by pore volume, relative injection pressure (ΔP) and reservoir injectivity (kh)

Also, it must be noted that outliers are disregarded during the construction of the rule-of-thumb. The outliers are not pure volume limited or rate limited, but in the transition zone. Therefore, the outliers do not follow the pure volume limited or pure rate limited trend. The rule-of-thumbs are constructed based on the simulations which are in line with the trend that correspond to a pure volume limited or pure rate limited storage capacity. Therefore, the volume limited and rate limited rule-of-thumb are not influenced by the presence of the outliers.

12 Conclusion

The following conclusions can be drawn from this study:

Geologic parameters
In total 17 formations are identified as potential CO_2 storage formations from the lower Cretaceous, Late Jurassic, Triassic and Permian geologic age. The collected data from these formations include the porosity [-], permeability [mD], net thickness [m] and depth [m]. The acquired geologic data shows a wide range in porosity, permeability and depth between the 17 considered CO_2 storage formations. Therefore a grouping system is used in order to cover all unique combinations. This ensures that there is a representative base case for every formation with a corresponding sensitivity range.

Operating constraint
In this study a maximum allowed bottomhole pressure (BHP) and maximum allowed injection rate (STG) are used as operation constraints. Both operating constraints are a function of depth.
For shallow reservoirs from 800 to 1600 meters depth, the BHP is determined by the leak-off pressure. From 1600 to 3200 meters the BHP is determined by the weight of the CO_2 column, with a tophole pressure of 90 bar. With these BHP conditions and a hydrostatic reservoir pressure, the highest possible relative injection pressure is located at approximate 1600 meters depth. At this point the leak-off pressure and CO_2 pressure intersect. Moreover, the maximum injection depth is located at approximately 3200 meters depth. At this depth the relative injection pressure is zero and therefore injection of CO_2 into the subsurface at greater depths is not possible. The BHP and the reservoir pressure are of significant importance when estimating the storage potential of an aquifer.

Storage potential
Estimation of the storage potential can be subdivided into three storage mechanism categories: volume limited storage capacity, rate limited storage capacity and something in between, which we call the transition zone. This categorization is based on whether the pore volume or the injection rate is related to the mass of CO_2 that can be stored in a certain amount of time.
In the case of a volume limited storage capacity, the mass that can be stored is linearly related to the pore volume. The reservoir pressure increases significantly during CO_2 injection because of the limited amount of pore volume and the no-flow boundary. As the reservoir pressure increases, the relative injection pressure (ΔP) decreases because during injection a constant BHP is maintained. This results into a decrease in injection rate over time.
In the case of a rate limited storage capacity the pore volume is large enough for keeping the reservoir pressure more or less constant during CO_2 injection. Since the BHP is maintained constant, the relative injection pressure remains constant, and therefore the injection can be sustained at a plateau rate.
Between the volume and rate limited storage capacity the transition zone is present. The transition zone is a range in pore volume where the storage capacity is not pure volume or pure rate limited anymore. Instead, an aquifer with a pore volume that falls within the transition zone slowly starts to feel the reservoir boundary.
The pore volume of the transition zone is defined for 20, 40 and 100 years of injection. With the current knowledge it is not possible to define a rule-of-thumb for the transition zone. Therefore the storage capacity can be estimated with the volume limited and rate limited rule-of-thumb, which can be regarded as a minimum and maximum storage capacity.
Also, a look-up table from the sensitivity simulations is created such that the storage capacity of an aquifer with a pore volume which falls in the transition zone, can be approximated by finding the simulation that most resembles the case specific aquifer.

Rule-of-thumb
Since the volume limited and rate limited storage capacity estimations are related to different attributes, a rule-of-thumb is constructed for both storage mechanism categories.
A volume limited storage capacity can be estimated by a linear equation relating the storage capacity with the pore volume, including a storage efficiency factor E. The efficiency factor is a linear function of the relative injection pressure (ΔP). The other input parameters to calculate the storage capacity are the density of the CO_2 (ρ_{CO_2}) and the reservoir pore volume (V_p).

A convenient finding of this study is that the density of the CO_2 remains relatively constant under reservoir conditions when increasing the reservoir depth from 800 to 3200 meters. This results from the combination of the geothermal and pressure gradient in the reservoir. Due to the relatively constant CO_2 density, the results from the sensitivity study at different depths can be quantified on the basis of the efficiency factor.
Also, when calculating the mass of CO_2 with the rule-of-thumb, both for a volume limited and rate limited storage capacity a constant density can be assumed for simplicity.

Rate limited storage capacity can not be estimated with a volumetric calculation, because the mass of CO_2 that can be stored is not related to the pore volume. However, the storage capacity is easily estimated by multiplying the plateau rate with the total time of injection. The rule-of-thumb if the injection rate divided by the relative injection pressure (Q / ΔP) is a function of the reservoir injectivity (kh).

Practical application
The volume and rate limited rule-of-thumbs mentioned above can be applied during screening of several aquifers to select the aquifers with the highest possible storage potential. Additionally, the rule-of-thumbs can be used to estimate the reservoir properties necessary when injecting a certain mass of CO_2.
With the volume limited rule-of-thumb the reservoir pore volume necessary when injecting a certain mass of CO_2 can be calculated.

Moreover, when injecting a certain mass of CO_2 into a large aquifer with several wells, the minimum distance between the wells in order to prevent interference can be approximated with the plume radius. the plume radius can be estimated with the volume limited rule-of-thumb.

Additionally, the rate limited rule-of-thumb can be used to estimate the reservoir permeability and height (kh) or the relative injection pressure (ΔP) necessary when injecting CO_2 at a certain rate.
Also, below a certain efficiency factor the storage capacity is always rate limited. So even though the efficiency factor can not be used to estimate a rate limited storage capacity, the efficiency factor can be applied to calculate the pore volume necessary to inject a certain mass of CO_2 at plateau rate (=in the rate limited regime).
Last, the aquifer with a volume or rate limited storage capacity can be used for different project goals. Because the injection for volume limited aquifers is not at plateau rate, it might not be the best option to target a volume limited aquifer for projects where new facilities (platform and wells etc.) have to be developed. However, it might be very efficient to target a small, closed aquifer near-by existing gas platforms where facilities can be re-used. With the operational constraints assumed in this study, even a small, closed aquifer has a considerable storage capacity.
For rate limited aquifers the injection can be sustained at plateau rate. Therefore, aquifers with a rate limited storage capacity are a good target for projects where new facilities have to be developed.

13 Recommendations

Heterogeneity

More complexity could be added to the conceptual model used in this study. For instance, the effect of heterogeneous permeability could be included. Adding heterogeneity to the model could help to understand and quantify the effect of reservoir permeability on storage potential. This can either be done by a layered-cake approach, which is a simplification of the layered architecture of many geologic formations. In that case the radial model could be re-used. However, in the case that a heterogeneous permeability based on on environmental depositions is included, the radial model can not be re-used. Instead, the heterogeneity should be included into a Cartesian model. The effect of the non-ideal pressure distribution on the storage capacity, compared to the radial model, should be taken into account.

Moreover, the Cartesian grid could be used to quantify the effect of the structural dip of the aquifer on the storage capacity. The effect of the heterogeneous permeability, non-ideal pressure distribution resulting from the Cartesian grid and the structural dip could have a different effect on the volume limited and rate limited storage capacity.

Operational constraint

The relative injection pressure, which results from the BHP and the reservoir pressure, is of significant importance on the storage potential of CO_2 in saline aquifers. Therefore, the BHP with regards to technical and regulatory constraints should be studied into more depth.

For future work which focuses on aquifers at a depth of approximately 1600 to 3200 meters, the BHP pressure resulting from the CO_2 column could be refined. The density of the CO_2, which is used to calculate the BHP resulting from the CO_2 column, is currently estimated with a look-up table from a vertical lift profile calculation (VLP). The estimation of the CO_2 density along the well could be refined in order to estimate a more accurate BHP.

Moreover, the tophole pressure (THP) used for the calculation of the BHP resulting from the CO_2 column, could be studied into more depth in future work. Because, an increase in THP results into a direct increase in the relative injection pressure and storage potential. Additionally, every extra bar added to the tophole pressure results into an increase in maximum injection depth with 21.5 meters. Therefore, an accurate and optimal THP should be chosen in order to increase the storage potential.

For future work which focuses on aquifers at a reservoir depth of approximately 800 to 1600 meters, the geomechanical constraints could be refined by incorporating information from laboratory or insitu fracture tests. Moreover, in a case specific study the geomechanical fracture pressure from the case specific formation could be added, such that the relative injection pressure is more accurate.

Also, the regulatory constraints on the BHP should be considered in future studies. The regulatory constraints on the relative injection pressure often set a maximum allowed BHP or maximum allowed rise in reservoir pressure. The storage capacity is significantly impacted if the regulatory constraints decrease the maximum allowed BHP.

Because the relative injection pressure is of significant importance on both the volume and rate limited storage capacity, the reservoir pressure could be studied into more detail. For instance, by running extra simulations with varying reservoir salinity. The reservoir salinity increases the density of the brine and can therefore causes an increase in reservoir pressure. This results into a lower relative injection pressure and decrease in maximum injection depth. Therefore, studying the influence of brine salinity can be of significant importance on the storage capacity of aquifers. Moreover, several simulations could be added to include over and under pressured reservoirs.

This study includes a maximum allowed injection rate. However, it is also possible to set a minimum injection rate as operating constraint. At very low injection rates it is not economically feasible to continue with the injection of CO_2. In the case of a volume limited storage capacity, it is possible that the injection time is decreased due to the limit on the minimum allowed injection rate. Whereas in the case of a rate limited storage capacity, it is possible that the plateau rate is not economically feasible at all if it falls below the minimum allowed injection rate.

References

[1] BACHU, F. Review of CO_2 storage efficiency in deep saline aquifers. *International Journal of Greenhouse Gas Control 40* (2015), 188 – 202.

[2] BACHU, S & BENNION, B. Effects of in-situ condition on relative permeability characteristics of CO_2-brine systems. *Environmental Earth Sciences*.

[3] BENSON, S., PINI. R., REYNOLDS, C., KREVOR, S. Relative permeability analyses to describe multi-phase flow in CO_2 storage reservoirs. *Global CCS Institute* (2013).

[4] BIRKHOLZER, J.T. Large-scale impact of CO_2 storage in deep saline aquifers: a sensitivity study on pressure response in stratified systems. *Earth Sciences Division, Lawerence Berkeley National Laboratory* (2008).

[5] BONTÉ, D., VAN WEES, J., & VERWEIJ, J. Subsurface temperature of the onshore netherlands: New temperature dataset and modelling. *Netherlands Journal of Geosciences - Geologie En Mijnbouw* (2012).

[6] BOUZALAKOS, S. & MERCEDES MAROTO-VALER, M. Overview of carbon dioxide (CO_2) capture and storage technology. In *Development and Innovation in Carbon Dioxide (CO_2) Capture and Storage Technology, Volume 1 - Carbon Dioxide (CO_2) Capture, Transport and Industrial Applications*. Woodhead Publishing, 2011.

[7] BURNSIDE, N.M. & NAYLOR, M. Review and implications of relative permeability of CO_2/bine systems and residual trapping of CO_2. *International Journal of Greenhouse Gas Control* (2014).

[8] CELIA, M.A. & NORDBOTTEN, J.M. *Geolgical Storage of CO_2 Modelling Approaches for Large-Scale Simulation.* John Wiley & Sons, Inc., 2012.

[9] CHEN, X., KIANINEJAD, A., DICARLO, D. An experimental study of CO_2-brine relative permeability in sandstone. *SPE Symposium on Improved Oil Recovery* (2014).

[10] COMPUTER MODELLING GROUP LTD. CMG training: CO_2 sequestration using gem. Tech. rep., 2020.

[11] COMPUTER MODELLING GROUP LTD. *GEM User Guide 2020.10: Compositional & Unconventional Simulator*, 2020.

[12] DE SALIVA, P.N.K & RANJITH, P.G. A study of methodologies for CO_2 storage capacity estimations of saline aquifers. *Fuel 93* (2012), 13–27.

[13] DICKEY, P.A. Increasing concentration of subsurface brines with depth. *Chemical Geology 4*, 1-2 (1969), 361–370.

[14] EBN & GASUNIE. Transport en opslag van CO_2 in nederlands. Tech. rep., EBN & Gasunie, 2017.

[15] ERSHADNIA, R., HAJIREZAIE, S., AMOOIE, M., WALLACE, C.D., GERSHENZON, N.I., HOSSEINI, S.A., STURMER, D.M., RITZI, R.W., SOLTANIAN, M.R. CO_2 geological sequestration in multi scale heterogeneous aquifers: Effects of heterogeneity, connectivity, impurity, and hysteresis. *Advances in Water Resources* (2021).

[16] FLUDE, S. & ALCADE, J. *Carbon capture and storage has stalled needlessly - three reasons why fears of CO_2 leakage are overblown*. March 2020. Retrieved from: https://theconversation.com/carbon-capture-and-storage-has-stalled-needlessly-three-reasons-why-fears-of-co-leakage-are-overblown-130747.

[17] GEEL, C.R., VERDEL, A., PAAP, B, ORLIC, B. Feasibility of large scale CO_2 storage in aquifers performance of DAS technology and pressure limits for safe injection. TNO report TNO-2018-R1179, 2021.

[18] Goodman, A., Hakala, A., Bromhal, G., Deel, D., Rodosta, T., Frailey, S., Small, M., Allen, D., Romanov, V., Fazio, J., Huerta, N., McIntyre, D., Kutchko, B., Guthrie, G. U.S.DOE methodology for development of geologic storage potential for carbon dioxide at national and regional scale. *International Journal of Greenhouse Gas Control 5*, 4 (2011), 952–965.

[19] Krevor, S.C.M, Pini, R., Zuo, L., Benson, S.M. Relative permeability and trapping of CO_2 and water in sandstone rocks at reservoir conditions. *water resources research* (2012).

[20] Li, X., Wei, N., Liu, Y., Fang, Z., Dahowksi, R.T., Davidson, C.L. CO_2 point emission and geological storage capacity in china. *Energy Procedia 1*, 1 (2009), 2793–2800.

[21] Li, Y.K. & Nghiem, L.X. Phase equilibria of oil, gas and water/brine mixtures from a cubic equation of state and henry's law. *The Canadian Journal of Chemical Engineering* (1986).

[22] Madani Sani, F. Huizinga, S., Esaklul, K.A., Nesic, S. Review of the API RP 14E erosional velocity equation: origin, applications, misuses and limitations. *Wear* (2019).

[23] Marchal, V., Dellink, R., van Vuuren, D., Clapp, C., Château, J., Lanzi, E., Magné, D., van Vliet, J. Climate change. In *OECD environmental outlook to 2050*. 2011.

[24] McMinn, C.W., Szulcczewski, M.L., Juanes, R. CO_2 migration in saline aquifers, part 1: Capillary trapping under slope and groundwater flow. *Fluid Mechanics 662* (2010), 329–351.

[25] Metz, B., Davidson, O., de Coninck, H., Loos, M., and Meyer, L. IPCC special report: Carbon dioxide capture and storage. Tech. rep., Cambridge Univ Press, 2005.

[26] Monroe, M. Carbon dioxide levels hit record peak in may. Retrieved from: https://sioweb.ucsd.edu/programs/keelingcurve/2019/06/04/carbon-dioxide-levels-hit-record-peak-in-may/ , 2019.

[27] Neele, F., Nepveu, M., Hofstee, C., Meindertsma, W. CO_2 storage capacity assessment methodology. TNO report TNO-060-UT-2011-00810, 2011.

[28] Neele, F., ten Veen, J., Wilschut, F., Hofstee, C. Independent assessment of high-capacity offshore CO_2 storage options. TNO report TNO-060-UT-2012$_0$0414/B,2012.

[29] Nghiem, L.X., Shrivastava, V.K., Tran, D., Kohse, B.F., Hassam, M.S., Yang, C. Simulation of CO_2 storage in saline aquifers. *SPE International* (2009).

[30] Owken, R.T., Stewart, M.T., Cunningham, J.A. Analytical solution for estimating storage efficiency of geologic sequestration of CO_2. *International Journal of Greenhouse Gas Control 4*, 1 (2010), 102–107.

[31] Perrin, J. & Benson, S. An experimental study on the influence of sub-core scale heterogeneities on CO_2 distribution in reservoir rocks. *Transport in Porous Media* (2010).

[32] Pini, R. and Benson, S.M. Simultaneous determination of capillary pressure and relative permeability curves from core-flooding experiments with various fluid pairs. *Water Resources Research* (2013).

[33] Rackley, S.A. *Carbon Capture and Storage*. Butterworth-Heinemann, 2017.

[34] Ramdharee, S., Muzenda, E., Belaid, M. A review of the equations of state and their applicability in phase equilibrium modeling. *International Conference on Chemical and Environmental Engineering* (2013).

[35] Ramirez, A., Hegedoorn, S., Kramers, L., Wildenborg, T., Hendriks, C. Screening CO_2 storage options in the netherlands. *Energy Procedia 1*, 1 (2009), 2801–2808.

[36] Ramirez, A., Hegedoorn, S., Kramers, L., Wildenborg, T., Hendriks, C. Screening CO_2 storage options in the netherlands. *International Journal of Greenhouse Gas Control 1*, 1 (2010), 367–380.

[37] Ranjith, P.G., Perera, M.S.A., Khan, E. A study of safe CO_2 storage capacity in saline aquifers: a numerical study. *International Journal of Energy Research 37* (2012), 189–199.

[38] Szulczewski, M., MacMinn, C., Herzog, H., Ruanes, R. Lifetime of carbon capture and storage as a climate-change mitigation technology. *Proceeding of the National Acadamy of Sciences of the United States of America 109* (2012), 5185–9.

[39] TAQA. TAQA completion design Porthos, CO_2 transport and storage. Confidential report, 2021.

[40] Ter Borgh, M. M., Jaarsma, B., Rosendaal E.A. Structural developement of the northern dutch offshore: Paleozoic to present. *Geological Society, London, Special Publications 471* (2018), 115 – 131.

[41] Tucker, O. *Carbon Capture and Storage*. IOP Publishing, 2018.

[42] USDOE. Carbon sequestration atlas of united states and canada, 1st ed. Tech. rep., U.S. Department of Energy, 2007.

[43] van de Meer, B.L.G.H. & Yavuz, H. CO_2 storage capacity calculation for the dutch subsurface. *Energy Procedia 1*, 1 (2009), 2651 – 2611.

[44] van der Meer, L.G.H, Hofstee, C., Orlic, B. The fluid flow consequence of CO_2 migration from 1000 to 600 metres upon passing the critical conditions of CO_2. *Energy Procedia 1* (2009), 3213–3220.

[45] Vavra, C.L., Kaldi, J.G., Sneider, R.M. Geological applications of capillary pressure: A review. *AAPG Bulletin* (1992).

[46] Wang, Y. & Zhang, J. An optimized calculation method of critical erosion flow rates of UGS injection/production wells. *Natural Gas Industry B* (2020).

[47] Wetenhall, B., Race, J.M., Downie, M.J. The effect of CO_2 purity on the development of pipeline networks for carbon capture and storage schemes. *International Journal of Greenhouse Gas Control* (2014).

[48] White, A.J., Traugott, M.O., Swarbrick, R.E. The use of leak-off tests as means of predicting minimum in-situ stress. *Petroleum Geoscience* (2002).

[49] Witkowski, A.S., Majkut, M., Rulik, S. Analysis of pipeline transportation systems for carbon dioxide sequestration. *Archives of Thermodynamics* (2014).

[50] Wu, S., Dong, J., Wang, B., Fan, T., Li, H. A general purpose model for multiphase compositional simulation. *Society of Petroleum Engineers* (2018).

[51] Xu, T., Apps, J.A., Pruess, K. Numerical simulation of CO_2 disposal by mineral trapping in deep aquifers. *Applied Geochemistry* (2004).

[52] Zheng, Z., Larson, E.D., Li, Z., Liu, G., Williams, R.H. Near-term mega-scale CO_2 capture and storage demonstration opportunities in china. *Energy & Environmental Science 3* (2010), 1153–1169.

[53] Zhou, Q., Birkholzer, J.T., Tsang, C.F., Rutqvist, J. A method for quick assessment of CO_2 storage capacity in closed and semi-closed saline formations. *International Journal of Greenhouse Gas Control 2*, 4 (2008), 626–639.

Main Nomenclature

A	Area
BHP	Bottomhole pressure
CC	Geometric factor
D	Distance
E	Efficiency factor
$\mathbf{f}_{i,\alpha}$	Fugacity of component i in phase α
ff	fraction of completion
g	Gravitational acceleration
H	Enthalpy
$\mathbf{H}_{h,i}$	Henry's coefficient of component i
h	Height
$\mathbf{I}_{pore}$	Pore size distribution index
k	Permeability
K	Rock permeability
M	Mass
$\mathbf{N}_{c}$	Number of components
$\mathbf{N}_{cap}$	Capillary number
$\mathbf{N}_{i}$	Number of moles
$\mathbf{N}_{p}$	Number of phases
P	Pressure
Q	Flow rate
r	Radius
R	Gas constant
S	Saturation
STG	Maximum allowed injection rate
s	Skin factor
T	Temperature
THP	Tophole pressure
t	time
V	Volume
$\mathbf{V}_{m}$	Molar volume
v	Velocity
WI	Well index
wfrac	Well fraction
x	Mole fraction
Z	Compressibility factor
z	Depth
λ	Mobility
μ	Viscosity
ϕ	Porosity
ρ	Density

Subscripts

avg	Average
BH	Bottomhole
CO_2	Carbon dioxide
c	Component
cap	Capillary
crit	Critical
e	Entry
eq	Equilibrium
g	Gas
I	Grid cell I
i	Component i
inj	Injector
ini	Initial
irr	Irreducible saturation
j	Component j
res	Reservoir
r	Rock
top	Top of reservoir
T	Total
THP	Top-hole
m	Mass
max	Maximum
n	Number
nw	Non-wetting phase
nwr	Irreducible non-wetting phase
p	Plateau
plume	plume
r	Relative
w	Water or wetting phase
well	Well
wr	Irreducible wetting phase
α	Phase α

Superscripts

*	Reference
$\tilde{}$	Partial
o	end-point
n+1	new time
**	ideal gas conditions

Appendix A

Table 41: Experimental data from Chen et al (2014).

f_w	S_w	K_{rw}	K_{rg}
1	**1.0000**	1.0105	
0.5	**0.7524**	0.6777	0.0545
0.1	**0.5797**	0.2616	0.1894
0.01	**0.3892**	0.0478	0.3809
0.0001	**0.3034**	0.0051	0.4091
0	**0.2509**		0.4813

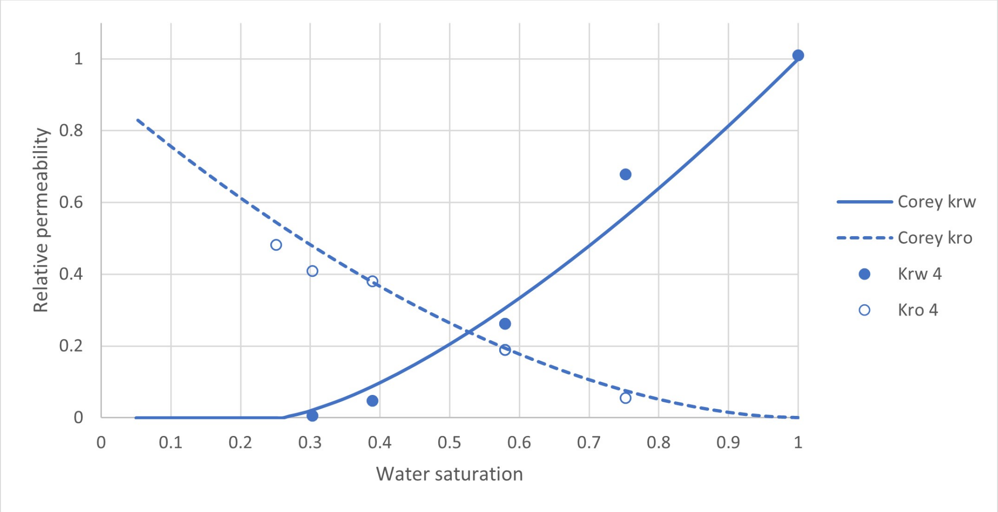

Figure 50: Chen *et al.* (2014) data fitted with the Corey equation 32 and 33.

Table 42: Fitting parameters for the relative permeability curve of Chen et al (2014) and Ershadnia et al (2021).

Corey-equation	**k_{rw}**	**k_{rwCO2}**	**n_w**	**n_{CO2}**	**S_{wr}**	**S_{nwr}**
Chen et al (2014)	1	0.5442	1.4372	1.7912	0.2509	0
Chen et al (2014): strong wetting	1	0.5442	1.4372	1.7912	0.29	0
Chen et al (2014): weak wetting	1	0.5442	1.4372	1.7912	0.2	0
Chen et al (2014): high capillary number	1	0.63	1.2	1.3	0.2509	0
Chen et al (2014): low capillary number	1	0.28	2.5	4	0.1509	0
Ershadnia et al (2021)	1	0.73	4	2.1	0.24	0
Brooks-Corey equation	**Pe**	**S_{wi}**	**λ**			
Ershadnia et al (2021)	0.020	0.176	0.900			

Table 43: Detailed overview of parameter input of group 1.

Group 1								
Parameter	**Base case**	**Sensitivity**		**Parameter**	**Base case**		**Parameter**	**Base case**
Depth [m]	1800	800-3000		STG [sm^3/day]	4.24E+06		S_{hys} [-]	0.4
$\varphi[-]$	0.2	0.05-0.40		BHP [bar]	235		Salinity [M]	0.5
k_{ij} [mD]	10	1-100		P_{res} [bar]	202		k_k [mD]	k_{ij} / 10
h [m]	100	20 - 250		T_{res} [C]	64		t_{inj} [y]	40
r [km]	2	1 - 1000		T_{inj} [C] ^{*a}	35		Z_{por} [1/kPa]	1.04E-04

*a: Only for thermal option turned on

Table 44: Detailed overview of parameter input of group 3.

Group 3						
Parameter	**Base case**	**Sensitivity**	**Parameter**	**Base case**	**Parameter**	**Base case**
Depth [m]	1800	800-3000	STG [sm^3/day]	4.24E+06	S_{hys} [-]	0.4
$\varphi[-]$	0.2	0.05-0.40	BHP [bar]	235	Salinity [M]	0.5
k_{ij} [mD]	500	1-1E+05	P_{res} [bar]	202	k_k [mD]	k_{ij} / 10
h [m]	100	20 - 250	T_{res} [C]	64	t_{inj} [y]	40
r [km]	2	1 - 1000	T_{inj} [C] ^{*a}	35	Z_{por} [1/kPa]	1.04E-04

*a: Only for thermal option turned on

Table 45: Detailed overview of parameter input of group 4.

Group 4						
Parameter	**Base case**	**Sensitivity**	**Parameter**	**Base case**	**Parameter**	**Base case**
Depth [m]	1800	800-3000	STG [sm^3/day]	4.24E+06	S_{hys} [-]	0.4
$\varphi[-]$	0.1	0.05-0.25	BHP [bar]	235	Salinity [M]	0.5
k_{ij} [mD]	50	1-1E+03	P_{res} [bar]	202	k_k [mD]	k_{ij} / 10
h [m]	100	20 - 250	T_{res} [C]	64	t_{inj} [y]	40
r [km]	2	1 - 1000	T_{inj} [C] ^{*a}	35	Z_{por} [1/kPa]	1.04E-04

*a: Only for thermal option turned on

Table 46: Detailed overview of parameter input of group 5.

Group 5						
Parameter	**Base case**	**Sensitivity**	**Parameter**	**Base case**	**Parameter**	**Base case**
Depth [m]	1800	800-3000	STG [sm^3/day]	4.24E+06	S_{hys} [-]	0.4
$\varphi[-]$	0.1	0.05-0.25	BHP [bar]	235	Salinity [M]	0.5
k_{ij} [mD]	10	1-100	P_{res} [bar]	202	k_k [mD]	k_{ij} / 10
h [m]	100	20 - 250	T_{res} [C]	64	t_{inj} [y]	40
r [km]	2	1 - 1000	T_{inj} [C] ^{*a}	35	Z_{por} [1/kPa]	1.04E-04

*a: Only for thermal option turned on

Table 47: Detailed overview of parameter input of group 6.

Group 6						
Parameter	**Base case**	**Sensitivity**	**Parameter**	**Base case**	**Parameter**	**Base case**
Depth [m]	3000	800-3200	STG [sm^3/day]	4.12E+06	S_{hys} [-]	0.4
$\varphi[-]$	0.1	0.05-0.25	BHP [bar]	343	Salinity [M]	0.5
k_{ij} [mD]	100	1-1E+04	P_{res} [bar]	336	k_k [mD]	k_{ij} / 10
h [m]	100	20 - 250	T_{res} [C]	100	t_{inj} [y]	40
r [km]	2	1 - 1000	T_{inj} [C] ^{*a}	35	Z_{por} [1/kPa]	1.04E-04

*a: Only for thermal option turned on

Table 48: Detailed overview of parameter input of group 7.

Group 7						
Parameter	**Base case**	**Sensitivity**	**Parameter**	**Base case**	**Parameter**	**Base case**
Depth [m]	3000	800-3200	STG [sm^3/day]	4.12E+06	S_{hys} [-]	0.4
$\varphi[-]$	0.1	0.05-0.25	BHP [bar]	343	Salinity [M]	0.5
k_{ij} [mD]	50	1-1E+03	P_{res} [bar]	336	k_k [mD]	k_{ij} / 10
h [m]	100	20 - 250	T_{res} [C]	100	t_{inj} [y]	40
r [km]	2	1 - 1000	T_{inj} [C] ^{*a}	35	Z_{por} [1/kPa]	1.04E-04

*a: Only for thermal option turned on

Table 49: Detailed overview of parameter input of group 8.

Group 8								
Parameter	**Base case**	**Sensitivity**		**Parameter**	**Base case**		**Parameter**	**Base case**
Depth [m]	3000	800-3200		STG [sm^3/day]	4.12E+06		S_{hys} [-]	0.4
$\varphi[-]$	0.2	0.05-0.40		BHP [bar]	343		Salinity [M]	0.5
k_{ij} [mD]	500	1-1E+05		P_{res} [bar]	336		k_k [mD]	k_{ij} / 10
h [m]	100	20 - 250		T_{res} [C]	100		t_{inj} [y]	40
r [km]	2	1 - 1000		T_{inj} [C] ^{*a}	35		Z_{por} [1/kPa]	1.04E-04

*a: Only for thermal option turned on

Table 50: Detailed overview of parameter input of group 9.

Group 9								
Parameter	**Base case**	**Sensitivity**		**Parameter**	**Base case**		**Parameter**	**Base case**
Depth [m]	3000	800-3200		STG [sm^3/day]	4.12E+06		S_{hys} [-]	0.4
$\varphi[-]$	0.2	0.05-0.40		BHP [bar]	343		Salinity [M]	0.5
k_{ij} [mD]	50	1-1E+03		P_{res} [bar]	336		k_k [mD]	k_{ij} / 10
h [m]	100	20 - 250		T_{res} [C]	100		t_{inj} [y]	40
r [km]	2	1 - 1000		T_{inj} [C] ^{*a}	35		Z_{por} [1/kPa]	1.04E-04

*a: Only for thermal option turned on

Appendix B

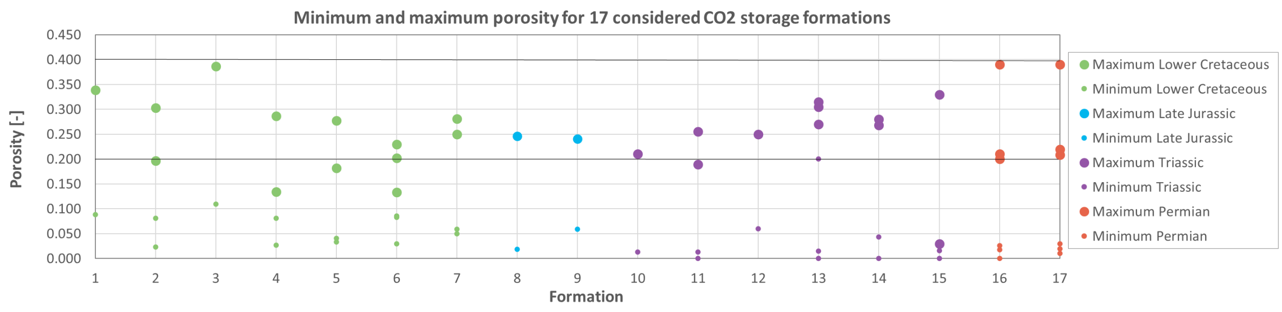

Figure 51: Collected porosity data for the 17 formations considered for CO_2 storage.

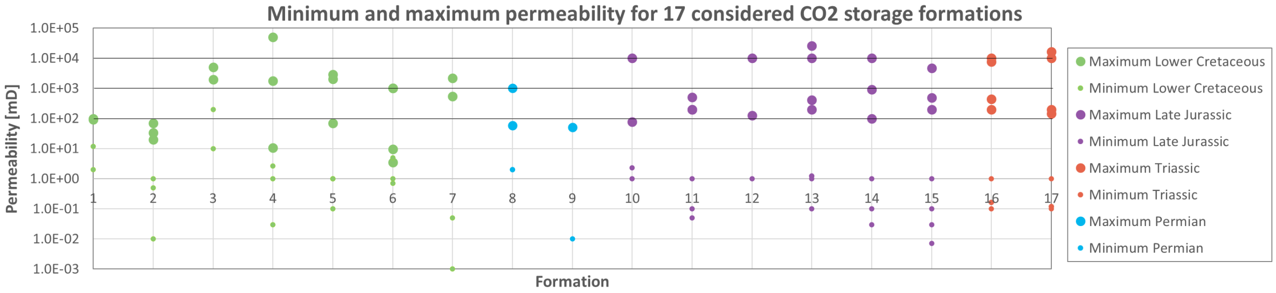

Figure 52: Collected permeability data for the 17 formations considered for CO_2 storage.

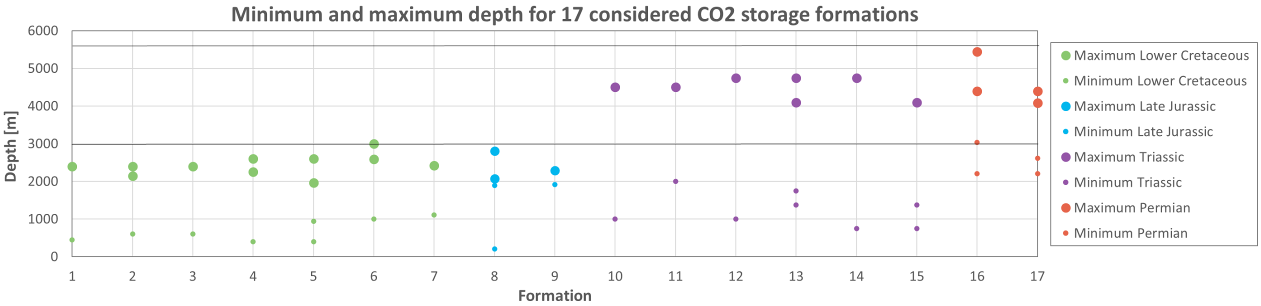

Figure 53: Collected depth data for the 17 formations considered for CO_2 storage.

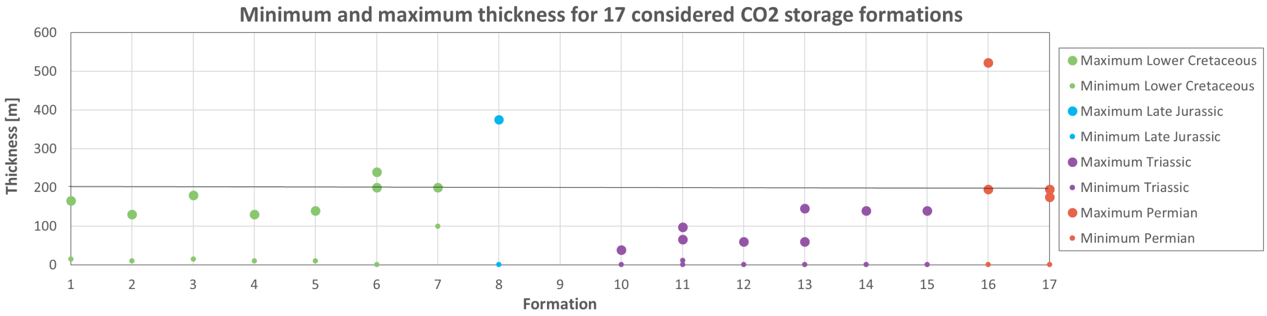

Figure 54: Collected thickness data for the 17 formations considered for CO_2 storage.

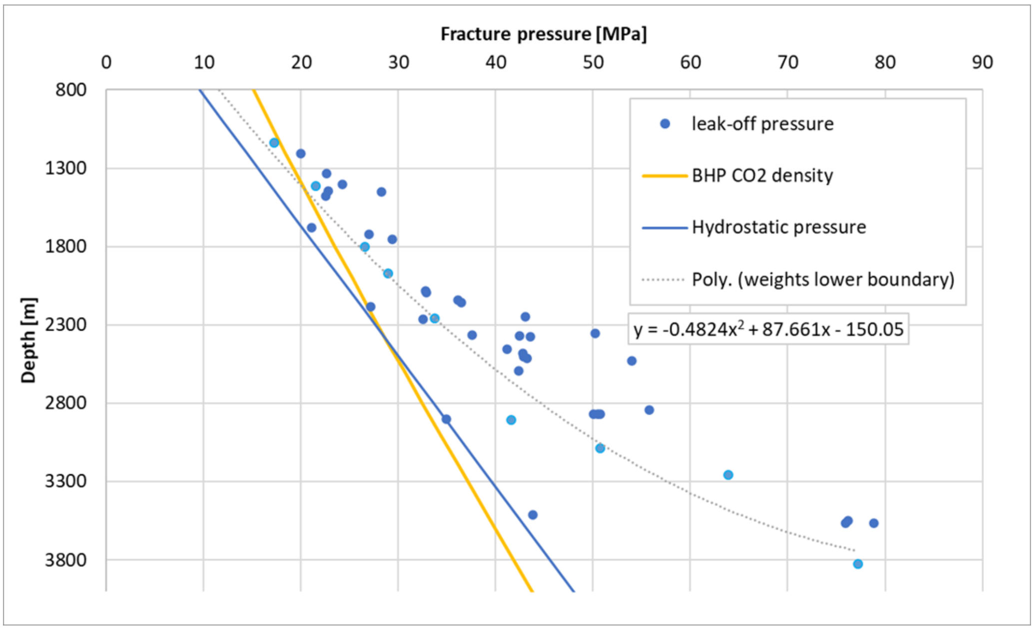

Figure 55: Fitted curve of the leak-off pressure as a function of depth.

Table 51: Volume limited: E factor for various depth when applying the BHP operating constraint from this study for an injection period of 20, 40 and 100 years.

Depth [m]	Δ P [bar]	E20	E40	E100
800	32	0.34	0.36	0.36
1000	28	0.30	0.32	0.33
1200	28	0.30	0.32	0.33
1400	32	0.34	0.36	0.36
1600	38	0.41	0.43	0.44
1800	33	0.36	0.38	0.38
2000	29	0.31	0.32	0.33
2200	24	0.26	0.27	0.27
2400	19	0.21	0.22	0.22
2600	15	0.16	0.17	0.17
2800	11	0.12	0.12	0.13
3000	7	0.08	0.08	0.08
3200	3	0.04	0.04	0.04

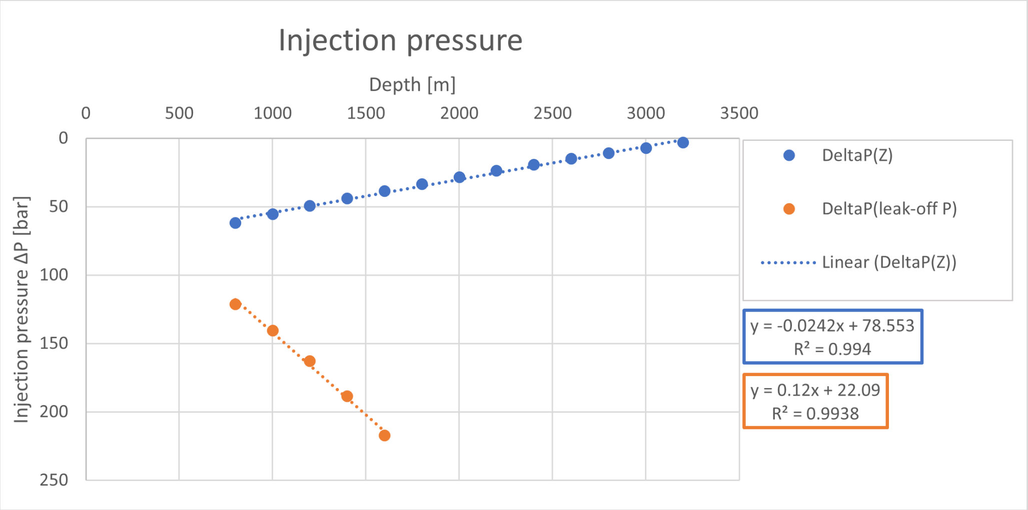

Figure 56: Fitted curve of the injection pressure ΔP as a function of depth. The injection pressure results from the hydrostatic reservoir pressure and the BHP (leak-off pressure and weight of the CO_2 column.

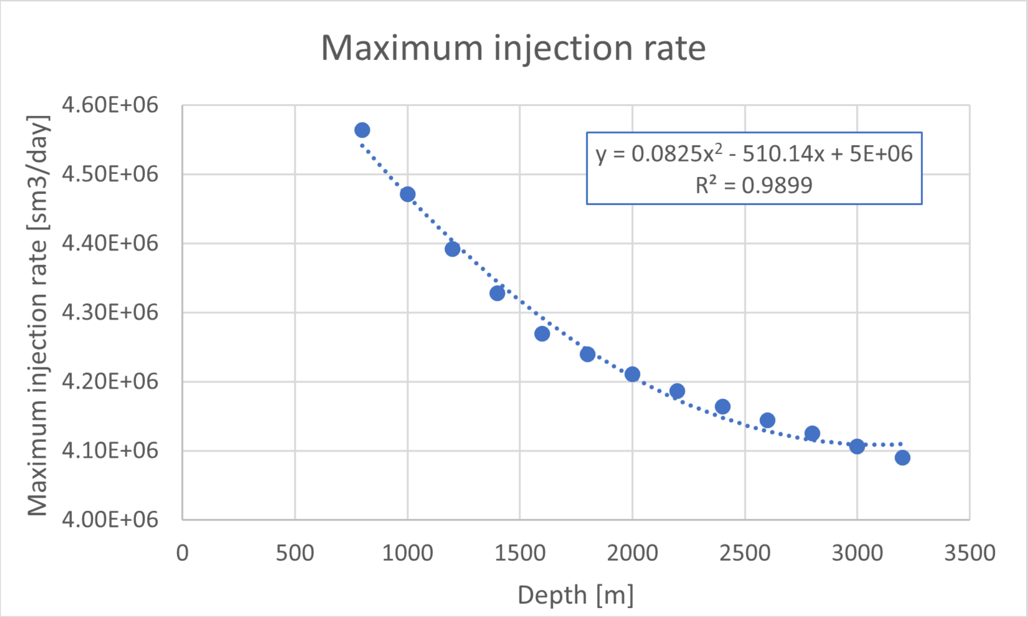

Figure 57: Fitted curve of the injection rate [sm^3/day]versus depth.

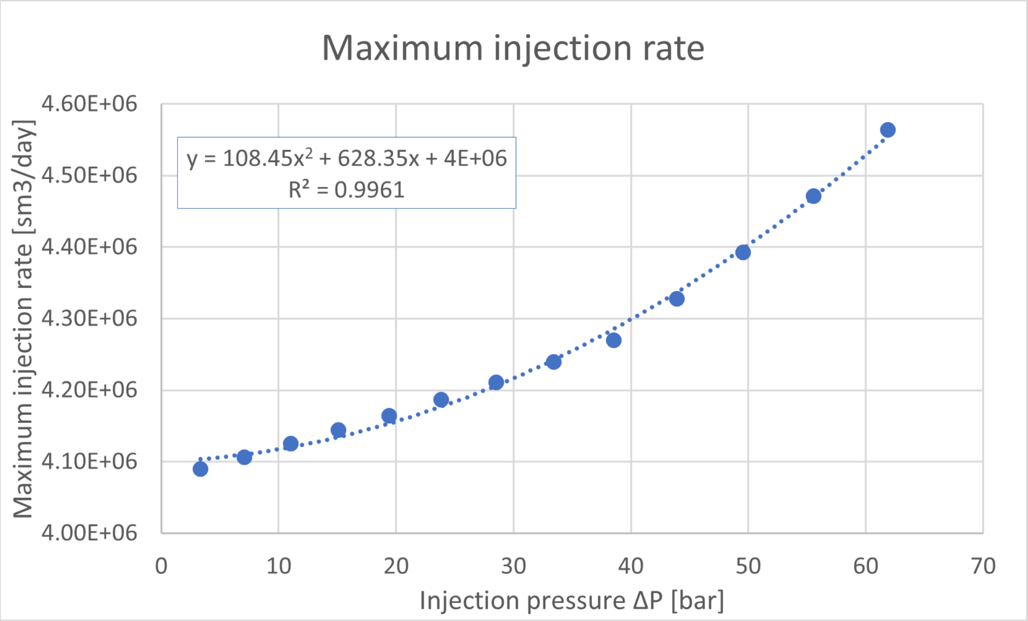

Figure 58: Fitted curve of the injection rate [sm^3/day] versus injection pressure.

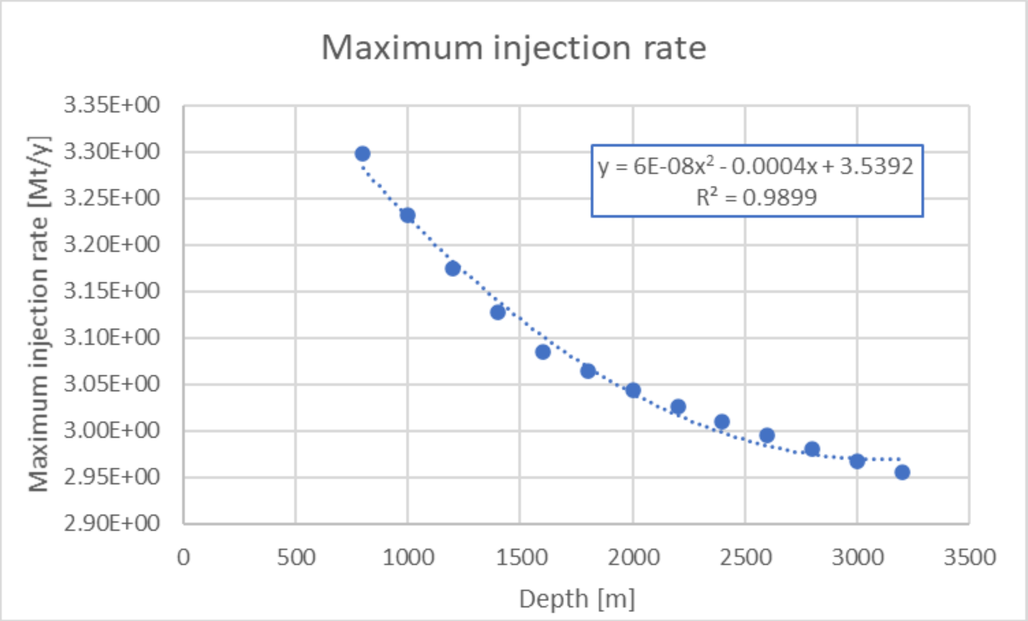

Figure 59: Fitted curve of the injection rate [Mt/y] versus depth.

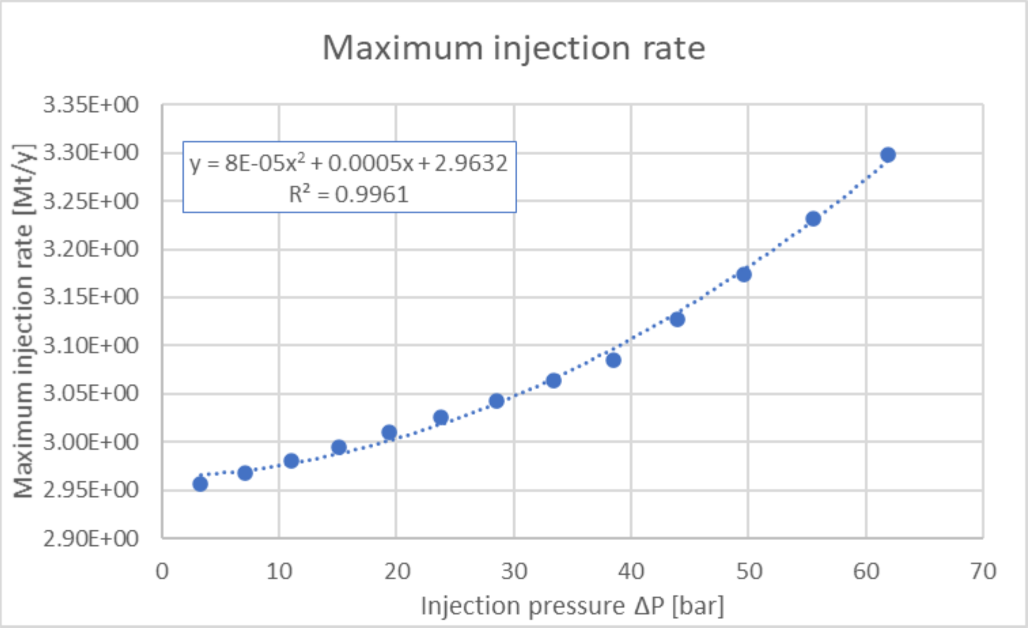

Figure 60: Fitted curve of the injection rate [Mt/y] versus injection pressure.

Appendix C

This appendix contains the look-up tables for 20, 40 and 100 years of injection. Within the table, the injection rate and cumulative gas mass are sorted by the pore volume, then by reservoir depth, then by permeability and thickness (KH). Also, the last column indicates whether the aquifer is volume or rate limited at 20, 40 or 100 years of injection.

Table 52: Look-up table for the injection rate and cumulative gas mass for aquifers with a pore volume that falls within the transition zone at 20 years of injection.

Pore volume $[m^3]$	**Depth [m]**	**KH [mD m]**	**Injection rate** $[sm^3/day]$	**Cumulative gas mass [Mt]**	**Category [-]**
6.30E+07	1600	5000	4.07E+05	5.03	Volume
6.30E+07	1600	10000	5.29E+03	3.83	Volume
6.30E+07	1800	500	1.81E+05	3.91	Rate
6.30E+07	1800	1000	3.17E+05	4.54	Rate
6.30E+07	1800	1000	3.22E+05	5.75	Rate
6.30E+07	1800	1000	3.17E+05	5.03	Rate
6.30E+07	1800	2500	5.09E+05	4.26	Volume
6.30E+07	1800	3000	1.30E+04	3.53	Volume
6.30E+07	1800	4000	9.30E+03	2.82	Volume
6.30E+07	1800	5000	3.55E+05	2.14	Volume
6.30E+07	1800	10000	9.66E+04	1.48	Volume
6.30E+07	1800	10000	9.78E+04	0.85	Volume
6.30E+07	1800	50000	7.06E+03	4.26	Volume
6.30E+07	2400	5000	1.94E+05	0.53	Volume
6.30E+07	2400	10000	4.07E+03	5.03	Volume
6.30E+07	2800	10000	3.39E+03	39.80	Volume
6.30E+07	3000	2000	7.44E+04	2.56	Volume
6.30E+07	3000	2500	9.36E+04	23.16	Volume
6.30E+07	3000	3000	7.82E+04	4.75	Volume
6.30E+07	3000	4000	7.36E+04	4.93	Volume
6.30E+07	3000	5000	7.16E+04	4.99	Volume
6.30E+07	3000	5000	7.03E+04	5.03	Volume
6.30E+07	3000	5000	7.03E+04	5.05	Volume
6.30E+07	3000	5000	6.74E+04	4.89	Volume
6.30E+07	3000	10000	3.94E+04	5.02	Volume
7.10E+07	1600	1000	3.78E+05	5.75	Rate
7.10E+07	1600	5000	5.25E+05	2.81	Volume
7.10E+07	1600	5000	5.25E+05	9.69	Volume
7.10E+07	1600	10000	1.64E+05	13.90	Volume
7.10E+07	1800	1000	3.27E+05	17.59	Rate
7.10E+07	1800	2000	5.05E+05	5.03	Volume
7.10E+07	1800	2000	5.05E+05	9.86	Volume
7.10E+07	1800	3000	5.52E+05	14.54	Volume
7.10E+07	1800	3000	5.52E+05	18.98	Volume
7.10E+07	1800	4000	5.20E+05	5.03	Volume
7.10E+07	1800	4000	5.20E+05	2.59	Volume
7.10E+07	1800	5000	4.52E+05	39.80	Volume
7.10E+07	2400	1000	1.79E+05	32.53	Rate
7.10E+07	2400	5000	1.34E+05	32.60	Volume
7.10E+07	2400	5000	2.47E+05	37.07	Volume
7.10E+07	2800	1000	9.34E+04	45.99	Rate
7.10E+07	2800	10000	6.90E+04	39.80	Volume
7.10E+07	3000	2000	8.06E+04	33.43	Volume
7.10E+07	3000	2000	8.06E+04	27.45	Volume
7.10E+07	3000	3000	8.90E+04	21.80	Volume
7.10E+07	3000	3000	8.90E+04	16.44	Volume
7.10E+07	3000	4000	8.79E+04	11.35	Volume
7.10E+07	3000	4000	8.79E+04	6.51	Volume
7.10E+07	3000	5000	8.25E+04	36.61	Volume
7.10E+07	3000	10000	5.33E+04	0.53	Volume

Pore volume [m^3]	Depth [m]	KH [mD m]	Injection rate [sm^3/day]	Cumulative gas mass [Mt]	Category [-]
1.30E+08	800	1000	3.03E+05	5.03	Rate
1.30E+08	800	5000	9.81E+05	39.80	Volume
1.30E+08	800	5000	9.81E+05	57.88	Volume
1.30E+08	800	10000	7.11E+05	23.16	Volume
1.30E+08	1000	1000	2.71E+05	57.57	Rate
1.30E+08	1200	1000	2.76E+05	16.18	Rate
1.30E+08	1200	5000	8.53E+05	28.39	Volume
1.30E+08	1200	5000	8.53E+05	35.59	Volume
1.30E+08	1200	10000	6.30E+05	39.80	Volume
1.30E+08	1400	1000	3.18E+05	42.41	Rate
1.30E+08	1400	5000	9.50E+05	16.24	Volume
1.30E+08	1600	1000	4.01E+05	4.87	Rate
1.30E+08	1600	5000	1.15E+06	2.38	Volume
1.30E+08	1600	5000	1.15E+06	1.31	Volume
1.30E+08	1600	10000	8.29E+05	4.10	Volume
1.30E+08	1800	100	3.73E+04	4.14	Rate
1.30E+08	1800	100	3.73E+04	30.59	Rate
1.30E+08	1800	500	1.85E+05	35.44	Rate
1.30E+08	1800	500	1.80E+05	16.69	Rate
1.30E+08	1800	1000	3.49E+05	8.71	Rate
1.30E+08	1800	1000	3.49E+05	9.69	Rate
1.30E+08	1800	1000	3.49E+05	13.90	Rate
1.30E+08	1800	1000	3.49E+05	17.59	Rate
1.30E+08	1800	1000	3.49E+05	39.80	Rate
1.30E+08	1800	1000	3.49E+05	9.86	Rate
1.30E+08	1800	1000	3.49E+05	14.54	Rate
1.30E+08	1800	1000	3.49E+05	18.98	Rate
1.30E+08	1800	2000	6.34E+05	39.80	Rate
1.30E+08	1800	2000	6.34E+05	20.77	Rate
1.30E+08	1800	3000	8.30E+05	57.57	Volume
1.30E+08	1800	3000	8.30E+05	53.17	Volume
1.30E+08	1800	4000	9.43E+05	56.98	Volume
1.30E+08	1800	4000	9.43E+05	58.30	Volume
1.30E+08	1800	5000	1.02E+06	57.57	Volume
1.30E+08	1800	5000	9.87E+05	52.06	Volume
1.30E+08	1800	5000	9.87E+05	44.14	Volume
1.30E+08	1800	5000	9.87E+05	35.82	Volume
1.30E+08	1800	5000	9.87E+05	27.60	Volume
1.30E+08	1800	5000	9.87E+05	19.67	Volume
1.30E+08	1800	5000	9.87E+05	12.00	Volume
1.30E+08	1800	5000	9.87E+05	57.77	Volume
1.30E+08	1800	10000	7.14E+05	0.53	Volume
1.30E+08	1800	10000	7.14E+05	39.80	Volume
1.30E+08	1800	10000	7.14E+05	57.88	Volume
1.30E+08	1800	25000	1.34E+05	57.57	Volume
1.30E+08	1800	50000	6.58E+04	33.09	Volume
1.30E+08	1800	50000	6.58E+04	48.27	Volume
1.30E+08	2000	1000	2.95E+05	57.57	Rate
1.30E+08	2000	5000	8.21E+05	57.88	Volume
1.30E+08	2000	5000	8.21E+05	16.86	Volume
1.30E+08	2000	10000	6.02E+05	37.17	Volume
1.30E+08	2200	1000	2.43E+05	57.57	Rate

Pore volume **[m^3]**	**Depth** **[m]**	**KH** **[mD m]**	**Injection rate** **[sm^3/day]**	**Cumulative gas mass** **[Mt]**	**Category** **[-]**
1.30E+08	2400	1000	1.94E+05	33.05	Rate
1.30E+08	2400	5000	5.34E+05	19.95	Volume
1.30E+08	2400	5000	5.34E+05	16.33	Volume
1.30E+08	2400	10000	4.01E+05	18.57	Volume
1.30E+08	2600	1000	1.47E+05	23.06	Rate
1.30E+08	2600	5000	3.98E+05	19.95	Volume
1.30E+08	2800	1000	1.02E+05	16.75	Rate
1.30E+08	2800	5000	2.76E+05	13.75	Volume
1.30E+08	2800	5000	2.76E+05	10.91	Volume
1.30E+08	2800	10000	2.22E+05	8.23	Volume
1.30E+08	3000	100	6.29E+03	5.68	Rate
1.30E+08	3000	100	6.29E+03	3.26	Rate
1.30E+08	3000	1000	5.82E+04	18.34	Rate
1.30E+08	3000	1000	5.82E+04	0.52	Rate
1.30E+08	3000	1000	5.82E+04	4.93	Rate
1.30E+08	3000	2000	1.03E+05	28.39	Rate
1.30E+08	3000	2000	1.03E+05	19.95	Rate
1.30E+08	3000	2500	1.42E+05	33.09	Volume
1.30E+08	3000	3000	1.33E+05	14.21	Volume
1.30E+08	3000	3000	1.33E+05	19.95	Volume
1.30E+08	3000	4000	1.51E+05	22.13	Volume
1.30E+08	3000	4000	1.51E+05	23.16	Volume
1.30E+08	3000	5000	1.60E+05	23.71	Volume
1.30E+08	3000	5000	1.60E+05	15.31	Volume
1.30E+08	3000	5000	1.60E+05	17.74	Volume
1.30E+08	3000	5000	1.60E+05	4.36	Volume
1.30E+08	3000	5000	1.60E+05	8.80	Volume
1.30E+08	3000	5000	1.60E+05	11.74	Volume
1.30E+08	3000	5000	1.60E+05	13.85	Volume
1.30E+08	3000	5000	1.60E+05	19.95	Volume
1.30E+08	3000	5000	1.60E+05	9.49	Volume
1.30E+08	3000	10000	1.41E+05	13.54	Volume
1.30E+08	3000	10000	1.41E+05	17.02	Volume
1.30E+08	3000	10000	1.41E+05	19.95	Volume
1.30E+08	3000	10000	1.41E+05	37.23	Volume
1.30E+08	3000	10000	1.41E+05	10.39	Volume
1.30E+08	3000	10000	1.41E+05	4.93	Volume
1.30E+08	3000	10000	1.41E+05	3.78	Volume
1.30E+08	3000	25000	3.23E+04	3.85	Volume
1.30E+08	3200	5000	5.87E+04	4.46	Volume
1.30E+08	3200	10000	6.74E+04	5.65	Volume
1.40E+08	1600	1000	4.08E+05	4.93	Rate
1.40E+08	1600	5000	1.26E+06	4.18	Volume
1.40E+08	1600	10000	1.05E+06	3.46	Volume
1.40E+08	1800	1000	3.56E+05	2.76	Rate
1.40E+08	1800	2000	6.54E+05	2.09	Rate
1.40E+08	1800	2000	6.54E+05	1.45	Rate
1.40E+08	1800	3000	8.70E+05	0.83	Volume
1.40E+08	1800	3000	8.70E+05	4.21	Volume
1.40E+08	1800	4000	1.01E+06	0.52	Volume
1.40E+08	1800	4000	1.01E+06	4.93	Volume
1.40E+08	1800	10000	9.09E+05	28.39	Volume
1.40E+08	1800	50000	1.30E+05	2.51	Volume

Pore volume [m^3]	**Depth [m]**	**KH [mD m]**	**Injection rate [sm^3/day]**	**Cumulative gas mass [Mt]**	**Category [-]**
1.40E+08	2400	1000	1.98E+05	19.95	Rate
1.40E+08	2400	10000	4.94E+05	4.75	Volume
1.40E+08	2800	5000	3.00E+05	4.93	Volume
1.40E+08	2800	10000	2.69E+05	4.99	Volume
1.40E+08	3000	2000	1.06E+05	5.03	Rate
1.40E+08	3000	3000	1.39E+05	5.05	Volume
1.40E+08	3000	4000	1.61E+05	4.85	Volume
1.40E+08	3000	5000	1.74E+05	5.56	Volume
1.90E+08	1800	1000	3.56E+05	2.70	Rate
1.90E+08	1800	1000	3.56E+05	1.41	Rate
1.90E+08	1800	5000	1.32E+06	8.80	Volume
1.90E+08	1800	10000	1.43E+06	11.74	Volume
1.90E+08	1800	50000	5.38E+05	13.85	Volume
1.90E+08	3000	5000	2.10E+05	4.93	Volume
1.90E+08	3000	5000	2.10E+05	9.49	Volume
1.90E+08	3000	10000	2.44E+05	13.54	Volume
1.90E+08	3000	50000	6.85E+04	17.02	Volume
2.50E+08	800	1000	3.06E+05	4.93	Rate
2.50E+08	800	5000	1.39E+06	33.37	Rate
2.50E+08	800	10000	1.96E+06	2.55	Volume
2.50E+08	800	50000	1.59E+06	4.73	Volume
2.50E+08	1000	1000	2.75E+05	23.72	Rate
2.50E+08	1000	10000	1.73E+06	32.87	Volume
2.50E+08	1000	50000	1.02E+06	23.81	Volume
2.50E+08	1200	1000	2.80E+05	15.51	Rate
2.50E+08	1200	5000	1.23E+06	8.13	Rate
2.50E+08	1200	10000	1.71E+06	4.73	Volume
2.50E+08	1200	50000	1.10E+06	1.64	Volume
2.50E+08	1400	1000	3.24E+05	26.77	Rate
2.50E+08	1400	10000	1.90E+06	0.09	Volume
2.50E+08	1400	50000	2.21E+06	0.83	Volume
2.50E+08	1600	1000	4.11E+05	4.73	Rate
2.50E+08	1600	10000	2.31E+06	3.26	Volume
2.50E+08	1600	50000	4.27E+06	2.89	Rate
2.50E+08	1600	50000	4.27E+06	4.73	Rate
2.50E+08	1800	100	3.80E+04	5.83	Rate
2.50E+08	1800	100	3.80E+04	6.51	Rate
2.50E+08	1800	100	3.80E+04	6.96	Rate
2.50E+08	1800	500	1.83E+05	3.17	Rate
2.50E+08	1800	1000	3.59E+05	20.88	Rate
2.50E+08	1800	1000	3.59E+05	5.30	Rate
2.50E+08	1800	1000	3.59E+05	1.44	Rate
2.50E+08	1800	1000	3.59E+05	1.91	Rate
2.50E+08	1800	1000	3.59E+05	2.26	Rate
2.50E+08	1800	1000	3.59E+05	4.73	Rate
2.50E+08	1800	1000	3.59E+05	1.58	Rate
2.50E+08	1800	1000	3.59E+05	2.23	Rate
2.50E+08	1800	2000	6.98E+05	2.78	Rate
2.50E+08	1800	2000	6.98E+05	4.73	Rate
2.50E+08	1800	2000	7.15E+03	6.92	Volume
2.50E+08	1800	3000	1.01E+06	2.75	Rate
2.50E+08	1800	3000	1.01E+06	3.26	Rate

Pore volume [m^3]	Depth [m]	KH [mD m]	Injection rate [sm^3/day]	Cumulative gas mass [Mt]	Category [-]
2.50E+08	1800	4000	1.27E+06	16.33	Rate
2.50E+08	1800	4000	1.27E+06	23.06	Rate
2.50E+08	1800	5000	1.49E+06	16.75	Rate
2.50E+08	1800	5000	1.49E+06	10.91	Rate
2.50E+08	1800	5000	1.49E+06	5.68	Rate
2.50E+08	1800	10000	1.98E+06	3.26	Volume
2.50E+08	1800	10000	1.98E+06	1.03	Volume
2.50E+08	1800	10000	1.98E+06	18.34	Volume
2.50E+08	1800	10000	1.98E+06	0.09	Volume
2.50E+08	1800	10000	1.98E+06	0.83	Volume
2.50E+08	1800	10000	1.98E+06	4.73	Volume
2.50E+08	1800	10000	1.98E+06	3.26	Volume
2.50E+08	1800	10000	1.98E+06	2.37	Volume
2.50E+08	1800	10000	1.86E+06	3.26	Volume
2.50E+08	1800	50000	3.38E+06	3.63	Volume
2.50E+08	1800	50000	3.38E+06	3.83	Volume
2.50E+08	1800	50000	3.38E+06	3.94	Volume
2.50E+08	1800	50000	3.38E+06	2.52	Volume
2.50E+08	1800	50000	3.38E+06	17.74	Volume
2.50E+08	1800	50000	3.38E+06	8.35	Volume
2.50E+08	1800	50000	3.38E+06	1.44	Volume
2.50E+08	1800	100000	4.24E+06	1.91	Rate
2.50E+08	1800	100000	4.24E+06	2.26	Rate
2.50E+08	2000	1000	3.04E+05	3.26	Rate
2.50E+08	2000	5000	1.24E+06	1.58	Volume
2.50E+08	2000	10000	1.64E+06	2.23	Volume
2.50E+08	2000	50000	1.28E+06	2.78	Volume
2.50E+08	2000	50000	1.28E+06	3.26	Volume
2.50E+08	2200	1000	2.52E+05	4.42	Rate
2.50E+08	2200	10000	1.34E+06	1.93	Volume
2.50E+08	2200	50000	5.40E+05	12.00	Volume
2.50E+08	2400	1000	2.01E+05	52.86	Rate
2.50E+08	2400	5000	8.06E+05	58.30	Volume
2.50E+08	2400	10000	1.07E+06	52.06	Volume
2.50E+08	2400	50000	2.99E+05	35.82	Volume
2.50E+08	2400	50000	2.99E+05	19.67	Volume
2.50E+08	2600	1000	1.53E+05	12.00	Rate
2.50E+08	2600	10000	7.95E+05	4.74	Volume
2.50E+08	2600	50000	1.98E+05	0.09	Volume
2.50E+08	2800	1000	1.06E+05	6.51	Rate
2.50E+08	2800	5000	4.16E+05	12.00	Volume
2.50E+08	2800	10000	5.52E+05	9.32	Volume
2.50E+08	2800	50000	1.56E+05	12.00	Volume
2.50E+08	2800	50000	1.56E+05	14.44	Volume
2.50E+08	3000	100	6.37E+03	12.00	Rate
2.50E+08	3000	1000	6.05E+04	6.51	Rate
2.50E+08	3000	1000	6.05E+04	3.83	Rate
2.50E+08	3000	2000	1.16E+05	18.46	Rate
2.50E+08	3000	3000	1.64E+05	19.53	Rate
2.50E+08	3000	4000	2.06E+05	12.81	Volume

Pore volume [m^3]	**Depth [m]**	**KH [mD m]**	**Injection rate [sm^3/day]**	**Cumulative gas mass [Mt]**	**Category [-]**
2.50E+08	3000	5000	2.39E+05	6.69	Volume
2.50E+08	3000	5000	2.39E+05	3.83	Volume
2.50E+08	3000	5000	2.39E+05	1.15	Volume
2.50E+08	3000	5000	2.39E+05	20.42	Volume
2.50E+08	3000	5000	2.39E+05	0.09	Volume
2.50E+08	3000	5000	2.39E+05	0.85	Volume
2.50E+08	3000	5000	2.39E+05	6.51	Volume
2.50E+08	3000	10000	3.21E+05	3.83	Volume
2.50E+08	3000	10000	3.21E+05	12.00	Volume
2.50E+08	3000	10000	2.39E+05	2.37	Volume
2.50E+08	3000	10000	3.21E+05	3.26	Volume
2.50E+08	3000	10000	3.21E+05	3.63	Volume
2.50E+08	3000	20000	2.77E+05	3.83	Volume
2.50E+08	3000	50000	1.24E+05	3.94	Volume
2.50E+08	3000	50000	1.25E+05	2.34	Volume
2.50E+08	3000	50000	1.24E+05	16.54	Volume
2.50E+08	3000	50000	1.25E+05	7.77	Volume
2.50E+08	3000	50000	1.25E+05	1.41	Volume
2.50E+08	3000	50000	1.25E+05	1.84	Volume
2.50E+08	3000	50000	1.25E+05	2.13	Volume
2.50E+08	3000	50000	1.25E+05	3.39	Volume
2.50E+08	3200	5000	7.57E+04	23.98	Rate
2.50E+08	3200	50000	9.26E+04	5.92	Volume
3.10E+08	1800	1000	3.61E+05	1.61	Rate
3.10E+08	1800	1000	3.61E+05	2.29	Rate
3.10E+08	1800	5000	1.58E+06	2.88	Rate
3.10E+08	1800	10000	2.36E+06	3.83	Volume
3.10E+08	1800	50000	4.24E+06	1.66	Rate
3.10E+08	3000	5000	2.57E+05	2.43	Rate
3.10E+08	3000	5000	2.57E+05	3.15	Rate
3.10E+08	3000	10000	3.78E+05	3.83	Volume
3.10E+08	3000	50000	1.99E+05	2.27	Volume

Table 53: Look-up table for the injection rate and cumulative gas mass for aquifers with a pore volume that falls within the transition zone at 40 years of injection.

Pore volume [m^3]	**Depth [m]**	**KH [mD m]**	**Injection rate [sm^3/day]**	**Cumulative gas mass [Mt]**	**Category [-]**
1.30E+08	800	1000	2.91E+05	8.28	Rate
1.30E+08	800	5000	3.51E+05	26.83	Volume
1.30E+08	800	10000	7.41E+04	30.51	Volume
1.30E+08	1000	1000	2.58E+05	7.41	Rate
1.30E+08	1000	5000	3.16E+05	23.84	Volume
1.30E+08	1200	1000	2.59E+05	7.51	Rate
1.30E+08	1200	5000	3.11E+05	23.78	Volume
1.30E+08	1200	10000	8.54E+04	27.26	Volume
1.30E+08	1400	1000	2.95E+05	8.66	Rate
1.30E+08	1400	5000	3.44E+05	26.81	Volume
1.30E+08	1600	1000	3.67E+05	10.91	Rate
1.30E+08	1600	5000	4.08E+05	32.95	Volume
1.30E+08	1600	10000	9.92E+04	37.44	Volume
1.30E+08	1800	100	3.66E+04	1.03	Rate
1.30E+08	1800	500	1.81E+05	5.10	Rate
1.30E+08	1800	500	1.75E+05	4.93	Rate
1.30E+08	1800	1000	3.17E+05	9.50	Rate
1.30E+08	1800	2000	4.71E+05	17.04	Volume
1.30E+08	1800	3000	4.89E+05	22.42	Volume
1.30E+08	1800	4000	4.37E+05	26.06	Volume
1.30E+08	1800	5000	3.41E+05	29.31	Volume
1.30E+08	1800	5000	3.52E+05	28.45	Volume
1.30E+08	1800	10000	9.41E+04	32.38	Volume
1.30E+08	1800	25000	1.30E+04	33.54	Volume
1.30E+08	2000	1000	2.66E+05	8.02	Rate
1.30E+08	2000	5000	2.97E+05	23.86	Volume
1.30E+08	2000	10000	8.38E+04	27.25	Volume
1.30E+08	2200	1000	2.18E+05	6.62	Rate
1.30E+08	2200	5000	2.46E+05	19.57	Volume
1.30E+08	2400	1000	1.73E+05	5.27	Rate
1.30E+08	2400	5000	1.98E+05	15.54	Volume
1.30E+08	2400	10000	6.55E+04	17.91	Volume
1.30E+08	2600	1000	1.30E+05	3.99	Rate
1.30E+08	2600	5000	1.53E+05	11.74	Volume
1.30E+08	2800	1000	8.93E+04	2.76	Volume
1.30E+08	2800	5000	1.10E+05	8.14	Volume
1.30E+08	2800	10000	4.79E+04	9.60	Volume
1.30E+08	3000	100	6.18E+03	0.17	Rate
1.30E+08	3000	100	6.18E+03	0.17	Rate
1.30E+08	3000	1000	5.15E+04	1.58	Rate
1.30E+08	3000	2000	7.56E+04	2.79	Volume
1.30E+08	3000	2500	93610.29	3.87	Volume
1.30E+08	3000	3000	8.11E+04	3.66	Volume
1.30E+08	3000	4000	7.77E+04	4.29	Volume
1.30E+08	3000	5000	7.01E+04	4.74	Volume
1.30E+08	3000	10000	3.93E+04	5.79	Volume
1.30E+08	3200	5000	3.37E+04	1.64	Volume

Pore volume [m^3]	Depth [m]	KH [mD m]	Injection rate [sm^3/day]	Cumulative gas mass [Mt]	Category [-]
1.40E+08	1600	1000	3.77E+05	11.12	Rate
1.40E+08	1600	5000	5.22E+05	35.54	Volume
1.40E+08	1600	10000	1.60E+05	41.79	Volume
1.40E+08	1800	1000	3.27E+05	9.69	Rate
1.40E+08	1800	2000	5.05E+05	17.60	Volume
1.40E+08	1800	3000	5.52E+05	23.51	Volume
1.40E+08	1800	4000	5.18E+05	27.73	Volume
1.40E+08	1800	10000	1.43E+05	36.12	Volume
1.40E+08	2400	1000	1.79E+05	5.39	Rate
1.40E+08	2400	10000	9.19E+04	19.88	Volume
1.40E+08	2800	5000	1.33E+05	8.72	Volume
1.40E+08	2800	10000	6.86E+04	10.61	Volume
1.40E+08	3000	2000	8.07E+04	2.88	Volume
1.40E+08	3000	3000	8.89E+04	3.83	Volume
1.40E+08	3000	4000	8.77E+04	4.53	Volume
1.40E+08	3000	5000	8.22E+04	5.05	Volume
1.90E+08	1800	1000	3.40E+05	9.75	Rate
1.90E+08	1800	5000	7.13E+05	35.69	Volume
1.90E+08	1800	10000	3.48E+05	46.06	Volume
1.90E+08	3000	5000	1.21E+05	5.84	Volume
1.90E+08	3000	10000	8.69E+04	7.86	Volume
2.50E+08	800	1000	3.03E+05	8.41	Rate
2.50E+08	800	5000	9.80E+05	36.73	Volume
2.50E+08	800	10000	7.05E+05	53.62	Volume
2.50E+08	1000	1000	2.71E+05	7.56	Rate
2.50E+08	1000	10000	6.34E+05	47.65	Volume
2.50E+08	1000	50000	3.82E+04	55.95	Volume
2.50E+08	1200	1000	2.76E+05	7.70	Rate
2.50E+08	1200	5000	8.52E+05	32.70	Volume
2.50E+08	1200	10000	6.25E+05	47.52	Volume
2.50E+08	1200	50000	4.35E+04	55.86	Volume
2.50E+08	1400	1000	3.18E+05	8.92	Rate
2.50E+08	1400	10000	6.91E+05	53.58	Volume
2.50E+08	1400	50000	4.65E+04	62.56	Volume
2.50E+08	1600	1000	4.01E+05	11.29	Rate
2.50E+08	1600	10000	8.22E+05	65.84	Volume
2.50E+08	1600	50000	7.87E+04	76.08	Volume
2.50E+08	1800	100	3.73E+04	1.05	Rate
2.50E+08	1800	500	1.79E+05	5.02	Rate
2.50E+08	1800	1000	3.49E+05	9.86	Rate
2.50E+08	1800	2000	6.34E+05	18.99	Rate
2.50E+08	1800	2000	3.55E+05	10.65	Rate
2.50E+08	1800	3000	8.30E+05	27.09	Volume
2.50E+08	1800	4000	9.43E+05	34.06	Volume
2.50E+08	1800	5000	9.86E+05	39.94	Volume
2.50E+08	1800	10000	7.08E+05	56.86	Volume
2.50E+08	1800	10000	7.17E+05	53.72	Volume
2.50E+08	1800	50000	6.52E+04	66.18	Volume
2.50E+08	1800	50000	6.55E+04	66.19	Volume

Pore volume [m^3]	Depth [m]	KH [mD m]	Injection rate [sm^3/day]	Cumulative gas mass [Mt]	Category [-]
2.50E+08	2000	1000	2.95E+05	8.35	Rate
2.50E+08	2000	5000	8.20E+05	33.53	Volume
2.50E+08	2000	10000	5.97E+05	47.69	Volume
2.50E+08	2000	50000	6.42E+04	55.92	Volume
2.50E+08	2200	1000	2.43E+05	6.91	Rate
2.50E+08	2200	10000	4.94E+05	39.11	Volume
2.50E+08	2200	50000	6.64E+04	46.32	Volume
2.50E+08	2400	1000	1.94E+05	5.52	Rate
2.50E+08	2400	5000	5.33E+05	21.85	Volume
2.50E+08	2400	10000	3.98E+05	31.07	Volume
2.50E+08	2400	50000	4.99E+04	37.33	Volume
2.50E+08	2600	1000	1.46E+05	4.19	Rate
2.50E+08	2600	10000	3.07E+05	23.48	Volume
2.50E+08	2800	1000	1.02E+05	2.90	Rate
2.50E+08	2800	5000	2.76E+05	11.36	Volume
2.50E+08	2800	10000	2.21E+05	16.28	Volume
2.50E+08	3000	100	6.27E+03	0.18	Rate
2.50E+08	3000	1000	5.79E+04	1.66	Rate
2.50E+08	3000	2000	1.03E+05	3.15	Rate
2.50E+08	3000	3000	1.33E+05	4.46	Volume
2.50E+08	3000	4000	1.51E+05	5.57	Volume
2.50E+08	3000	5000	1.60E+05	6.52	Volume
2.50E+08	3000	10000	1.40E+05	9.47	Volume
2.50E+08	3000	10000	1.38E+05	6.92	Volume
2.50E+08	3000	10000	1.40E+05	9.47	Volume
2.50E+08	3000	20000	1.16E+05	9.37	Volume
2.50E+08	3000	50000	3.01E+04	12.82	Volume
2.50E+08	3200	5000	5.86E+04	2.06	Volume
3.10E+08	1800	1000	3.53E+05	9.93	Rate
3.10E+08	1800	5000	1.18E+06	42.56	Volume
3.10E+08	1800	10000	1.10E+06	65.05	Volume
3.10E+08	1800	50000	1.99E+05	81.97	Volume
3.10E+08	3000	5000	1.89E+05	6.96	Volume
3.10E+08	3000	10000	1.94E+05	10.71	Volume
3.10E+08	3000	50000	4.58E+04	15.78	Volume
3.80E+08	1800	1000	3.56E+05	9.98	Rate
3.80E+08	1800	10000	1.43E+06	71.27	Volume
3.80E+08	1800	50000	5.29E+05	96.60	Volume
3.80E+08	3000	5000	2.10E+05	7.27	Volume
3.80E+08	3000	50000	6.81E+04	18.63	Volume
4.40E+08	1800	1000	3.57E+05	10.01	Rate
4.40E+08	1800	10000	1.73E+06	76.01	Volume
4.40E+08	1800	50000	1.50E+06	108.61	Volume
4.40E+08	3000	5000	2.27E+05	7.49	Volume
4.40E+08	3000	50000	9.48E+04	21.36	Volume
5.00E+08	1800	1000	3.59E+05	10.05	Rate
5.00E+08	1800	2000	6.55E+05	18.55	Rate
5.00E+08	1800	10000	1.97E+06	79.69	Volume
5.00E+08	1800	20000	1.94E+06	101.05	Volume
5.00E+08	1800	50000	3.38E+06	115.20	Volume
5.00E+08	1800	100000	3.54E+06	115.49	Rate
5.00E+08	3000	5000	2.39E+05	7.65	Volume
5.00E+08	3000	10000	2.39E+05	8.85	Volume
5.00E+08	3000	50000	1.24E+05	24.00	Volume

Table 54: Look-up table for the injection rate and cumulative gas mass for aquifers with a pore volume that falls within the transition zone at 100 years of injection.

Pore volume [m^3]	Depth [m]	KH [mD m]	Injection rate [sm^3/day]	Cumulative gas mass [Mt]	Category [-]
1.90E+08	1800	1000	2.63E+05	22.16	Volume
1.90E+08	1800	5000	8.38E+04	47.78	Volume
1.90E+08	1800	10000	1.70E+04	49.63	Volume
1.90E+08	3000	5000	2.87E+04	8.36	Volume
2.50E+08	800	1000	2.79E+05	20.44	Rate
2.50E+08	800	5000	1.95E+05	57.33	Volume
2.50E+08	800	10000	2.27E+04	61.64	Volume
2.50E+08	1000	1000	2.46E+05	18.26	Rate
2.50E+08	1000	10000	2.84E+04	55.28	Volume
2.50E+08	1200	1000	2.46E+05	18.47	Rate
2.50E+08	1200	5000	1.80E+05	50.86	Volume
2.50E+08	1200	10000	3.29E+04	55.28	Volume
2.50E+08	1400	1000	2.79E+05	21.24	Volume
2.50E+08	1400	10000	4.08E+04	62.09	Volume
2.50E+08	1600	1000	3.45E+05	26.66	Volume
2.50E+08	1600	10000	4.72E+04	75.84	Volume
2.50E+08	1800	100	3.64E+04	2.55	Rate
2.50E+08	1800	500	1.71E+05	12.22	Rate
2.50E+08	1800	1000	2.97E+05	23.18	Volume
2.50E+08	1800	2000	3.94E+05	39.98	Volume
2.50E+08	1800	2000	2.19E+05	22.35	Volume
2.50E+08	1800	3000	3.60E+05	50.61	Volume
2.50E+08	1800	4000	2.80E+05	56.97	Volume
2.50E+08	1800	5000	2.06E+05	60.64	Volume
2.50E+08	1800	10000	3.79E+04	65.65	Volume
2.50E+08	1800	10000	6.84E+04	63.67	Volume
2.50E+08	2000	1000	2.48E+05	19.55	Volume
2.50E+08	2000	5000	1.75E+05	50.9	Volume
2.50E+08	2000	10000	3.43E+04	55.26	Volume
2.50E+08	2200	1000	2.03E+05	16.1	Volume
2.50E+08	2200	10000	3.41E+04	45.55	Volume
2.50E+08	2400	1000	1.61E+05	12.82	Volume
2.50E+08	2400	5000	1.20E+05	33.23	Volume
2.50E+08	2400	10000	3.35E+04	36.47	Volume
2.50E+08	2600	1000	1.21E+05	9.69	Volume
2.50E+08	2600	10000	3.17E+04	27.86	Volume
2.50E+08	2800	1000	8.32E+04	6.69	Volume
2.50E+08	2800	5000	6.97E+04	17.5	Volume
2.50E+08	2800	10000	2.97E+04	19.72	Volume
2.50E+08	3000	100	6.15E+03	0.43	Rate
2.50E+08	3000	1000	4.78E+04	3.83	Volume
2.50E+08	3000	2000	6.41E+04	6.53	Volume
2.50E+08	3000	3000	6.25E+04	8.31	Volume
2.50E+08	3000	4000	5.60E+04	9.48	Volume
2.50E+08	3000	5000	4.89E+04	10.28	Volume
2.50E+08	3000	10000	2.46E+04	12.01	Volume
2.50E+08	3200	5000	2.60E+04	3.69	Volume
3.10E+08	1800	1000	3.17E+05	23.73	Rate
3.10E+08	1800	5000	3.51E+05	71.2	Volume
3.10E+08	1800	10000	9.25E+04	81.01	Volume

Pore volume [m^3]	Depth [m]	KH [mD m]	Injection rate [sm^3/day]	Cumulative gas mass [Mt]	Category [-]
3.10E+08	3000	5000	7.00E+04	11.85	Volume
3.10E+08	3000	10000	3.93E+04	14.47	Volume
3.80E+08	1800	1000	3.29E+05	24.06	Rate
3.80E+08	1800	10000	1.69E+05	95.53	Volume
3.80E+08	3000	5000	9.27E+04	13.13	Volume
4.40E+08	1800	1000	3.37E+05	24.28	Rate
4.40E+08	1800	10000	2.81E+05	108.98	Volume
4.40E+08	1800	50000	1.46E+04	116.56	Volume
4.40E+08	3000	5000	1.11E+05	14.17	Volume
5.00E+08	1800	1000	3.42E+05	24.43	Rate
5.00E+08	1800	2000	5.55E+05	43.48	Volume
5.00E+08	1800	10000	4.13E+05	121.23	Volume
5.00E+08	1800	20000	1.59E+05	127.09	Volume
5.00E+08	1800	50000	2.92E+04	132.97	Volume
5.00E+08	3000	5000	1.31E+05	15.02	Volume
7.90E+08	1800	1000	3.54E+05	24.2	Rate
7.90E+08	1800	2000	6.83E+05	48.06	Rate
7.90E+08	1800	3000	9.40E+05	70.4	Rate
7.90E+08	1800	4000	1.11E+06	90.5	Volume
7.90E+08	1800	5000	1.20E+06	108.1	Volume
7.90E+08	3000	2000	1.11E+05	8.02	Rate
7.90E+08	3000	3000	1.51E+05	11.65	Rate
7.90E+08	3000	4000	1.80E+05	14.9	Volume
7.90E+08	3000	5000	1.97E+05	17.76	Volume
7.90E+08	3000	10000	1.84E+05	27.18	Volume